DRILLED SHAFT FOUNDATION DEFECTS
Identification, Imaging, and Characterization

Publication No. FHWA-CFL/TD-05-007 **October 2005**

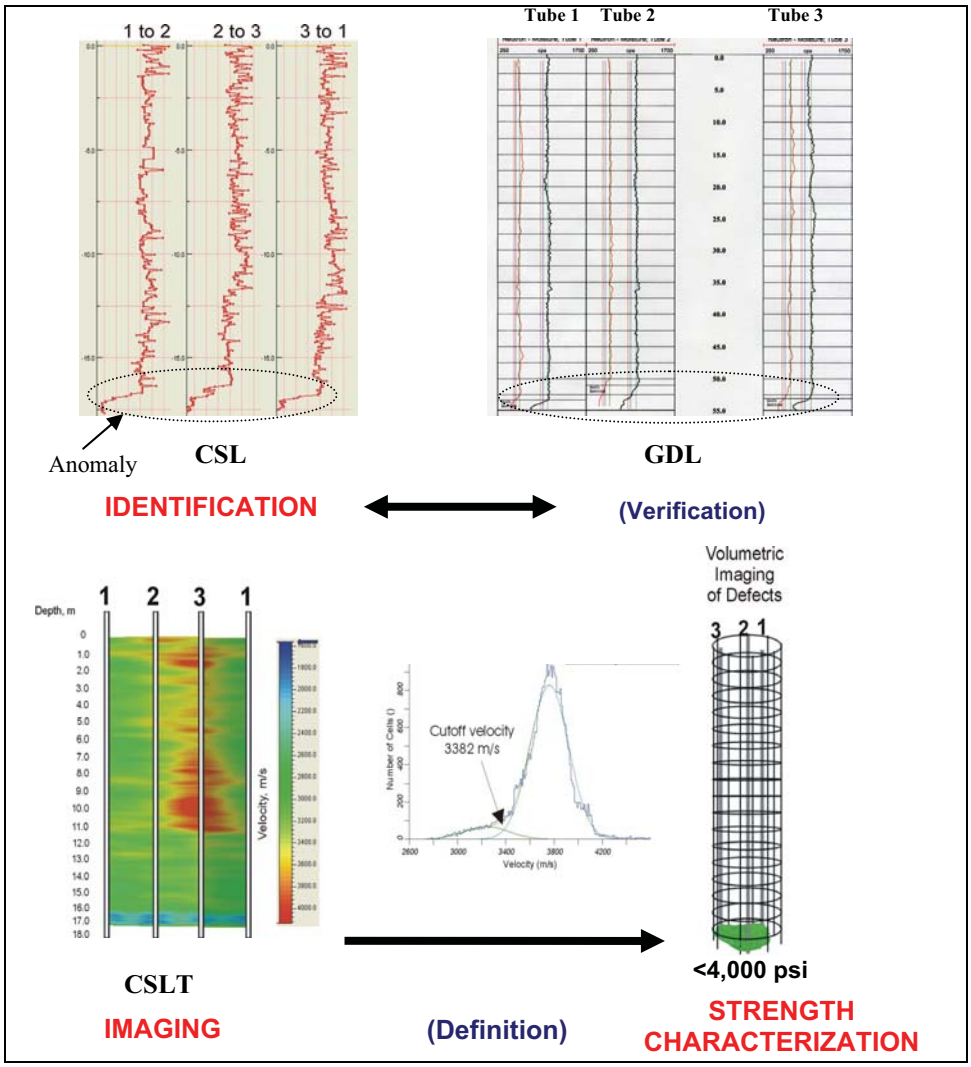

U.S. Department of Transportation
Federal Highway Administration

Federal Lands Highway
Commitment to Excellence

Central Federal Lands Highway Division
12300 West Dakota Avenue
Lakewood, CO 80228

FOREWORD

The Federal Lands Highway (FLH) of the Federal Highway Administration (FHWA) promotes development and deployment of applied research and technology applicable to solving transportation related issues on Federal Lands. The FLH provides technology delivery, innovative solutions, recommended best practices, and related information and knowledge sharing to Federal agencies, Tribal governments, and other offices within the FHWA.

Specifically, this report addresses what constitutes a defect in a newly constructed drilled shaft foundation and how to relate observed defects in a geophysical velocity tomogram to engineering strength information for integrity assessment. This study, therefore, closes the present decision making gap by the foundation engineer in deciding to accept, correct (remediate), or reject a given drilled shaft or a wall structure.

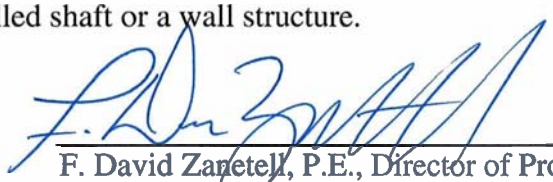

F. David Zanetell, P.E., Director of Project Delivery
Federal Highway Administration
Central Federal Lands Highway Division

Notice

Quality Assurance Statement

The Federal Highway Administration (FHWA) provides high-quality information to serve Government, industry, and the public in a manner that promotes public understanding. Standards and policies are used to ensure and maximize the quality, objectivity, utility, and integrity of its information. FHWA periodically reviews quality issues and adjusts its programs and processes to ensure continuous quality improvement.

Technical Report Documentation Page

1. Report No.	2. Government Accession No	3. Recipient's Catalog No
FHWA-CFL/TD-05-003		

4. Title and Subtitle	5. Report Date
Defects in Drilled Shaft Foundations: Identification, Imaging, and Characterization	March 2005
	6. Performing Organization Code

7. Authors	8. Performing Organization Report No.
Frank Jalinoos, MS Geophysics – Principal Investigator (PI); Natasa Mekic, MS Geophysics; Robert E. Grimm, Ph.D., Geophysics; Kanaan Hanna, MS, Mining Engineering	3755FHA

9. Performing Organization Name and Address	10. Work Unit No.
Blackhawk, a division of ZAPATA ENGINEERING 301 Commercial Road, Suite B Golden, Colorado 80401	11. Contract or Grant No. DTFH68-03-P-00116

12. Sponsoring Agency Name and Address	13. Type of Report and Period Covered
Federal Highway Administration Central Federal Lands Highway Division 12300 West Dakota Avenue Lakewood, Colorado 80228	Final Report, May 2003-March 2005
	14. Sponsoring Agency Code HFTS-16.4

15. Supplementary Notes

COTR: Khamis Haramy, FHWA-CFLHD. Advisory Panel: Scott Anderson, FHWA-FLH and Roger Surdahl FHWA-CFLHD. This project was funded under the Federal Lands Highway Technology Deployment Initiatives and Partnership Program (TDIPP.)

16. Abstract

This report addresses two key issues needed by the foundation engineer to assess the structural integrity of drilled shaft, or other concrete structures that contain access tubes; specifically:

a) What constitutes a defect in a drilled shaft?; and,
b) How to relate observed defect in a velocity tomogram to engineering strength information?

This study was conducted based on the development of a three-step approach:

1) *Anomaly Identification and Independent Verification* - This step allows the engineer to identify and independently verify suspected **"anomalies"** in drilled shafts. It is concluded that both crosshole sonic logging (CSL) and gamma-gamma density logging (GDL) must be used. For velocity imaging of the shaft's interior, three-dimensional crosshole sonic logging tomography (CSLT) is required.

2) Defect Definition – A statistical approach is presented to define a cut-off velocity to separate CSLT velocity distribution of sound concrete from the velocity distribution of anomalous concrete. The cut-off velocity is then used to volumetrically image a **"defect"** volume.

3) Defect Characterization – Finally, changes in velocity values in the defect volume is correlated to changes in concrete strength and a 3-D strength image is developed for integrity assessment by the engineer. The velocity-strength correlation is developed in the laboratory using cylinders with the same design mix as the shaft and allowing for maturity.

Therefore, this study proposes a complete analysis and technical information to assist the foundation engineer and owner agencies in deciding to accept, remediate, or reject a given shaft or a wall structure.

17. Key Words	18. Distribution Statement
Concrete Strength, Crosshole Sonic Logging (CSL), Defects, Drilled Shaft Foundations, Engineering Properties of Concrete, Integrity Testing, Gamma-Gamma Density Logging, Maturity, Nondestructive Testing (NDT), Temperature Monitoring, Tomography	No restriction. This document is available to the public from the sponsoring agency at the website http://www.cflhd.gov.

19. Security Classification (of this report)	19. Security Classification (of this page)	20. No. of Pages	21. Price
Unclassified	Unclassified	138	

Form DOT F 1700.7 (8-72) Reproduction of completed page authorized

SI* (MODERN METRIC) CONVERSION FACTORS

APPROXIMATE CONVERSIONS TO SI UNITS

Symbol	When You Know	Multiply By	To Find	Symbol
		LENGTH		
in	inches	25.4	millimeters	mm
ft	feet	0.305	meters	m
yd	yards	0.914	meters	m
mi	miles	1.61	kilometers	km
		AREA		
in^2	square inches	645.2	square millimeters	mm^2
ft^2	square feet	0.093	square meters	m^2
yd^2	square yard	0.836	square meters	m^2
ac	acres	0.405	hectares	ha
mi^2	square miles	2.59	square kilometers	km^2
		VOLUME		
fl oz	fluid ounces	29.57	milliliters	mL
gal	gallons	3.785	liters	L
ft^3	cubic feet	0.028	cubic meters	m^3
yd^3	cubic yards	0.765	cubic meters	m^3
		NOTE: volumes greater than 1000 L shall be shown in m^3		
		MASS		
oz	ounces	28.35	grams	g
lb	pounds	0.454	kilograms	kg
T	short tons (2000 lb)	0.907	megagrams (or "metric ton")	Mg (or "t")
		TEMPERATURE (exact degrees)		
°F	Fahrenheit	5 (F-32)/9 or (F-32)/1.8	Celsius	°C
		ILLUMINATION		
fc	foot-candles	10.76	lux	lx
fl	foot-Lamberts	3.426	$candela/m^2$	cd/m^2
		FORCE and PRESSURE or STRESS		
lbf	poundforce	4.45	newtons	N
lbf/in^2	poundforce per square inch	6.89	kilopascals	kPa

APPROXIMATE CONVERSIONS FROM SI UNITS

Symbol	When You Know	Multiply By	To Find	Symbol
		LENGTH		
mm	millimeters	0.039	inches	in
m	meters	3.28	feet	ft
m	meters	1.09	yards	yd
km	kilometers	0.621	miles	mi
		AREA		
mm^2	square millimeters	0.0016	square inches	in^2
m^2	square meters	10.764	square feet	ft^2
m^2	square meters	1.195	square yards	yd^2
ha	hectares	2.47	acres	ac
km^2	square kilometers	0.386	square miles	mi^2
		VOLUME		
mL	milliliters	0.034	fluid ounces	fl oz
L	liters	0.264	gallons	gal
m^3	cubic meters	35.314	cubic feet	ft^3
m^3	cubic meters	1.307	cubic yards	yd^3
		MASS		
g	grams	0.035	ounces	oz
kg	kilograms	2.202	pounds	lb
Mg (or "t")	megagrams (or "metric ton")	1.103	short tons (2000 lb)	T
		TEMPERATURE (exact degrees)		
°C	Celsius	1.8C+32	Fahrenheit	°F
		ILLUMINATION		
lx	lux	0.0929	foot-candles	fc
cd/m^2	$candela/m^2$	0.2919	foot-Lamberts	fl
		FORCE and PRESSURE or STRESS		
N	newtons	0.225	poundforce	lbf
kPa	kilopascals	0.145	poundforce per square inch	lbf/in^2

*SI is the symbol for the International System of Units. Appropriate rounding should be made to comply with Section 4 of ASTM E380. (Revised March 2003)

ACKNOWLEDGEMENTS

The authors would like to express their sincere appreciation to Mr. Khamis Y. Haramy, COTR of the Federal Highway Administration (FHWA), Central Federal Lands Highway Division (CFLHD) for his guidance, valuable technical assistance, and review during the course of this investigation. The authors would also like to thank Dr. Scott Anderson and Mr. Roger Surdahl of the FHWA-CFLHD for their technical support and review of this report.

TABLE OF CONTENTS

LIST OF FIGURES

LIST OF TABLES

EXECUTIVE SUMMARY

This study was conducted under the Federal Highway Administration (FHWA), Central Federal Lands Highway Division (CFLHD) contract number DTFH68-03-P-00116. The current practice in assessing the integrity of newly constructed drilled shaft foundations, or other concrete structures that contain access tubes, is through the use of nondestructive testing (NDT) methods. Most common NDT methods include crosshole sonic logging (CSL), gamma-gamma density logging (GDL), and crosshole sonic logging tomography (CSLT). Numerous studies and field investigations have been performed to evaluate the accuracy and effectiveness of these NDT methods in detecting defects in drilled shafts. However, most of these studies have fallen short to correctly identify and characterize defects for engineering decision making. Or, as stated by Jerry DiMaggio (2004), FHWA Principal Geotechnical Engineer, *"when using (NDT) methods, the key questions that often must be answered are:* (1*) Is the test result a false negative?* (2) *What are the next steps and who is responsible for incurred cost if a defect is suspected? and most importantly* (3) *Is the discontinuity a defect?"*

The purpose of this study was to address two key issues needed by the foundation engineer to assess the structural integrity of drilled shaft, more specifically:

- What constitutes a defect in a drilled shaft? and,
- How to relate observed defect in a velocity tomogram to engineering strength information?

The overall objectives of this study were:

- Review and evaluate the current state-of-practice of NDT methods;
- Use a statistical analysis to define a "defect" in a CSLT image;
- Monitor and model changes in concrete temperature (velocity, density, and moisture) in a drilled shaft after concrete placement;
- Establish empirical relationships that correlate changes in a CSLT velocity image to changes in concrete strength.

To address the above issues and objectives, the study was conducted based on the development of a three-step approach that allows the foundation engineer to evaluate and characterize a defect and assess its effects on the overall integrity of the drilled shaft foundation. The following presents the most significant results:

Step 1. Anomaly Identification and Independent Verification – This step allows the engineer to identify and independently verify suspected "anomalies" in a drilled shaft foundation inside and outside the rebar cage. It is concluded that both CSL and GDL must be used for this initial evaluation.

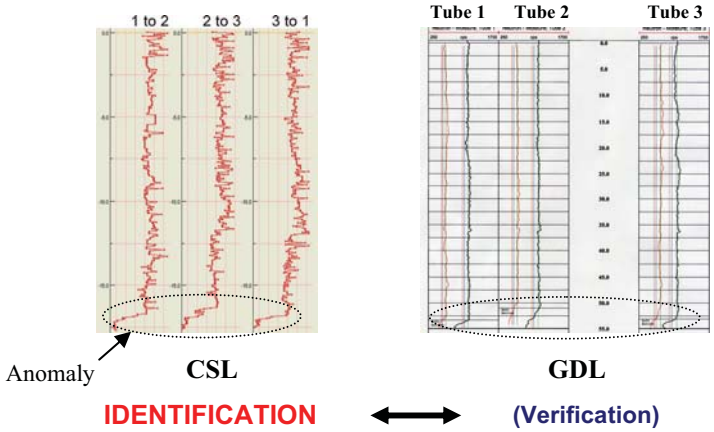

Once an anomaly is identified, three-dimensional CSLT is required for velocity imaging of the anomalous zones. This task is best achieved by using true 3-D tomographic inversion software. The 3-D imaging also requires a velocity equalization to be performed prior to tomographic imaging.

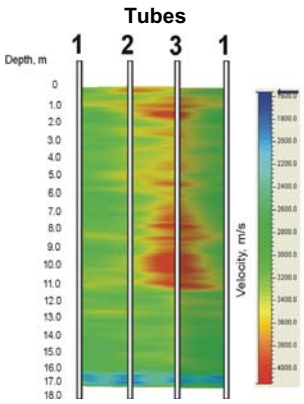

CSLT
IMAGING

Step 2. Defect Definition – In this step, a statistical approach is used to separate CSLT velocity distribution of sound concrete from the velocity distribution of anomalous concrete. With this analysis, a key cut-off velocity is determined that separates this two velocity distributions. As a result, a **"defect"** volume is defined as having a velocity lower than the cut-off velocity.

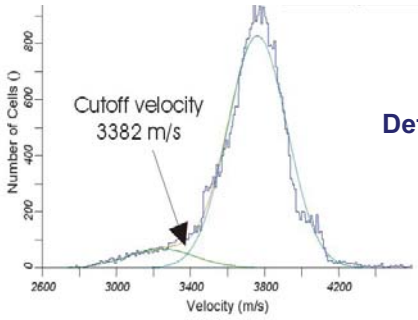

Defect Definition

Step 3. Defect Characterization – The third step relates changes in velocity values in the defect volume to changes in concrete strength. Using the cut-off velocity, a 3-D strength image is developed to characterize the defect. The velocity-strength correlation is developed in the laboratory using cylinders with the same design mix as the shaft and allowing for maturity. The strength image can now be inputted to the shaft design analysis program to evaluate the effect of the defect on the overall performance of the designed structure. This allows the engineer to decide whether the defective shaft is still serviceable, repairable by remediation, or unacceptable.

<4,000 psi
STRENGTH
CHARACTERIZATION

Therefore, this study has evolved onto the development of a basic guideline or "roadmap" that leads the engineer from the initial detected anomalies to the integrity assessment of the drilled shaft foundations. The outcome of this study has provided the foundation engineer and owner agencies with an improved tool in deciding to accept, remediate, or reject a given shaft or a wall structure.

REPORT ORGANIZATION

Chapter One contains a brief discussion of various nondestructive techniques along with advantages and their disadvantages.

Chapter Two describes in detail anomaly identification, independent verification, and imaging. A tomographic modeling study of shafts containing defects is presented.

Chapter Three describes the statistical analysis used for separating sound concrete velocity distribution from anomalous concrete velocity distribution. Using this analysis, a cut-off velocity is determined for volumetric imaging of a defect.

Chapter Four describes defect characterization (or, correlation of velocity to strength). Final tomographic "strength images" are developed for integrity assessment by the engineer. In order to better understand the correlation between velocity and strength, the results of a temperature modeling study is presented. In addition, data from a seven-day field monitoring of two shafts using temperature, velocity, density, and moisture logging is included. A description of the maturity method is presented.

Chapter Five presents data examples where the three-step approach (described in Chapters 2-4) is used. Data from 20 drilled shafts obtained from three (3) different projects are presented.

Chapter Six provides a summary and conclusions of the study.

In order to aid in defining some of the terms used in this report, a glossary of terms is provided.

In Appendix A, seven (7) case histories are presented where dual crosshole sonic logging (CSL) and gamma-gamma density logging (GDL) methods were used for correct identification and independent verification of anomalies in drilled shaft foundations.

Units. All units are expressed in both metric and English. However, when a reference is made to a figure or table which has only metric units, accordingly the units in the text are expressed in metric only.

CHAPTER 1 – INTRODUCTION

1.1 PURPOSE AND OBJECTIVES

The purpose of this study was to addresses what constitutes a defect in a newly constructed drilled shaft foundation and how to relate identified defects in a velocity tomogram to engineering strength information for integrity assessment.

The overall objectives of this study were:

- Review and evaluate the current state-of-practice of nondestructive test (NDT) methods;
- Use a statistical analysis to define a "defect" in a crosshole sonic logging tomography (CSLT) image;
- Monitor and model changes in concrete temperature (velocity, density, and moisture) in a drilled shaft after concrete placement;
- Establish empirical relationships that correlate changes in a CSLT velocity image to changes in concrete strength.

The scope of work was carried out based on a three-step approach to identify and image anomalies within a drilled shaft and to relate percentage changes in 3-D tomographic velocity image to changes in concrete strength for engineering decision making. The three steps approach included:

1. *Anomaly Identification and Independent Verification* – In this step, various NDT methods including crosshole sonic logging (CSL) and gamma-gamma density logging (GDL) are used to identify and independently verify suspected **"anomalies"** in drilled shafts. In addition, CSLT method is used to create three-dimensional (3-D) velocity images of these anomalies.
2. *Defect Definition* – The second step addresses what constitute a velocity **"defect"** or a flaw in a 3-D CSLT velocity tomogram?[1] A statistical analysis is used to separate velocity distribution of sound concrete from velocity distribution of anomalous concrete. Based on this analysis, a cut-off velocity is established as a key parameter that separates this two velocity distributions. In this report, a defect volume is defined as having a velocity lower than the cut-off velocity.
3. *Defect Characterization* – In this step, changes in velocity values in the defect volume are correlated to changes in concrete strength and hence 3-D strength images are developed. Empirical velocity-strength correlation is established in the laboratory using cylinders with the same design mix as the shaft and allowing for maturity. This strength image will allow the engineer to perform modeling to evaluate the overall integrity of the drilled shaft foundation.

[1] In this study, "anomaly" refers to a suspected deviation from homogeneity (uniformity) in a concrete structure. No determination is yet made regarding its exact size or extent. Statistical analysis is performed to obtain a cut-off velocity that is used in defining a "defect" volume with a velocity lower than the cut-off velocity.

This three-step approach was applied on twenty (20) drilled shafts from three (3) different projects:

- Dataset from two (2) research drilled shafts with planned defects from the National Geotechnical Experimentation Site (NGES), Amherst, Massachusetts;
- Dataset from twelve (12) production shafts (shafts used in a bridge project with unplanned defects) from the Jim Camp Bridge, Arizona Project;
- Dataset from six (6) production shafts from the Sevenmile Gooseberry, Utah Project.

1.2 DRILLED SHAFT FOUNDATION - BACKGROUND

Drilled shafts are deep or shallow foundation support elements formed by creating a drilled hole into which structural steel and concrete is cast or placed. The reinforcing steel is placed in the hole prior to concrete placement. Drilled shafts are typically used as deep foundations capable of supporting high, concentrated loads: they are the foundation of choice for heavily-loaded, seismically-sensitive structures as they can carry both axial and lateral loads.

The development of drilled shafts, more or less independently, in various parts of the world led to different terminologies (O'Neil and Reese, 1999). "Drilled shaft" is the term first used in Texas, while "drilled caisson" or "drilled pier" is more common in the Midwestern United States. "Cast-in-drilled-hole (CIDH) pile" is a term used by California Department of Transportation (CalTrans), and "bored pile" is common outside of the United States. These terms all describe essentially the same type of foundation.

Drilled shafts range from diameters of 46 cm (18 in) to greater than 3.6 m (12 ft) and to depths of 50 m (164 ft). The variation of shaft diameter is dependable on excavation depth. As the depth of excavation becomes greater, the diameter normally must increase. Several factors that influence the ratio of depth to diameter are: the nature of the soil profile, the position of the groundwater table, whether or not a rebar cage is required, the design of the concrete mix, and the need to support lateral loading. Ordinarily, the aspect ratio of drilled shaft, or its length divided by its diameter, should not exceed about 30. Cylindrical holes can be drilled with diameters of up to 6 m (20 ft), to depths of up to 73 m (243 ft), and with underreams up to 10 m (33 ft) in diameter, although such sizes are unusual. A typical schematic of drilled shaft construction with the loading is presentation in Figure 1 and a typical drilled shaft operation during construction is shown in Figure 2.

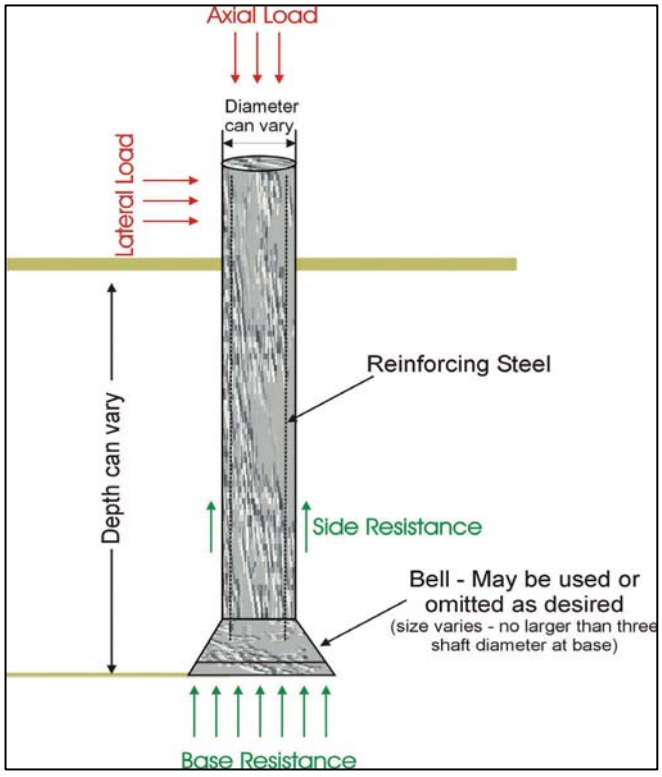

Figure 1. Schematic. Typical Drilled Shaft Foundation.

Figure 2. Photo. Drilled Shaft Construction.

Drilled shafts are designed and installed as either end bearing or friction type shafts or a combination. In the end bearing shaft, the structure loads bear on top of the solid rock in the rock socket. In the skin friction shaft, the structure loads bear on sides of the drilled shaft.

Drilled shafts are constructed straight, belled and rock-socketed using two different methods:

1. *Dry method* – construction of a shaft without excessive water interference. The dry construction method consists of drilling the shaft excavation, removing loose material from the excavation and placing the concrete in a relatively dry excavation. The rate of flow of water into the hole should not be more than 300 mm (12 inches) within a 1-hour period. No concrete is placed if there is more than 75 mm (3 inches) of water in the bottom of the hole. Casing can be used as temporary or permanent as described below:

   A. Temporary Casing Construction Method: The temporary casing construction method is used when excavations in the dry construction method, encounter water bearing or caving soil formations. A temporary casing is then placed into the impervious formation to produce a watertight seal at the bottom. During concrete placement, the casing is withdrawn.

   B. Permanent Casing Construction Method: This method consists of placing a casing to a prescribed depth before excavation begins. If, during dry drilling, caving or water

bearing soils is encountered, the hole is filled with water and the excavation is advanced by drilling. Pressure grouting is required to ensure contact (bearing) between the casing and any surrounding soil layer that is used for lateral support.

2. *Wet or slurry methods* – constructing a shaft either with ground water or under water using tremie concrete. In this type of operation, drilling slurry (typically commercial bentonite clay mixed with water) or polymer slurry is used to stabilize the excavation or when ground water is encountered in the excavation that cannot be dewatered.

1.3 CURRENT NDT METHODS USED FOR DETERMINING THE INTEGRITY OF DRILLED SHAFT FOUNDATIONS

Nondestructive test (NDT) methods are used for quality assurance (QA) integrity testing of drilled shaft foundations, or other concrete structures, such as diaphragm slurry walls, auger-cast in place (ACIP) piles, shear pin wall, and dams. NDT methods are often called "small strain test" tests because a small seismic energy source, such as a hammer, is used to generate the seismic waves. These methods are used to identify and image flaws or "defects". Common structural defects include shaft necking and bulbing, "soft bottom" condition, voids, poor quality concrete, delamination, and honey-combing.

These tests can be divided into two groups: Surface NDT method, if access is required only at the surface of a foundation, and in-hole NDT methods, if access tubes are installed to the inside of the reinforcing rebar cage prior to the concrete placement as shown in Figure 3. In the following section, three in-hole NDT methods are discussed. Surface NDT methods, such as sonic echo (SE)/ impulse response (IR) or ultraseismic test (UST) methods, are not covered in this report.

Figure 3. Photo. Rebar Cage and CSL Tubes of Completed Drilled Shaft.

1.3.1 Crosshole Sonic Logging (CSL) Method

In the standard CSL method (Figure 4), ultrasonic transmitter/receiver probes are initially lowered to the bottom of a pair of access tubes. The two probes are then pulled simultaneously as to maintain near horizontal ray paths between them (*zero-offset logging*). The system is calibrated to measure the sonic wavefield at 5 cm (2.4 in) depth intervals throughout the length of the shaft. This test is repeated for all test paths along the outer perimeter as well as across the inner diagonal of the shaft. Good concrete condition will result in a near continuous vertical alignment of the waterfall-displayed data (and travel time picks). Longer travel times and lower signal amplitudes characterize anomalous zones, defined as defects, due to soil intrusions, voids, or poor quality concrete.

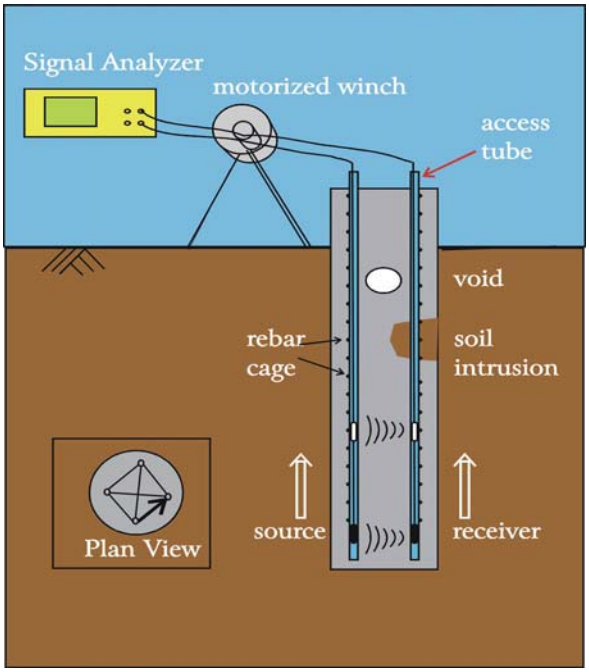

Figure 4. Schematic. Crosshole Sonic Logging (CSL) Field Setup.

1.3.1.1 Standard CSL Data Presentation Format

Figure 5 presents standard CSL logs (in waterfall 1-D display format) acquired between six (6) test panels on a test wall (with engineered defects) compared side by side. The wall geometry and defect locations are indicated on the top right hand side. In each CSL data plot, a full-waveform gray-scale vertical stack of the data traces is displayed as a function of depth in the right hand track. In the left hand track, the picked travel *time* arrivals (thin line) and signal amplitude (thick line) are also displayed. Depths, is shown on the vertical axis.

In Figure 6, the new format for the display of the CSL data on a single plot is shown. In this figure, the CSL results from a drilled shaft containing 5 tubes are plotted in 5 separate sub-plots from 5 different access-tube pair combinations, as indicated on the top label. Each individual sub-plot displays the velocity in black color and signal root mean squared (RMS) amplitude levels in magenta color. Also, in each separate sub-plot, the average velocity as well as 10%

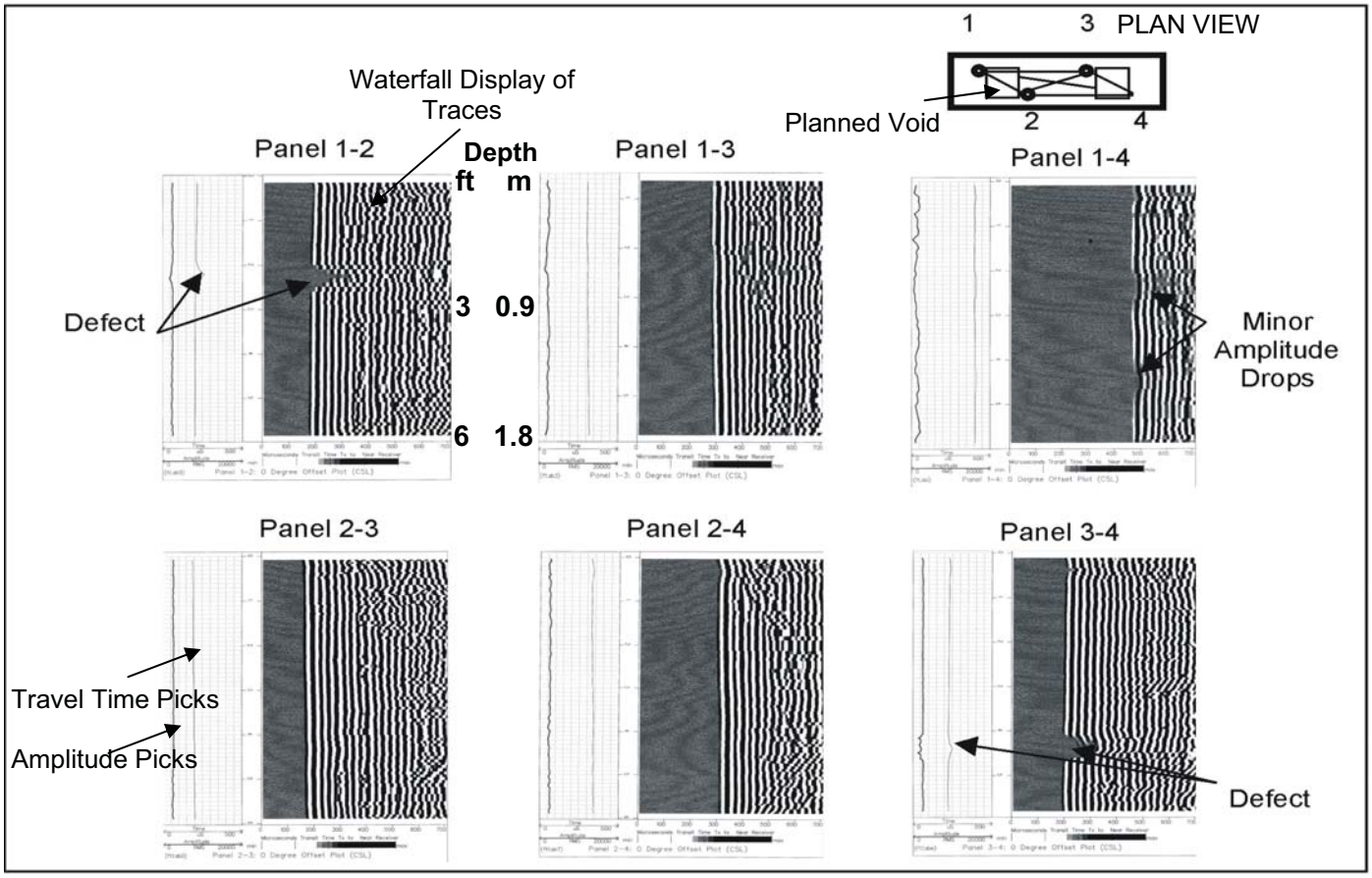

Figure 5. Graph. Zero-Offset CSL Dataset from a Test Wall with Engineered Defects. Data from All CSL Test Paths are Indicated.

drop in average velocity (questionable concrete) and 20% drop in average velocity (poor concrete) are displayed as vertical green, blue and red lines, respectively.

1.3.1.2 Defect Definition

Using standard CSL testing, "questionable" concrete condition is defined as a zone with a decrease (from median) in sonic velocity between 10% and 20% (or about 40%-65% of old strength); and, "poor" concrete condition is defined as a zone with greater than 20% decrease in sonic velocity (or about less than 40% of old strength)[2]. For details on the empirical relationship between sonic velocity and concrete strength, please refer to Sections 4.1.

[2] Example Specification: U.S. Federal Highway Administration (FHWA) Section 565 (1996) Specification for drilled shafts (construction requirement: integrity testing). Note that the correlation between velocity and concrete strength is from empirical relationships.

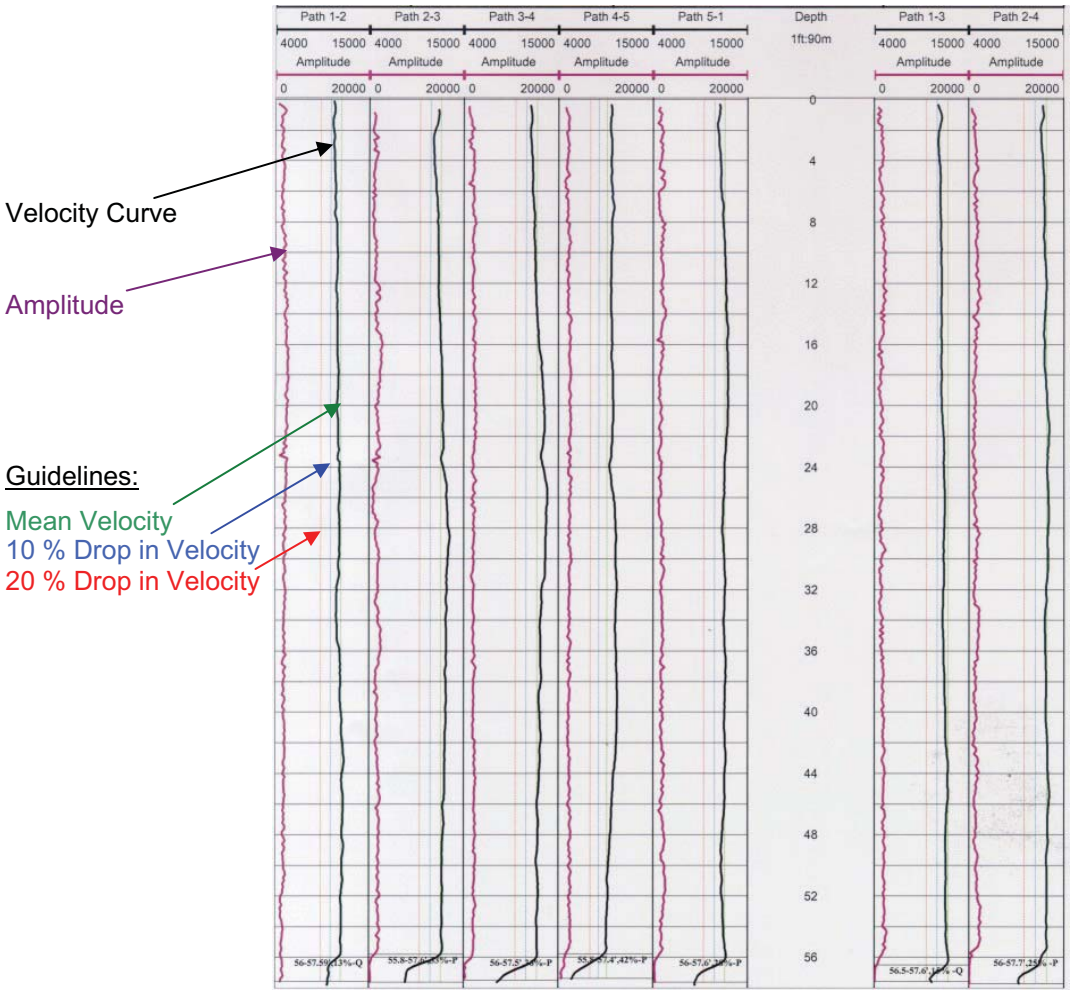

Figure 6. Graph. Single Plot Display Format for the CSL Data from a Drilled Shaft Foundation. Green Vertical Guideline Indicate Average Velocity and Blue and Red Vertical Guidelines Denote 10% Drop and 20% Drop in Velocity, Respectively.

1.3.1.3 Advantages of CSL

- Accurate characterization of soil intrusions or other anomalies throughout the shaft inside the rebar cage (between the tubes).
- Several defects at different depths can be detected by this method with high precision.
- It can be used to identify un-cured concrete especially in chemically retarded mixes.
- No special handling is required for the use of radioactive sources.

1.3.1.4 Limitations of CSL

- Tube debonding condition can occur with PVC access tubes especially above the groundwater table (where the temperatures are higher). No signal is obtained in the debonded zone.
- Only defects along the path of the sonic wave will be detected; it cannot detect anomalies outside the rebar cage.

- It cannot be used to detect shaft bulbing (increase in diameter).

1.3.2 Crosshole Sonic Logging Tomography (CSLT) Method - Offset Tomography

CSL data can be collected by initially offsetting either the source or the receiver and then pulling the two probes together as to maintain a constant non-zero angle between them (*Offset Logging*). In the CSLT method (Figures 7 and 8), data is collected by running a zero-offset log in combination with several positive offset (receiver is shallower) and negative offset (source is shallower) logs. This procedure is repeated for all possible access tube combinations to form a three-dimensional tomography dataset.

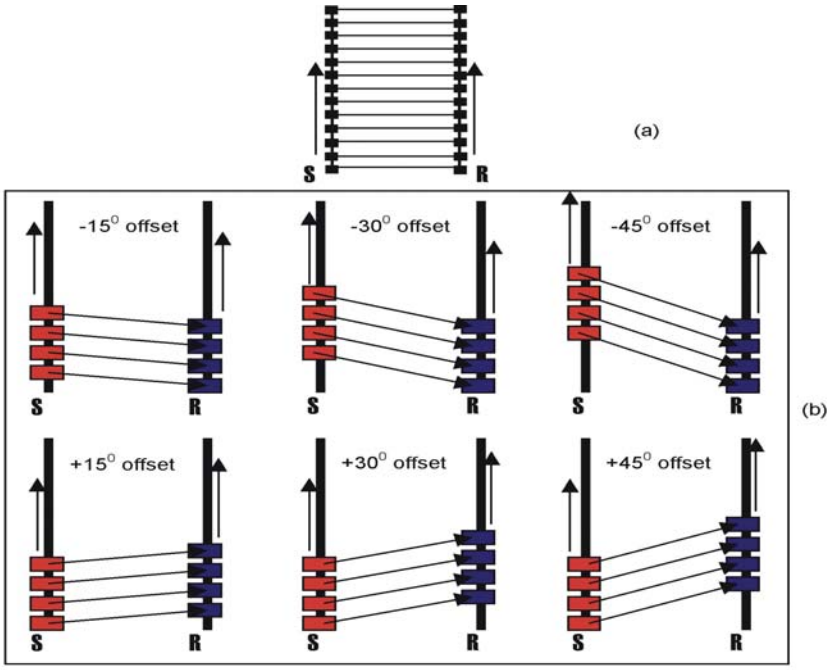

Figure 7. Schematic. Zero-Offset Vs Multi-Offset Tomographic Data Collection.

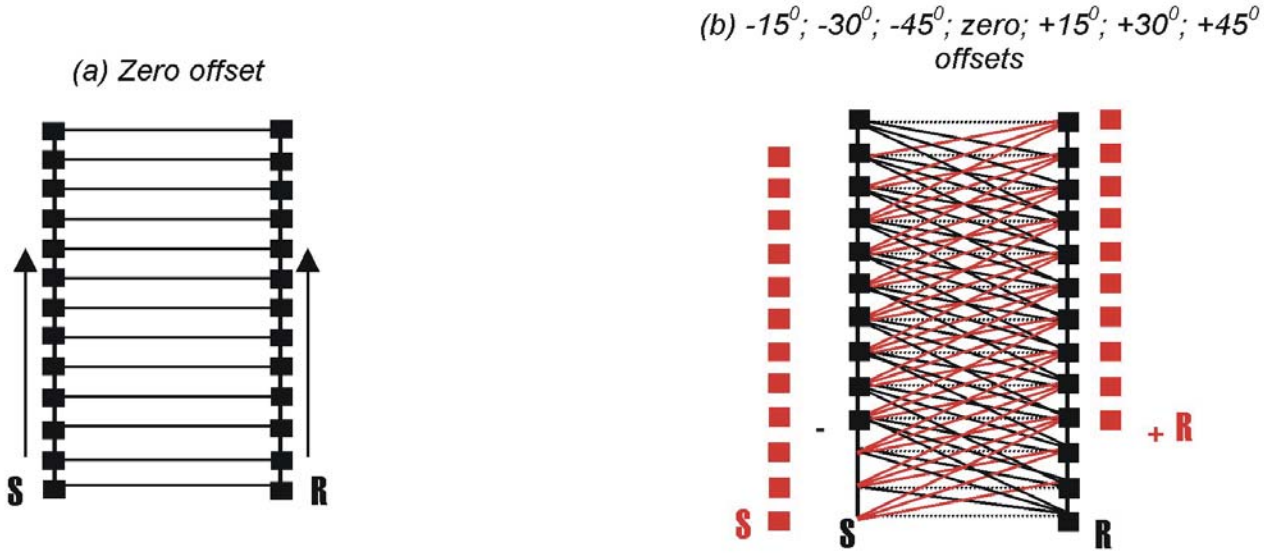

Figure 8. Schematic. Ray-Density with Zero-Offset Data Collection b) Tomographic Data Collection (Zero Plus Three Positive and Three Negative offsets).

1.3.2.1 CSLT Data Presentation Format

Typical three-dimensional tomography (CSLT) data presentation format is shown in Figure 9. In this figure, a soft bottom condition is indicated which extends to the interior of the shaft. 3-D images defined poor quality concrete zones shown in green and blue colors.

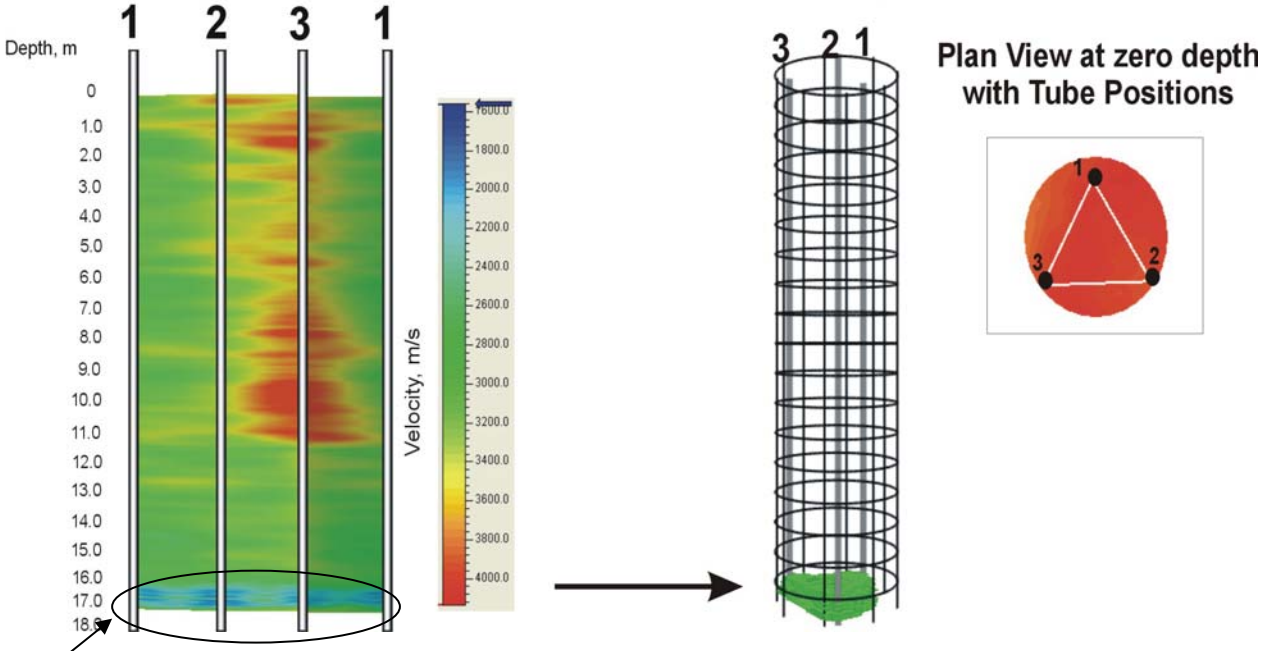

Figure 9. Schematic. Crosshole Sonic Logging Tomography (CSLT) Data Display Format.

1.3.2.2 Advantages of CSLT

- Provides for two-dimensional area or three-dimensional volumetric *imaging* of defect zones for immediate engineering remediation.
- Can identify small horizontally elongated defects, such as cold joints, missed by the standard CSL technique.
- Attenuation tomography can be used for possibly identifying soil intrusions that end at the rebar cage or the fracture zones.
- Can be used in before and after surveys for monitoring the effectiveness of remediation.

1.3.2.3 Limitations of CSLT

- Data-intensive for non-automated field systems.
- Specialized analyses software is required for true three-dimensional imaging.
- Due to limited ray coverage, artifacts[3] can be present due to edge effects.
-

1.3.3 Gamma-Gamma Density Logging (GDL)

In the 4-pi Gamma-Gamma Density Logging (GDL) test method (Figure 10), a weak Cesium-137 source is used to emit gamma rays into the surrounding material. A small fraction of the gamma ray photons are reflected back to the probe (due to Compton scattering) and their intensity are recorded by a NaI scintillation crystal as counts per second (cps). The measured count rate (cps) depends on the electron density of the surrounding medium, which is proportional to the mass per unit volume. The tool is calibrated by placing the probe in an environment of known density in order to convert the measured count rate (cps) into the units of density in g/cm^3 (lb/ft^3).

[3] Artifacts are erroneous velocity values produced by the tomographic matrix inversion process due to inadequate scanning (or aperture) of the test volume; inaccuracies in travel time picking; and non-linear and non-unique inversion of the travel time data. These artifacts mostly occur near the image boundaries.

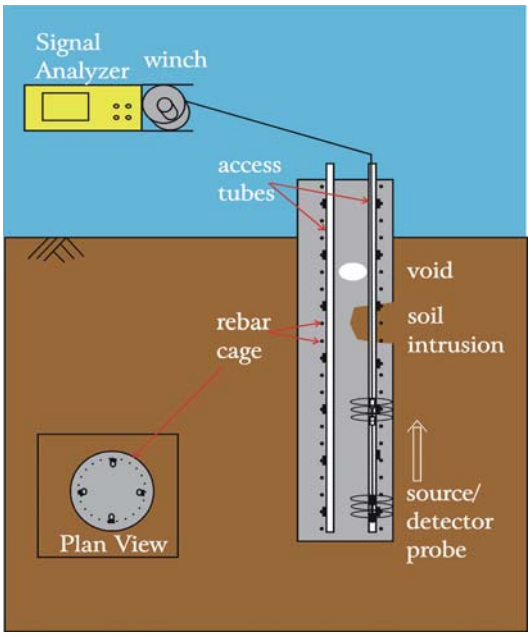

Figure 10. Schematic. Gamma-Gamma Density Logging (GDL) Field Setup.

In the GDL test, the radius of investigation is largely governed by 1/2 of the source-detector spacing. An optimal spacing is selected (generally about 35.6 cm (14 inch)) and the GDL test is performed from all tubes in order to obtain uniform coverage around the perimeter of the shaft. Good concrete condition will result in a near continuous alignment of the data. Anomalous zones—due to soil intrusions, poor concrete, or voids—are characterized by large low density (high count rate) deflection in the data.

1.3.3.1 Typical Data Presentation Format

In a typical GDL log (Figure 11), the measured gamma ray intensity count rate (cps) is presented in the units of g/cm^3 (lb/ft^3). In Figure 11, the GDL results are plotted in 4 separate sub-plots from the tested access tubes. Each individual sub-plot depicts the GDL results from 35.6 cm (14 inch) source-detector separation (corresponding to about 13-15 cm (5-6 inch) radius of investigation) presented in a magnified density scale of 2.1-2.9 g/cm^3 (130-180 lb/ft^3). Also, in each sub-plot, the mean as well as the -2 and the -3 standard deviation from mean curves are displayed as vertical guidelines. Depths, in meter (feet), are measured from the top of the shaft and are shown on the vertical axis.

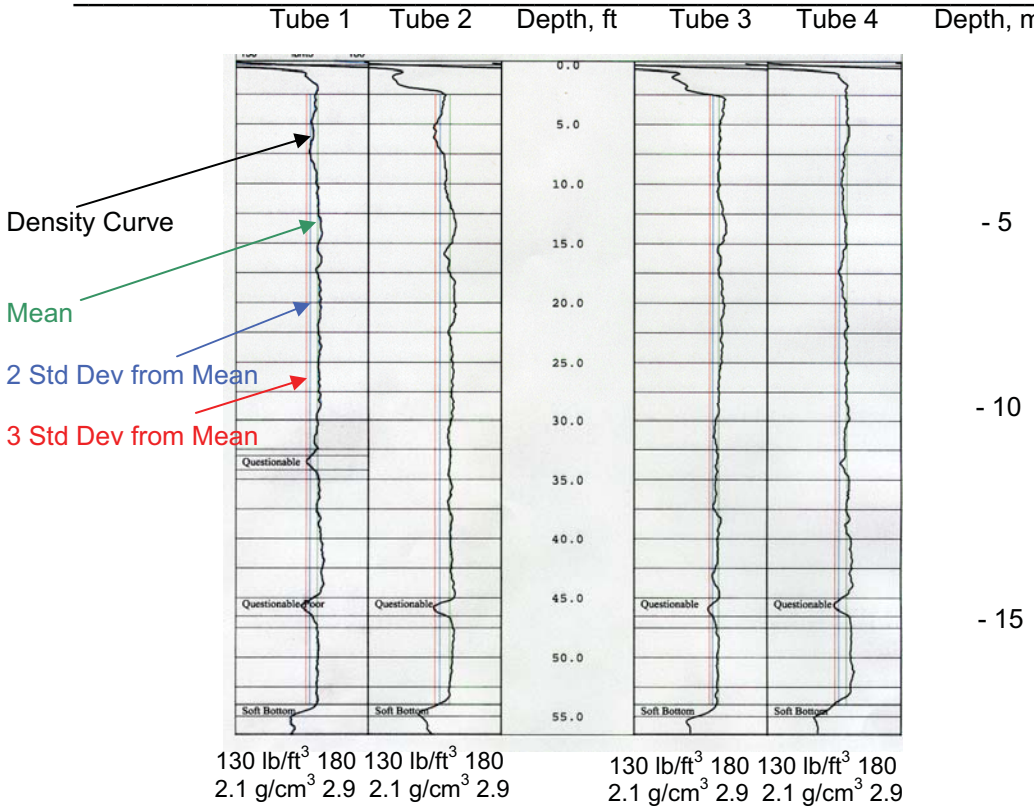

Figure 11. Graph. Gamma-Gamma Density Logging (GDL) Data Display Format.

1.3.3.2 Defect Definition

In the GDL testing, "questionable" concrete condition is defined as a zone with reduction in density between 2-3 standard deviations from mean and "poor" concrete condition is defined as a zone with reduction in density of greater than 3 standard deviations from mean.

1.3.3.3 Advantages of GDL

- Detects anomalies within a 13-15 cm (5-6 inch) radius around the inspection tubes both inside and *outside* of the rebar cage.
- Several defects at different depths can be detected by this method with high precision.
- Can be used for testing in fresh concrete while restoration is still feasible as the density of concrete changes minimally as it sets.
- Minimally is affected by the tube debonding condition.

1.3.3.4 Limitations of GDL

- Only measures concrete integrity along the outer perimeter of the shaft at about 13-15 cm (5-6 inch) radius from each tube (average tube-to-tube separation along the perimeter is about 76 cm (30 inches)). Therefore, no data is recorded along some portions of the perimeter and from the entire interior portion of the shaft.
- It cannot be used to identify young (heavily retarded) un-cured concrete.
- Special handling is required for the use of radioactive sources.

1.3.4 Other Specialized Logging Applications

Other geophysical logging probes can be used in this application to assess the condition of in-placed concrete. Currently, these single-hole logs are not in routine use by the industry, and include: 1) temperature logging for evaluating concrete curing condition; 2) neutron logging for measuring moisture content; 3) natural-gamma logging for assessing clay content; 4) optical and acoustic televiewer for visual inspection of defects through cored holes (or clear or PVC tubes); and 5) electrical and ground penetrating radar (GPR) logging for examining the condition and positioning of rebar within the cage.

In the next section, a brief description of neutron-moisture logging (NML) and temperature logging is presented. These two methods are used in this report. NML logs are used for verification of anomalies observed by CSL and GDL logs. Temperature logs are used for monitoring concrete curing rates in two (2) drilled shafts. Because of their limited use in this application, only brief method descriptions and advantages of these single-hole logging methods are provided.

1.3.4.1 Neutron Moisture Logging (NML)

In the neutron-moisture logging (NML) test method, an americium-beryllium neutron source in sizes of 1 to 5 Curies source is used to emit high energy neutrons into the surrounding material. Helium-3 detectors are typically used in recording the interactions that occur in the vicinity of the access tubes. Two different neutron-logging techniques can be used: 1)- geophysical neutron probes with a large source size (>1 Curie) and long spacing (>30 cm (11.8 in)) with radius of investigation of about 15-18 cm (6-7 inches) (as used in this report); and, 2)- engineering probes with a small source size (<100 millicuries) and short spacing (<30 cm (11.8 in)) with radius of investigation of 2.5-5 cm (1-2 inches). Three general types of neutron-porosity logs exist: neutron-epithermal neutron, neutron-thermal neutron (as used in this report), and neutron-gamma. Cadmium foil may be used to shield Helium-3 detector from thermal neutrons. Neutron-epithermal neutron logs are least affected by the chemical composition of surrounded material.

Fast neutrons, emitted by a source, undergo three basic types of reactions with matter adjacent to the access tubes (concrete, steel, and possibly moisture and soil) as they lose energy and ultimately are captured. These physical interactions include inelastic scatter, elastic scatter, and absorption or capture. In elastic scatter, the mass of the scattering element controls the loss of energy by the neutron. Light elements (mostly hydrogen element in water) are most effective in moderating, or slowing neutrons, whereas heavy elements have little effect on neutron velocity or energy. The moderating and capture processes result in the number of epithermal and thermal neutrons and capture gamma photons being inversely related to the hydrogen content of concrete, at source-to-detector spacing greater than approximately 30 cm (11.8 in). If detectors are located closer than 30 cm from the source, as in engineering moisture probes, the number of moderated and captured neutrons increases with increasing hydrogen content.

Typical NML logs are presented in a similar format as GDL logs with measured neutron counts per second (cps) displayed along with the mean and the -2 and the -3 standard deviation from

mean vertical guidelines. High moisture zones are indicated by low count rates deflection in the data.

Benefits of NML. NML can used to investigate the presence of excessive moisture in a defect zone; especially, when such moisture is in contact with the rebar cage (vulnerability to corrosion).

1.3.4.2 Temperature Logging

Temperature probes employ a glass-bead thermistor along with a solid-state IC device. Most thermistor probes have an accuracy, repeatability, and sensitivity on the order of 0.02°C. They also are very stable over long periods of time, but they have the disadvantage of a nonlinear temperature response.

The standard temperature log records temperature as a function of depth. The sensor in a temperature probe only responds to the fluid in its immediate vicinity reflecting the thermal gradient in concrete.

Calibration of temperature probes needs to be carried out in a constant temperature bath, using highly accurate mercury thermometers. The bath and probe need to reach equilibrium before a calibration value is established. Onsite standardization cannot be carried out with great accuracy because no portable substitute exists for a constant-temperature bath. The only temperature that can be achieved and maintained for sufficient time to permit a valid calibration is 0°C in an ice bath.

Movement of a logging probe disturbs the thermal profile in the fluid column; therefore, the most accurate temperature log is made before any other log, and it is recorded while moving slowly down the hole.

Benefits of Temperature Logging. 1) Temperature logging can be used to evaluate the negative effects of the cracking resulting from uncontrolled mass concrete placement. Care must be taken for the maximum temperature reached in the shaft not to exceed the specified maximum allowable temperature (typically, 57°C (135°F)). Also, with the use of thermocouples, readings can be taken to insure the differential temperature from the center of the shaft to the outside edge of the shaft not to exceed the tolerance specified in the standard provisions (typically, 19°C (35°F)). 2) Temperature logging, as described in this report, can also be used during the first 7 days after concrete placement to identify shaft bulbing.

CHAPTER 2 – ANOMALY IDENTIFICATION AND INDEPENDENT VERIFICATION

In this chapter, application of geophysical logging methods is evaluated to correctly identify and independently verify anomalies in a drilled shaft foundation. "Correct identification and verification" also includes elimination of false positives or false negatives as is discussed in Section 2.1. Once anomalies are correctly identified, 3-D tomographic imaging (CSLT) is used to image the anomalous zones inside the rebar cage of the shaft, as discussed in Section 2.2.

2.1 DUAL CSL/GDL TESTING

In the U.S., typically integrity testing is performed using either of crosshole sonic logging (CSL) or gamma-gamma density logging (GDL) methods; but rarely both. GDL is the method of choice by the California Department of Transportation (CalTrans) and, on some projects, by the Arizona Department of Transportation (ADOT). Other states mostly require CSL for integrity testing and, only on rare occasions, utilize GDL for anomaly verification.

This single test method approach is, however, seriously flawed for correct identification of anomalies. Occasionally, false positive or false negatives can result in incorrect interpretation of the data by the testing agencies. Example of false positives include observation of "anomalies" that are related to access tube placement (resulting in poor bonding of tubes with concrete) as reported by the CSL method or by the observation of density anomalies due to changes in rebar cage design (lower bar density) or the probe's incorrect readings at high temperatures as reported by the GDL method. Example of false negative includes non-detection of anomalies located outside the rebar cage by the CSL method or non-detection of anomalies located in the interior portion of the shaft or un-cured (green) young concrete by the GDL.

Due to the importance of this topic, six (6) case histories are presented separately in Appendix A where dual CSL/GDL testing was performed. Dual testing is proven to be critical for correct interpretation of anomalies both inside and outside the rebar cage. In addition, dual testing provides with independent verification of those anomalies observed by both methods. Therefore, dual testing is essential not only in elimination of false positives or false negatives in the data; but more importantly, eliminating construction theories as to what may have gone wrong.

2.2 VOLUMETRIC IMAGING OF ANOMALIES – CSLT

In the previous section and Appendix A, the importance of dual crosshole sonic logging (CSL) and gamma-gamma density logging (GDL) for accurate identification and verification of anomalies is discussed. Once an anomaly is identified, volumetric imaging is required which is commonly performed using crosshole sonic logging tomography (CSLT) method.

A brief theory of CSLT method is presented next.

2.2.1 Tomography Theory

The use of tomographic analysis for imaging subsurface materials between boreholes (or defect in concrete between access tubes) is now a well established technique in geophysics. In this

report, application of "travel time" tomography is discussed. This method uses time of flight (first arrival travel times and amplitudes) to derive velocity or attenuation images.

2.2.1.1 Travel Time Tomography

Travel time tomography (Dines and Lytle, 1979) involves imaging the seismic properties from the observation of the transmitted compressional or shear first arrival energy. The relationship between the velocity field v (x,y), travel time t_i, and distance ds is given by the line integral (for a ray i):

$$t_i = \int_{R_i} \frac{ds}{v(x,y)} \qquad (1)$$

where R_i denotes the curve connecting a source receiver pair which yields the least possible travel time according to Fermat's principle. Tomography is an attempt to match calculated travel times (model responses) to the observed data by inversion of these line integrals. Initially, the region of interest is divided into a rectangular grid of constant velocity cells (j) and a discrete approximation of the line integral is assumed as:

$$t_i = \sum_j \Delta S_{ij} \cdot n_j \qquad (2)$$

where ΔS_{ij} is the distance traveled by ray i in cell j, and n_j slowness within cell j. Using a first order Taylor expansion and neglecting residual error, Equation (2) can be written in matrix form as:

$$\underline{y} = \mathbf{A}\,\underline{x} \qquad (3)$$

where the vector $\underline{y}$ is defined as the difference between computed travel times (from the model) and the observed travel times, vector $\underline{x}$ as the difference between the true and the modeled slowness, and **A** is the Jacobian matrix. In travel time tomography, Equation (3) is solved using matrix inversion techniques.

In this inversion technique, Equation (3) is commonly solved by using two series expansion approaches from geophysics: 1) matrix inversion approach (e.g. Conjugate Gradient (CG) matrix inversion technique (Nolet, 1987; Scales, 1987)); and 2) "Back-projection" inversion technique, adapted from medical tomography (e.g. Simultaneous Iterative Reconstruction Technique (SIRT)) (e.g. Herman, 1980; Ivanson, 1986).

In both techniques, the acoustic wavefield is initially propagated through a presumed theoretical model and a set of travel times are obtained by ray-tracing (forward modeling step). The travel time equations are then inverted iteratively to reduce the root mean square (RMS) error between the observed and computed travel times (inversion step). The inversion results can be used for imaging the velocity (travel time tomography) and attenuation (amplitude tomography) distribution between boreholes or access tubes.

A number of software algorithms for performing travel time tomography exist. These algorithms utilize straight or curved rays for forward model, 2-D or 3-D matrix inversion, and 2-D or 3-D graphic packages to display the results.

For accurate volumetric imaging of anomalies in concrete structures, it is critical to use a software package with the following characteristics: a) curved ray tracing or wave propagation based forward modeling; b) True 3-D matrix inversion; c)- 3-D display of data.

A "true 3-D" tomographic program inverts for the full 3-D velocity *volume* in a single step. As is shown in the next section, software packages that, for example, use 2-D inversion followed by the 3-D display of the results, do not render an adequate volumetric definition of anomalies or defects. Two-dimensional tomographic inversion produces defect images with lower resolution than 3-D inversion as imaging is done independently in 2-D planes (panels). In addition, in the next section, a critical velocity equalization Quality Control (QC) processing step is described. Velocity equalization is performed prior to the tomographic inversion for minimizing artifacts in the imaged space.

2.2.2 Tomography Pre-Processing – Velocity Equalization

Three-dimensional tomographic velocity inversion requires the critical step of velocity equalization. Velocity equalization is also important for 2-D velocity inversion. Velocity equalization involves in static shifts of zero and offset CSL logs in order to equalize background (shaft) velocity in all the test panels. Velocity equalization is necessitated due to inaccurate measurements of tube geometries in the field—such as inaccurate measurement of tube separation due to the bending of tubes at the surface. It can also be due to the "cycle skipping" (missing the right leg in picking travel times) especially in picking high angled offset logs.

Proprietary three-dimensional velocity equalization software is used which normalizes the background (shaft) velocity in three-dimensions prior to the tomographic inversion. This step is important for CSLT imaging as edge (boundary) artifacts are reduced. For true 3-D imaging, however, velocity equalization is critical; otherwise false anomalies can be created if large velocity contrasts exist between the panels.

To demonstrate the importance of velocity equalization step, 2-D and 3-D tomographic results from Amherst-NGES Shaft 1 are shown in Figure 12 before and after velocity equalization (top and bottom figures, respectively). As described in Section 5.1 in detail, this shaft was constructed in Amherst, MA with known engineered defects. In Figure 12, results using 3-D matrix inversion are shown on the left hand side and results using 2-D matrix inversion is shown on the right hand side. All CSLT images are displayed with the same velocity scale for comparison.

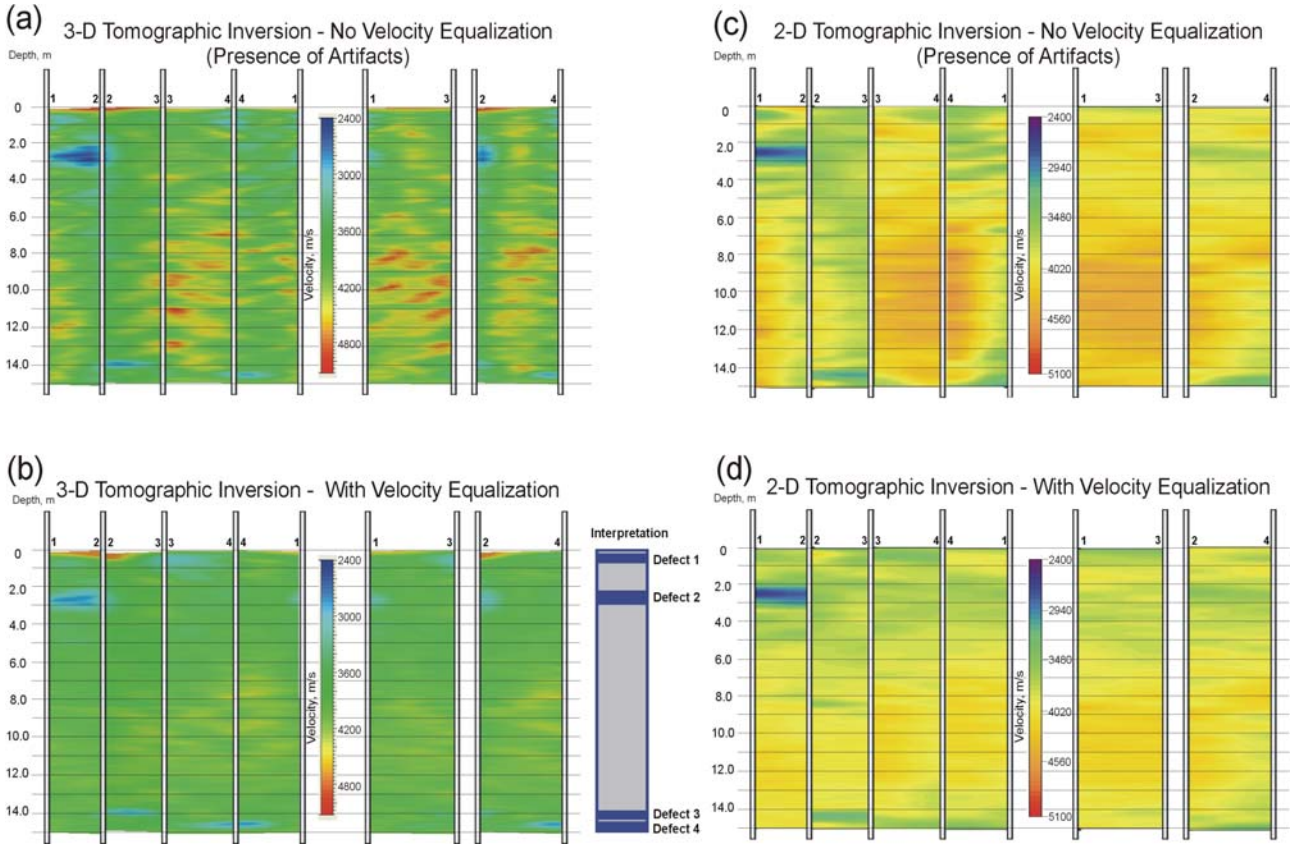

Figure 12. Schmeatic. Comparison of 2-D and 3-D Tomographic Imaging With and Without Velocity Equalization- Shaft 1, NGES, Amherst, MA.

Four defects are interpreted from the equalized 3-D tomography results of Figure 12-b and is shown to the right of this figure. For the shallow Defect 1 between the depths of 0.2-1 m, only 3-D inversion resolves this defect near Tube 3. This defect is not imaged in the 2-D inversion results of Figure 12-d. For Defect 2 between the depths of 2-3 m, both 2-D and 3-D inversions image this defect; however, 3-D inversion resolves this defect better, especially between Panels 1-3 and 2-4. For Defect 3 between the depths of 13.8-14.2 m, both 2-D and 3-D inversions image this defect between Panel 2-3. Finally, for the Defect 4 between the depths of 14.3-14.8 m, only 3-D inversion images this defect near Tube 4. Therefore, it is evident that 3-D inversion produces sharper defined images with better spatial definition.

From this figure it is also clear that artifacts are considerably reduced by the velocity equalization step. Artifacts are indicated by red and yellow colors in the 3-D inversion results shown in Figures 12-a and 12-b and by orange color in the 2-D inversion results shown in Figures 12-c and 12-d.

As a second example, results from Amherst Shaft 4 (also with known defects) are displayed in Figure 13. From this figure, three defects are interpreted from the equalized 3-D tomography results of Figure 13-b and is shown to the right of this figure. For the shallow Defect 1 (between 2.8-3.4 m depths), both the 2-D and 3-D inversions indicate this anomaly; however, 3-D

inversion resolves this defect better, especially between Panel 1-3. For Defect 2 between the depths of 5.5-6.2 m, both 2-D and 3-D inversions indicate this anomaly; however, 3-D inversion resolves this defect better. For Defect 3 between the depths of between the depths of 14.6-14.9 m, both 2-D and 3-D inversions indicate this anomaly; however, 3-D inversion resolves this defect better, especially between Panel 2-3 and 1-3. Therefore, it is evident that 3-D inversion produces sharper images with better spatial definition.

From this figure it is also evident that artifacts are considerably reduced by the velocity equalization step, especially in 3-D inversion. Artifacts are indicated by red and yellow colors in the 3-D inversion results shown in Figures 13-a and 13-b. Note, for example, that in Panel 3-4, Defects 1, 2, and 3 are masked in 3-D inversion. In 2-D inversion, notice the dramatic effect of velocity equalization in higher average velocities in Panel 2-3 (blue) before velocity equalization in Figures 13-c as compared to after velocity equalization in Figure 13-d (green).

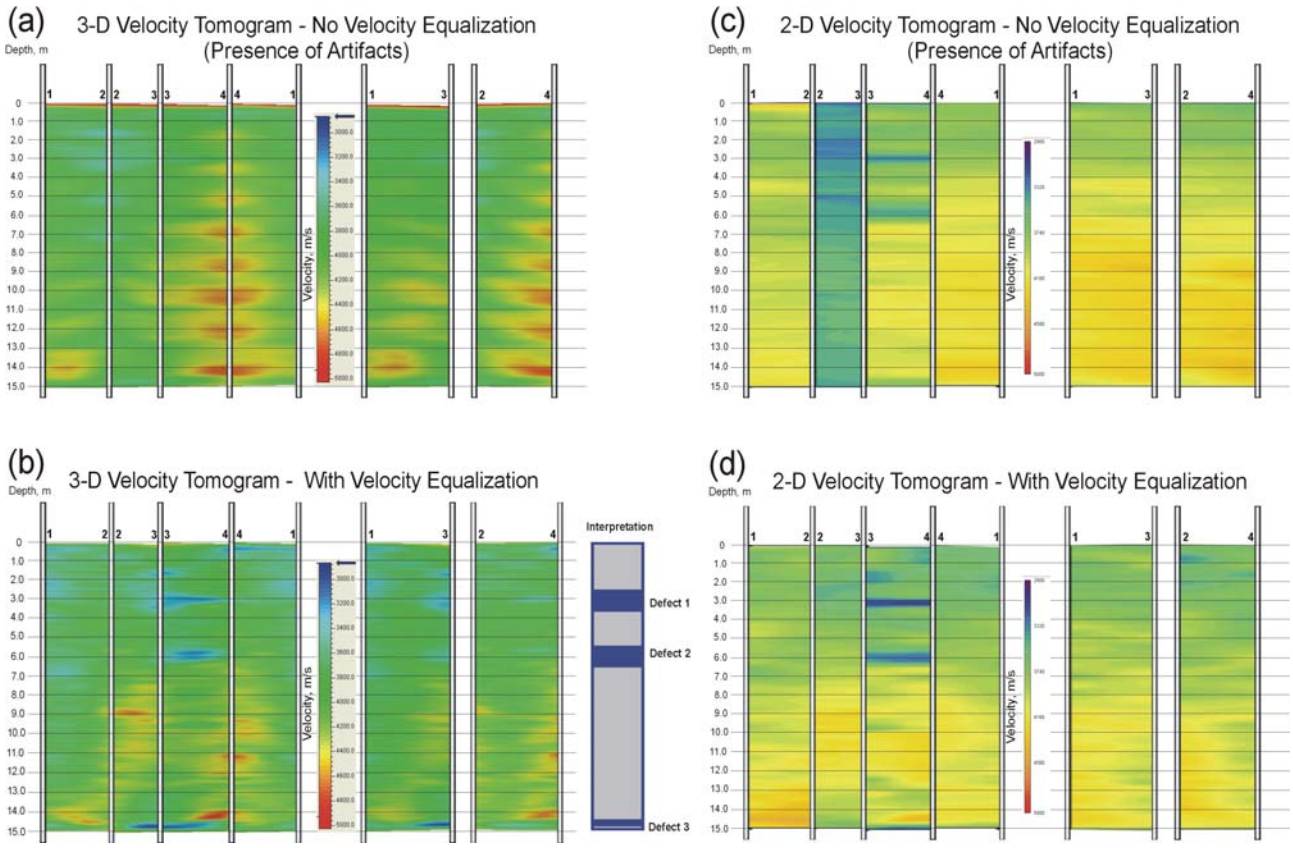

Figure 13. Schematic. Comparison of 2-D and 3-D Tomographic Imaging With and Without Velocity Equalization- Shaft 4, NGES, Amherst, MA.

Therefore, it is recommended to use velocity equalization followed by true 3-D tomographic inversion of the data in order to obtain best resolution in defining defects and in minimizing artifacts in the imaged space.

2.2.3 Tomography Modeling

Synthetic forward modeling was performed to examine the resolution and accuracy of typical CSLT acquired data. The first task addresses how well typical offset tomography field acquisition images or resolves defects. The second task addresses how well these final tomography images represent the true velocity field so that it can be correlated it to concrete strength.

2.2.3.1 CSLT Offset Tomography as an Imaging Tool

The degree tomography can image or resolve a defect depends on how completely one can surround the test volume with sources and receivers and scan it (aperture). Since a full 360º scanning is not possible, and tomography is an iterative a priori based error reduction process, a perfect image of defects can never be obtained, even under ideal modeling where perfect data picking is assumed.

To examine the effectiveness of typical CSLT field acquired data in resolving defects in a drilled shaft foundation, three synthetic models are created:

Model 1: Shaft with a Small Defect**.** As shown in the left hand side of Figure 14-a, a 2-D model is created consisting of two access tubes 1.0 m apart with a (0.4x0.5m) defect representing 2% of total area. The model consists of sound concrete at 4,000 m/s, shown in light purple, and defect at 2,000 m/s, shown in dark purple. This model is used to examine the resolving power of different combinations of CSLT field acquired offset log data.

First, the results using standard zero probe offset CSL process is shown next to the model in Figure 14-a. These images were obtained by inputting a single "zero-offset" CSL log into the tomographic imaging software. It is apparent from Figure 14-a that standard CSL horizontally smears (elongates) defects due to the lack of angular ray coverage. The zero-offset image is shown with and without ray paths superimposed.

Next, in order to systematically observe the improvement in CSLT images, the zero-offset CSL log is progressively combined with just one other offset log. These two combination logs are formed by combining 0º CSL logs with one other offset log ±11.25º, or ±22.5º, or ±45º as shown in Figures 14-b to 14-d, respectively. As expected improvement in image resolution is observed; however, the best improvement is observed by combining zero-offset logs with ±45º logs as high angled rays delineate the defect edges better.

Finally, zero offset logs were combined with two offset log of ±22.5º and ±45º in forming three combination logs in Figure 14-e and four combination logs of ±11.25º, ±22.5º, and ±45º in Figure 14-f. Obviously, the best image is formed using all four combinations of angled logs. Notice, however, that this image is not a "perfect" reconstruction of the model and has a slight velocity "shadow" which is typical of tomography images, as previously discussed. Nonetheless, the ray path diagram clearly delineates the four edges of the defect as points where rays are sharply turning (refracted) out.

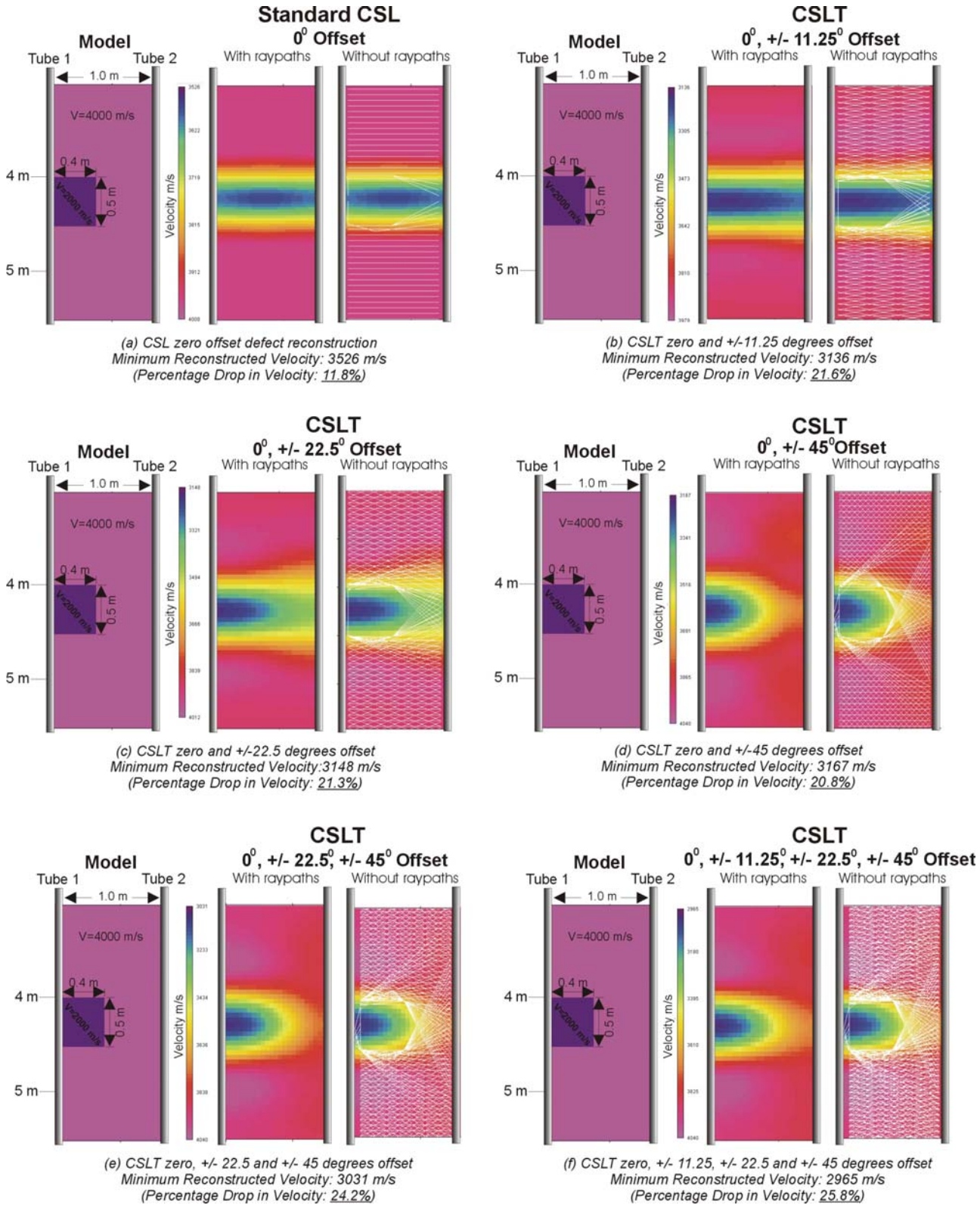

Figure 14. Schematic. Computer Based Synthetic Modeling of a Shaft with a Small Defect. Tomographic Imaging Results Comparing Standard Zero-Offset CSL Image (Top Left Hand Side) With Different Combination of Multi-Offsets CSLT Images.

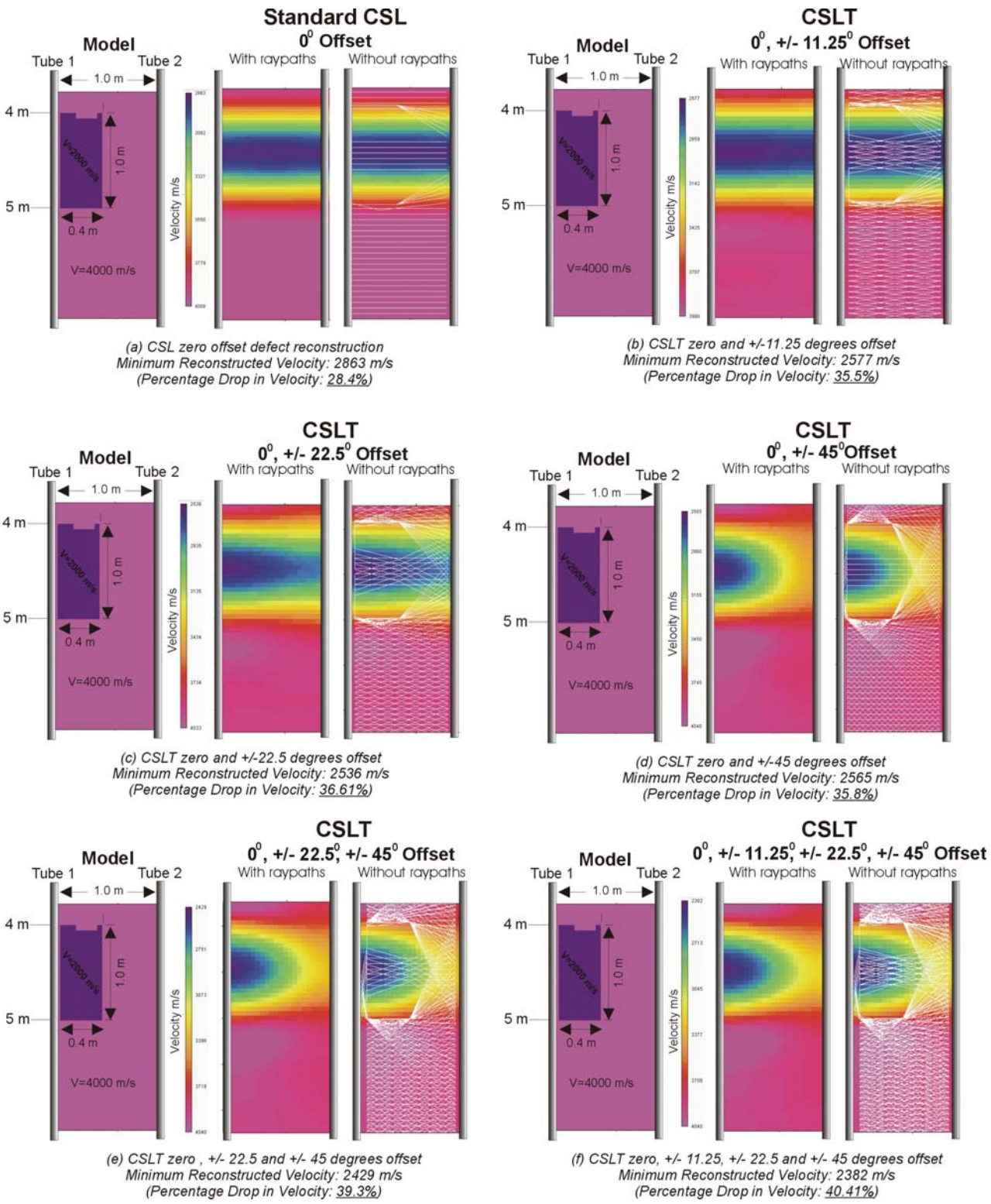

Figure 15. Schematic. Computer Based Synthetic Modeling of a Shaft with a Large Defect. Imaging Results Comparing Standard Zero-Offset CSL Image (Top Left Hand Side) With Different Combination of Multi-Offsets CSLT Images.

Surprisingly, note that just two combination of 0º and ±45º logs in Figure 14-d gave an image similar to the four combination logs of Figure 14-f, but only slightly oversized. It is apparent that even with a very coarse angular coverage (0 and 45 degree logs only), offset tomography can resolve defect boundaries sufficiently due to the fine depth sampling involved. Therefore, it is not necessarily the ray density that governs image resolution, but the presence of high angled rays. For this model of a shaft with "small" defect and the velocity contrast presented the ray paths all go around the defect with no raypath coverage (therefore, velocity reconstruction) inside.

Model 2: Shaft with Large Defect. As a second example, as shown in Figure 15, another 2-D model is created consisting of two access tubes 1.0 m apart with a defect twice as long (0.4x1m) which constitutes 4% of total 2D area. Again, similar results are obtained with 2-D CSLT using just 0º and ±45º logs in Figure 15-d producing an image similar to the four combination logs of Figure 15-f. However, due to the larger size of the defect, in all offset log combinations, few rays *are* traced inside the defect zone. Therefore, defect velocities are better reconstructed, as is described further in Section 2.2.3.2. Once again, CSLT reconstruction of offset log acquired data slightly elongates and over sizes the defect.

Model 3: Shaft with Multiple Levels of Defects. Finally, Figure 16 illustrates the results of a shaft with multiple defect levels. Multi-offset CSLT images are compared with zero-offset standard CSL "image". (This model has different velocity scale or color display than previous examples). Again, four offset CSLT acquisition provides with a good image of the defects even though multiple defect levels are present. However, CSLT exaggerate the size of anomaly, especially for smaller more elongated defects.

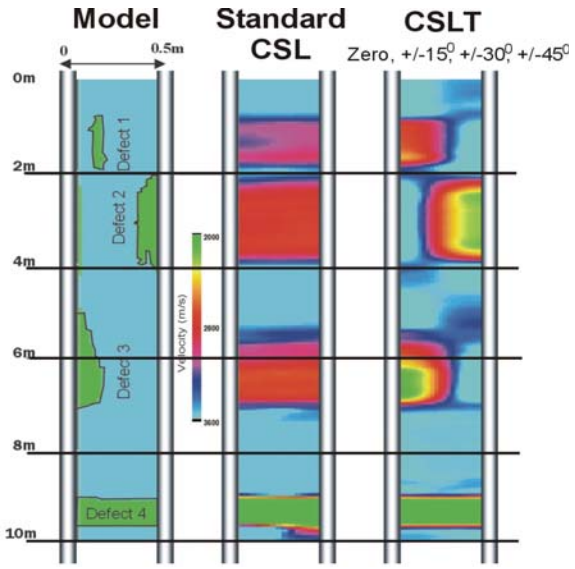

Figure 16. Schematic. Synthetic Modeling of a Shaft with Multiple Levels of Defects. Tomographic Imaging Results Comparing Standard Zero-Offset CSL Image With Multi-Offset CSLT Image.

Therefore, it is concluded that multi-offset CSLT reconstruction is a good *imaging* tool, but slightly over sizes defects.

2.2.3.2 Tomography as an Accurate Representation of the Velocity Field

To examine how well CSLT represents the velocity field (especially the defect velocity), percentage drops in minimum defect velocity as compared to the shaft velocity is presented in Figure 17. The percentage values are presented for the small and large defects in Figs. 14 and 15 with the solution (model) corresponding to 50% drop from 4,000 m/s to 2,000 m/s.

Note that tomography does not provide a perfect reconstruction of velocity field, especially for small defect or low velocity defects such as void. Larger, or higher velocity defects (low velocity contrast), provide a better reconstruction of velocity as rays travel inside the defect. Since most common defects in drilled shaft are relatively larger size with low velocity contrast, it appears the defect velocities must be reduced by about 30% for 2-D inversion and slightly less in 3-D (as described in Section 2.2.2)—even though more modeling is needed.

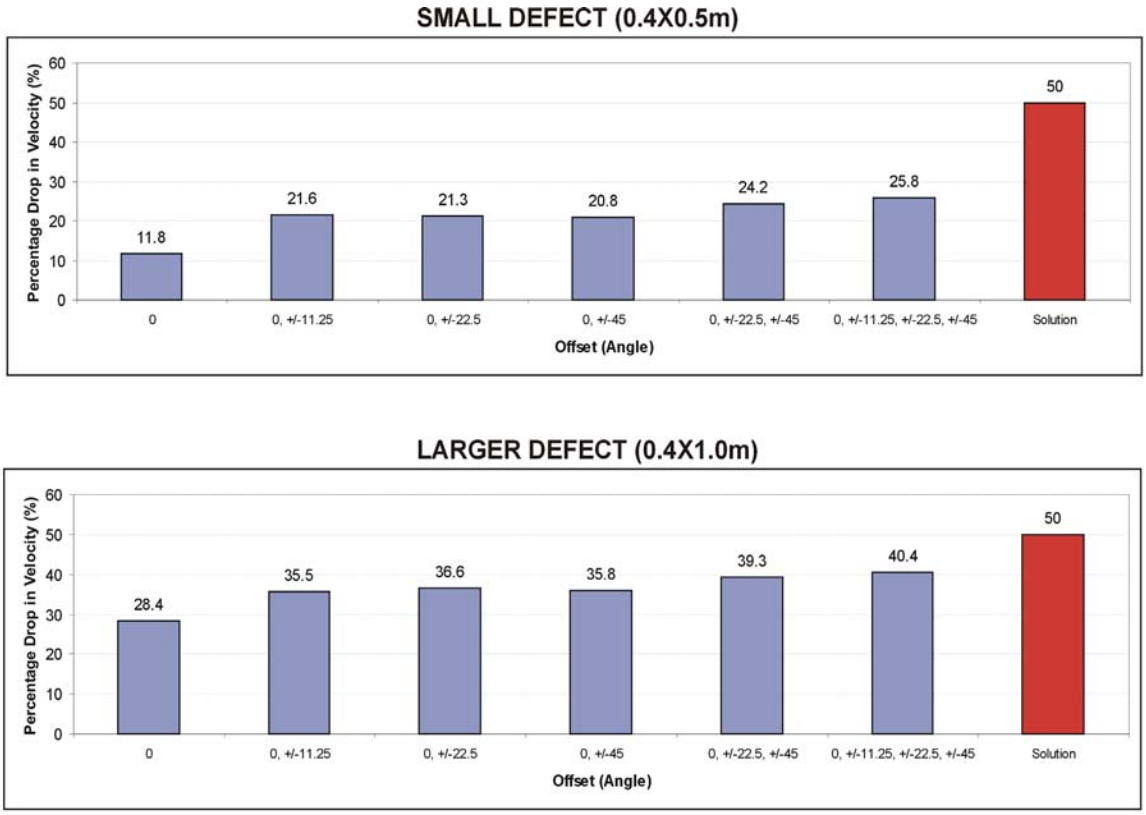

Figure 17. Schematic. Correlation between Percentages Drops in Velocity of Standard CSL Versus Number of Combination of CSLT Tomography.

In conclusion, tomography slightly over sizes and elongate defects but underestimates their velocities. Therefore, there is a compensation effect; nevertheless, a corrective factor needs to be applied to the defect velocities to accurately calibrate their values to concrete strength (for details, refer to Chapter 4).

CHAPTER 3 – DEFECT DEFINITION

In Chapter 2, velocity images obtained from three-dimensional tomographic reconstruction method (CSLT) were discussed. The principal use of CSLT is the identification of low-velocity regions indicative of anomalies in a drilled shaft. However, the velocity distributions or histograms are often smoothly varying so that identification of a single cutoff velocity, below which the shaft is considered to be defective, is difficult. In this chapter, a statistically definition of a "defect" in a drilled shaft foundation is presented. By fitting classical normal probability distributions to the velocity histogram, the probability that any element (velocity bin) in the model volume is defective is quantified. In this approach, the probability of the total defective volume exceeding some threshold can be defined, and therefore engineers can make risk-based assessments of shaft integrity.

In the next section, a robust curve-fitting technique is presented to decompose histograms of crosshole sonic logging (CSL) velocity tomograms into one, two, or three constituent normal distributions (Gaussians). The crossover between the Gaussian with the lowest mean velocity and its nearest neighbor provides a practical definition of cutoff velocity for low-velocity flaw definition. Although the approach is limited in the test data by the presence of artifacts from the tomographic inversion, velocities below 85-90% of the median shaft velocity appear to be indicative of flaws.

3.1 STATISTICAL MODELING - GAUSSIAN PROBABILITY DISTRIBUTION CURVES

The statistical Gaussian curve-fitting technique is used for the final 3-D velocity distribution produced by tomographic inversion, following all data editing, velocity equalization corrections, and processing. The velocity histogram is the primary data; results are relatively insensitive to velocity bin widths <50 m/s. Therefore, in these examples, an optimum velocity bin size of 25 m/s is used. A robust (L1-norm) curve-fitting procedure is used to decompose the observed histogram into 1, 2, or 3 normal distributions (Gaussians). The mean (μ), standard deviation (σ), and amplitude (A) of each Gaussian component are the fitted parameters. An F-test is used to determine the probability that the additional Gaussian have actually improved the fit. PF_{12} is, therefore, the probability that the 2-Gaussian fit is better than the 1-Gaussian fit; similarly PF_{23} is the probability that 3 Gaussians is superior to 2. The quantity PF_{13} is also reported for completeness. PF values near 50% indicate there is no significant improvement using additional Gaussian, whereas PF = 100% means that the more complex fitting is unquestionably more accurate.

One of the Gaussians is identified as being associated with the anomalies of interest. For the 2-Gaussian case this is obviously the distribution with the smaller mean velocity, but for the 3-Gaussian fits either of the smaller-mean distributions could be relevant. For the data analyzed here, however, the Gaussian with the lowest mean velocity is inferred as anomalous concrete.

3.2 STATISTICAL MODELING RESULTS

The best fits for one-, two-, and three-Gaussian applied to two shafts at the Amherst test site are summarized in Table 1. Note that for each shaft, some trial-and-error adjustment of the starting parameter values was necessary in order to obtain reasonable results. In other words, the procedure is not yet completely automated and some analyst skill is required.

Multi-offset CSL data for Amherst Shaft 1 was tomographically inverted using low and high smoothing values of 0.1 and 1.0, respectively. The smoothing parameter controls the trade-off between data goodness-of-fit and model smoothness. The best fit may lead to a model with unrealistic (rough) velocity variations, whereas an over smoothed model may not have an acceptable model fit. The statistical fits reflect the differences in model smoothness.

Analysis of the low-smoothing solution for Shaft 1 is shown in Figure 18. A single Gaussian is a reasonable approximation to the velocity distribution as a whole. A second Gaussian fits a visually obvious low-velocity extension to the main distribution, but the F-test does not indicate this is statistically significant. Adding the third Gaussian does result in a significant improvement according to the F-test. The transition from the anomalous low-velocity portion occurs at 3,625 m/s (12,000 ft/s), which is 90% of both the mean and median velocity. The 3-D distributions of portions of the shaft indicated by the tomography to lie below this cutoff, and hence be part of a flaw, are also depicted in Figure 18.

High smoothing (Figure 19) during the tomographic inversions produces a smoother model as expected, but a pronounced hump in the histogram is now apparent at intermediate velocity (~3,900 m/s, 12,800 ft/s). Although a very low-velocity tail is again visually obvious, statistically only the 2nd Gaussian is important in making up the large misfits to a single Gaussian introduced by the intermediate-velocity hump. Selecting the high side of this feature as the flaw cutoff results in a cutoff velocity fully 95% of the mean or median velocities and therefore too much of the shaft is interpreted as flawed. Selecting the low side transition to the low-velocity tail yields a cutoff velocity of 91% of the mean or median, now in better agreement with the low-smoothing result for the same shaft. The intermediate-velocity feature is interpreted as a tomographic artifact, but its origin is unknown. These velocities are distributed around the regions of the inferred flaws and are not simply streaked along one side, as would be the case if one panel had not been properly static corrected. The artifact appears to be intrinsic to the Tomographic inversion procedure.

For Amherst Shaft 4, the intermediate-velocity artifact is now very pronounced, having the highest amplitude of any of the sub-distributions (Figure 20). However, this is now for a low-smoothing tomographic solution, not high smoothing as previously. (In view of that, the high smoothing results is not presented). Now the cause of the artifact can be likely identified as incomplete or ineffective static corrections, because the intermediate-velocity anomalies are vertically streaked throughout the shaft. Again, this intermediate-velocity distribution allows two locations to be picked for a velocity cutoff: the high-side value of 96% of the median or mean is clearly incorrect; the low-side value of 89% of the median or 90% of the mean is in better agreement with previous results. In both of these last two cases, the inferred upper cutoff may have been influenced by the artifacts.

The Gaussian fitting statistical analysis result presented in this section on Amherst Shafts 1 and 4 are developed for demonstrating the basic concept. In Section 5.2, the Amherst tomography results are presented based on multi-zone statistical analysis of the data with more refined definition of defects at each separate defect zone.

Table 1. Normal-Distribution Fitting to Amherst CSL Tomography (CSLT).

	Shaft 1 Low Smoothing	Shaft 1 High Smoothing	Shaft 4 Low Smoothing
μ_{11} (m/s)	4,050	4,130	3,760
σ_{11} (m/s)	210	110	270
A_{11} (counts/bin)	4,900	8,400	5,450
μ_{12} (m/s)	4,050	4,140	3,830
σ_{12} (m/s)	210	100	230
A_{12} (counts/bin)	4,910	8,800	3,600
μ_{22} (m/s)	3,290	3,880	3,590
σ_{22} (m/s)	150	80	50
A_{22} (counts/bin)	190	2,100	3,400
PF_{12}	66%	100%	100%
V_{cutoff} (m/s)	3,450	3,950	3,625
V_{cutoff}/μ_{11}	85%	96%	96%
V_{cutoff}/V_{median}	85%	96%	96%
μ_{13} (m/s)	4,210	4,140	3,800
σ_{13} (m/s)	150	100	230
A_{13} (counts/bin)	4,000	8,800	3,560
μ_{23} (m/s)	3,520	3,890	3,590
σ_{23} (m/s)	290	60	50
A_{23} (counts/bin)	250	2,100	3,750
μ_{33} (m/s)	3,900	3,630	3,150
σ_{33} (m/s)	120	200	70
A_{33} (counts/bin)	3,200	260	90
PF_{23}	100%	69%	35%
PF_{13}	100%	100%	100%
V_{cutoff} (m/s)	3,625	3,925 (3,750)	3,625 (3,375)
V_{cutoff}/μ_{11}	90%	95% (91%)	(90%)
V_{cutoff}/V_{median}	90%	95% (91%)	(89%)

* μ_{12} : mean velocity of the first Gaussian in a 2-Gaussian fit
σ_{23} : standard deviation of the second Gaussian in a 3-Gaussian fit
A_{33}: amplitude of the third Gaussian in a 3-Gaussian fit
PF_{23}: the probability that 3 Gaussians is superior to 2
V_{cutoff}: cut-off velocity
V_{median}: median velocity

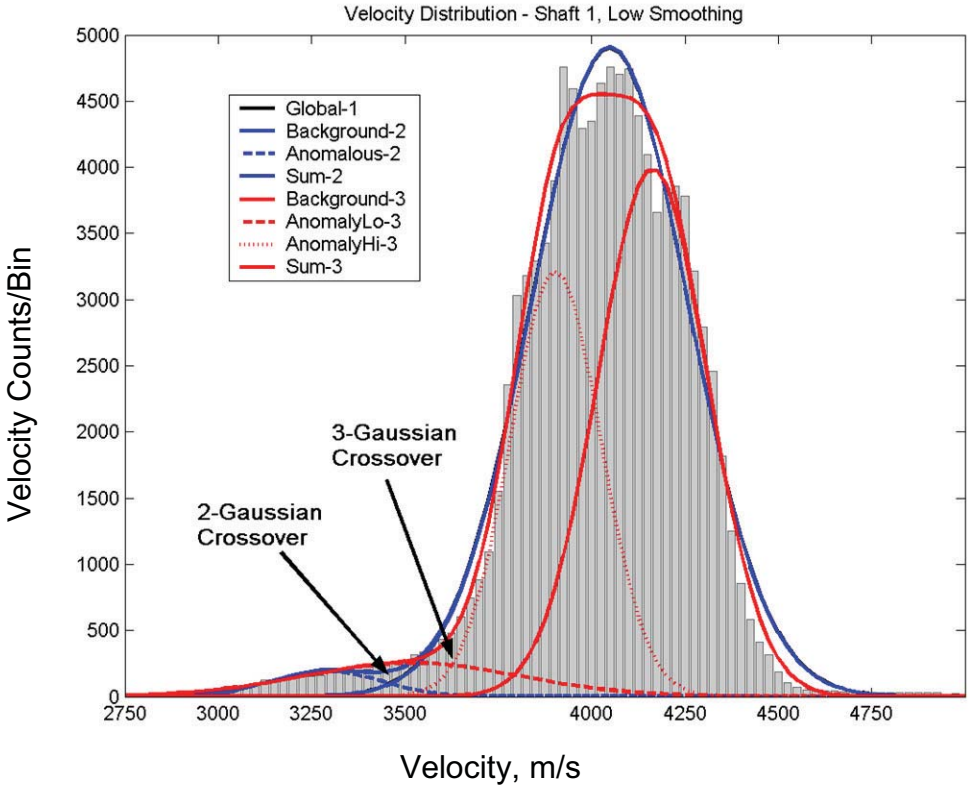
Velocity Distribution - Shaft 1, Low Smoothing
Global-1
Background-2
Anomalous-2
Sum-2
Background-3
AnomalyLo-3
AnomalyHi-3
Sum-3
3-Gaussian Crossover
2-Gaussian Crossover
Velocity Counts/Bin
Velocity, m/s
5000
4500
4000
3500
3000
2500
2000
1500
1000
500
0
2750
3000
3250
3500
4000
4250
4500
4750

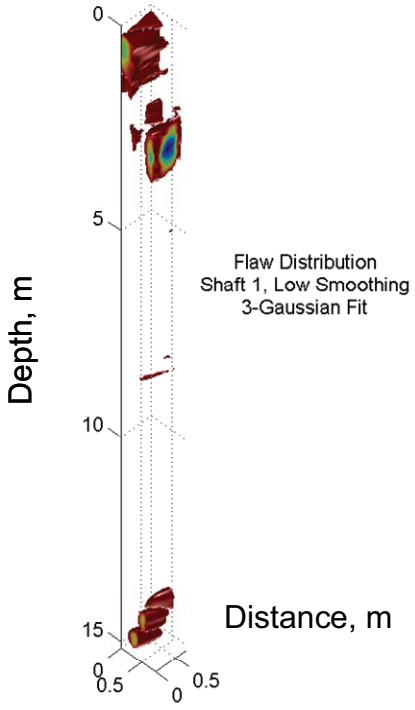

Figure 18. Schematic. Top. Histogram of Velocities from 3-D Tomography (CSLT) (Shown in Gray) of Amherst Shaft 1 under Low Smoothing, with Multi-Gaussian Fits Superimposed. Bottom. Visualization of Inferred Flawed Portions of the Shaft.

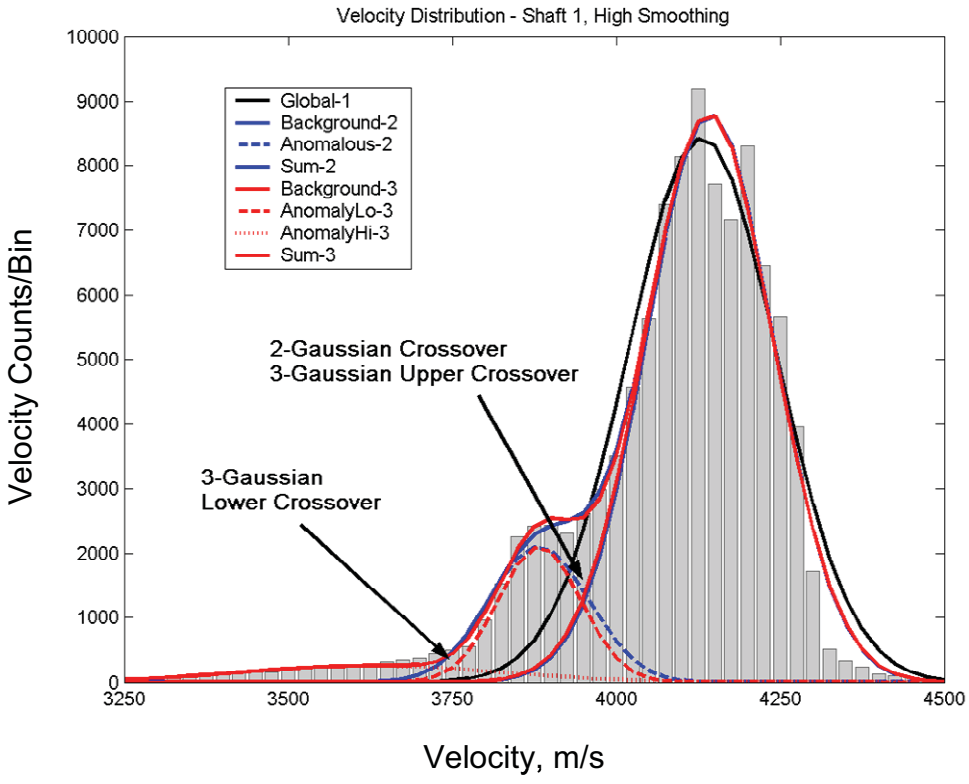

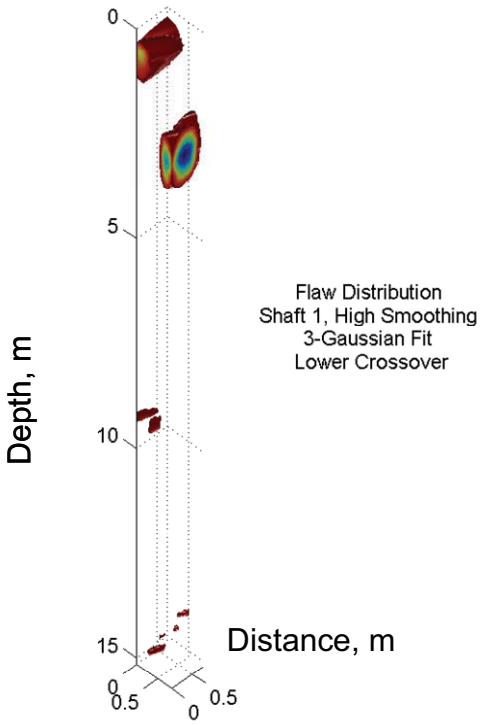

Figure 19. Schematic. As Figure 18 for Amherst Shaft 1, but for High Smoothing. Note Development of Anomalous Zone at Intermediate Velocities.

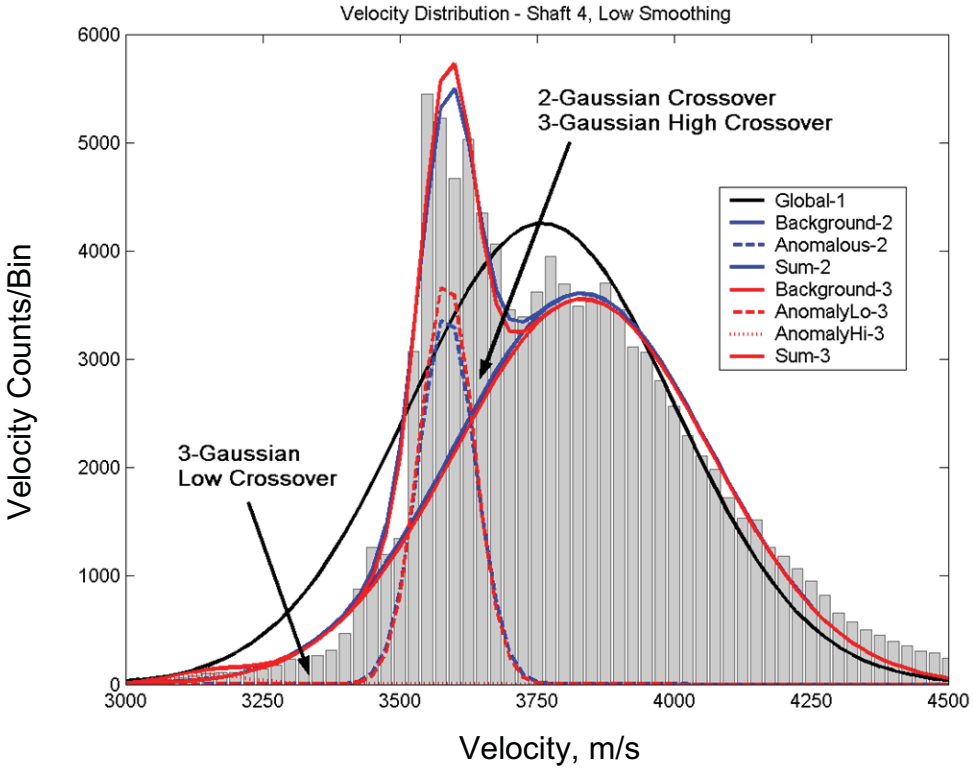

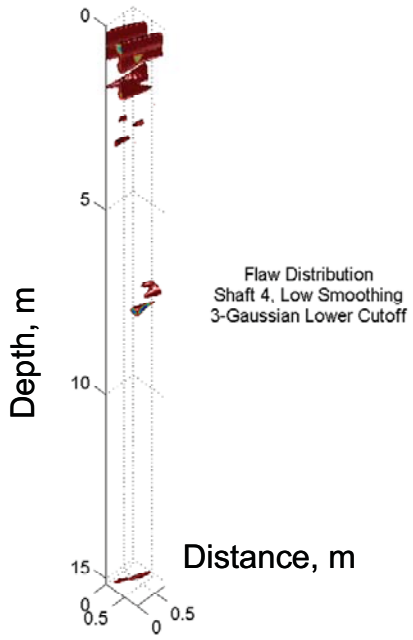

Figure 20. Schematic. Velocity Histogram and Flaw Interpretation for Amherst Shaft 4, Low Smoothing. Note Very Pronounced Intermediate-Velocity Artifact.

CHAPTER 4 – DEFECT CHARACTERIZATION AND IMAGING

This chapter addresses the third task of the investigation regarding defect characterization. To accomplish this, changes in concrete velocities are correlated with the changes in concrete strength and 3-D strength images are provided. The correlation of field measured CSL velocities and laboratory measured concrete velocity values to concrete strength values is established, as described next. The laboratory values are acquired from ultrasonic pulse velocity (UPV) testing obtained from 5 concrete cylinders at 4, 7, 14, 21, and 28-day intervals.

4.1 ESTABLISHMENT OF EMPERICAL RELATIONSHIP BETWEEN CSL VELOCITY AND STRENGTH

In present drilled shaft construction practice, the unconfined compressive strength of concrete f'_c is in the range of 20,700- 34,500 kPa (3,000-5,000 psi) for normal density cast-in-place concrete. High strength concretes, with f'_c to about 82,800 kPa (12,000 psi), are used mostly for pre-stressed long-span bridges. The strength data is usually obtained through tests after 28 days after concrete placement.

The modulus of elasticity of concrete E_c (in units of psi) is defined as the slope of the initial straight portion of the stress-strain curve. For concretes with compressive strength to about 41,400 kPa (6,000 psi), the following empirical relationship from the ACI code is used (Nilson and Winter, 1986)[4]:

$$E_c = 33\,\rho_c^{1.5}\sqrt{f'_c} \qquad (4)$$

where f'_c is the strength in psi and ρ_c is density of hardened structural concrete (in lb/ft^3) in the range of 1.44-2.5 g/cm^3 (90-155 lb/ft^3). For normal sand-and-stone concretes, with ρ_c = 2.32 g/cm^3 (145 lb/ft^3), Equation (4) becomes:

$$E_c = 57{,}000\sqrt{f'_c} \qquad (5)$$

From the theory of elasticity, compressional wave velocity V_p in an homogeneous, isotropic and elastic media is given by:

$$V_p = \sqrt{(E_c / \rho_c)} \qquad (6)$$

In narrow bars with lateral dimensions comparable to the transmitted wavelength, V_p is extensional wave velocity and E_c becomes Young's modulus. Using Equations (5) and (6)

[4] This universal concrete modulus to strength relationship (4) is developed without a good (high) R^2 correlation value. This is obviously due to the vast variety of aggregates, cements, and additives used by the concrete industry. As described in Section 4.1.3, it is more desirable to develop a shaft-specific strength to modulus (or velocity) relationship.

$$f'_c \approx V_p^4 \ \rho_c^2 \qquad (7)$$

Therefore, a fourth power relationship is assumed between unconfined compressive strength of concrete and compressional wave velocity (and only a second power relationship with density). This fourth power velocity-strength relationship is the current industry standard. It is used to characterize defective concrete in drilled shafts typically of less than 28 days in age even though the above strength relationships is usually obtained through tests made 28 days after the concrete placement. It is also used herein in developing strength images in Chapter 5.

Obviously, using a universal relationship such as Equation (7) between velocity and strength is very desirable. However, as described in section 4.1.3, a shaft specific relationship between strength and velocity is preferred that is developed for concrete of less than 28 days in age.

4.1.1 Example Calculation

A defect zone with 20% drop in velocity ($V_{new} = 0.8\ V_{old}$) and using Equation (7) implies:

$$f_{new} \approx 0.8^4\ f_{old} = 0.4\ f_{old} \qquad (8)$$

Therefore, the strength in the defect zone is about 40% of old strength. Similarly, a concrete with a 10% drop in velocity implies the strength in the defect zone is 65% of old strength.

4.1.2 Current Industry Standards for Defect Definition

Using standard CSL or CSLT testing, "questionable" concrete condition is defined as a zone with a decrease (from median) in sonic velocity between 10% and 20% (or about 40%-65% of old strength); and, "poor" concrete condition is defined as a zone with greater than 20% decrease in sonic velocity (or about less than 40% of old strength). (Please refer to footnote 2 for example specification).

4.1.3 Empirical Relationship Between Core Strength and CSL Velocity

As mentioned above, developing a universal relationship that relates either the maturity parameters or velocity to strength parameters of concrete (such as Equation (7)) is, obviously very desirable. However, this is not typically achievable because of wide variations in three categories of parameters used in construction of a shaft (Yuan, Nazarian, and Medichetti, 2003), namely:

1. *Mix-Related Parameters* – Referring to the vast variety of aggregates, cements and additives that are used in the concrete industry;
2. *Environmental-Related Parameters* – Referring to varying subsurface conditions; specifically, changes in stiffness, moisture, and temperature;
3. *Construction-Related Parameters* – Referring to changes in shaft diameter and differing reinforcement designs.

In this study, Equation (7) is sought to be determined empirically for the same concrete mix used in the construction of the shaft. To that end, concrete cylinders from 20 different cylinders from the Sevenmile Gooseberry, Utah project were tested using the ultrasonic pulse velocity (UPV, ASTM-C597) method at 4, 7, 14, 21, and 28-day intervals, as described below.

4.1.3.1 Ultrasonic Pulse Velocity (UPV) Method

The ultrasonic pulse velocity (UPV) method determines the velocity of propagation of ultrasonic energy pulse through a concrete member by transmitting a short duration, high voltage resonant frequency signal by a pulser to a transducer coupled to the opposite concrete surface. When the pulse is received the timer is turned off and the elapsed travel time is measured. The pulse velocity is obtained by dividing the direct path length between the transducers by the travel time.

For a given concrete mixture, as the compressive strength increases with age, there is a proportionally smaller increase in the pulse velocity (Jones, 1954). At early ages (typically 2-7 days), the pulse velocity is very sensitive to the gain in strength.

UPV results are operator dependent and for longer travel paths the test results are not constant. The accuracy of measurements also depends on factors such as moisture content (Jones and Facaoaru, 1969) and density of steel reinforcement (Chung, 1978) in the concrete member.

The results of the laboratory UPV testing from the Sevenmile-Gooseberry Project are shown in Figures 21 and 22. In these figures, UPV testing was performed by two groups (Olson Engineering and CFLHD) which is referred to as Batch 1 and Batch 2. Compressive strength measurements were all obtained by CFLHD. Each group tested two (2) samples at each time interval for statistical considerations; however, UPV measurements were not performed at 4 day testing (only strength measurements). The fourth power velocity-strength curve is also shown. For such a limited range in strength values, a conclusive power relationship cannot be inferred.

4.1.3.2 Maturity Method

To obtain a more representative empirical relationship between velocity and strength, the maturity method (Saul, 1951) must be considered. The maturity method assumes: 1) concrete derives its strength from the hydration of cement; 2) this hydration of cement produces heat; 3) if one can monitor this heat, then an estimation of the extent of the hydration reaction can be made and—as a result—the strength of the concrete can be predicted. The temperature-time approach, described herein, approximates the heat production as the area under the temperature-time curve. From the measured maturity, the strength of a concrete mass is determined by reference to the previously determined relationship between maturity and strength.

Two different methods are described in ASTM C1074 for analyzing concrete maturity. The first is the temperature time factor method (TTF), which utilizes the Nurse-Saul equation (Saul, 1951) as:

$$M(t) = \sum (T_a - T_0)\Delta t \qquad (9)$$

Batch 1					
Sample	Age	Strength (kPa)	Strength (PSI)	Velocity (m/s)	Velocity (ft/s)
03-801-CC	7	31440	4560	4150	13615
03-802-CC	7	31030	4501	4160	13648
03-803-CC	14	34010	4933	4260	13976
03-804-CC	14	32900	4772	4220	13845
03-805-CC	21	35140	5097	4230	13878
03-806-CC	21	35330	5124	4160	13648
03-807-CC	28	37090	5379	4260	13976
03-808-CC	28	36320	5268	4260	13976

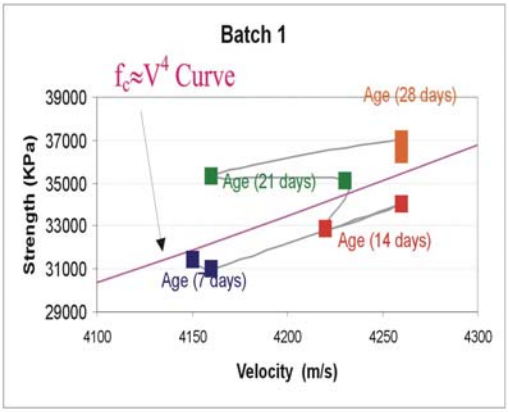

Figure 21. Chart. Velocity Versus. Strength Curve for Batch 1.

Batch 2					
Sample	Age	Strength (kPa)	Strength (PSI)	Velocity (m/s)	Velocity (ft/s)
03-811-CC	7	31370	4550	4140	13583
03-812-CC	7	30920	4485	4170	13681
03-813-CC	14	33090	4799	4210	13812
03-814-CC	14	32300	4685	4130	13550
03-815-CC	21	33680	4885	4270	14009
03-816-CC	21	35650	5171	4190	13747
03-817-CC	28	34270	4970	4280	14042
03-818-CC	28	35590	5162	4250	13944

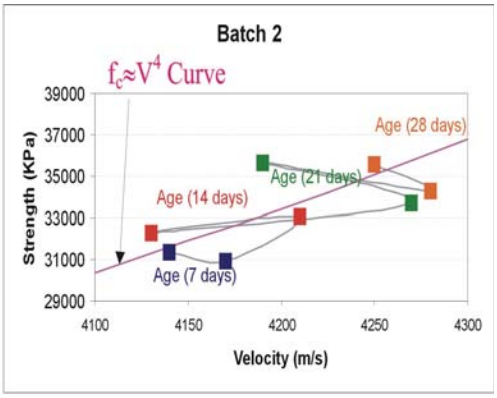

Figure 22. Chart. Velocity versus Strength Curve for Batch 2.

where M(t) is a "time-temperature factor" (TTF) at time t, T_0 is the lowest temperature at which a gain in strength is observed, T_a is the average temperature during time interval Δt between consecutive measurements. An examination of Equation 9 shows that it is an integration of the temperature-time curve utilizing the trapezoidal method. Basically, in this formulation, the maturity is the area under the temperature-time curve.

The second approach for analyzing maturity is the equivalent age (EQA) method, which is computed using the Nurse-Saul function as:

$$t_e = \sum \frac{(T_a - T_0)}{(T_r - T_0)} \Delta t \qquad (10)$$

where the equivalent age (t_e) is defined as the duration of the curing period at the reference temperature (T_r) resulting in the same maturity value as the curing period at any other temperature. Equation (10) can be written as:

$$t_e = \sum \alpha \Delta t \; ; \qquad (11)$$

where $\alpha = \frac{(T_a - T_0)}{(T_r - T_0)}$ is known as the age conversion factor as it converts Δt to the equivalent curing interval at the reference temperature. Alternatively, using the Arrhenius equation, Equation (10) becomes:

$$t_e = \sum e^{-Q\left(\frac{1}{T_a} - \frac{1}{T_r}\right)}.\Delta t \qquad (12)$$

where Q is the apparent activation energy divided by the universal gas constant. Like the TTF method, the equivalent age (EQA) method is an integration of time and temperature, except the temperature difference is embedded an exponential function.

Maturity measurement in the field primarily consists of monitoring the internal temperature of the concrete with respect to time by either a maturity meter or a temperature data-logger. Maturity meters are basically temperature-measuring devices that monitor temperature by attaching thermocouple wires inserted into the fresh concrete. ASTM C1074 summarizes the procedure for applying the maturity method as:

1) In the laboratory, a strength-maturity relationship is developed on the mixture to be used;
2) In the field, the temperature history of the concrete being tested is recorded from placement to the time the strength estimate is needed;
3) the maturity index is calculated; and
4) the strength at that maturity is estimated from the strength-maturity relationship.

For NDT testing programs of drilled shafts of less than 7 days in age, it is recommended to conduct a maturity and a UPV test in the laboratory prior to the strength test. A plot between the average compressive or flexural strengths and average maturity values (TTF value or equivalent age t_e) must be made and a best-fit curve obtained. The curve is used for estimating the strength of concrete based on maturity. Additionally, a plot between the average strengths and average velocity (or seismic modulus) and between average velocity and average maturity must be developed. The maturity method can then be used to compare CSL velocities, obtained at field cured temperature of less than 7 days in age, to the laboratory obtained UPV velocities as it is correlated to strength.

In addition to the above mentioned effect of temperature on velocity, several other correction factors needs to be considered, as is described next.

4.2 DIFFERENCES BETWEEN LABORATORY AND FIELD MEASUREMENTS

One important consideration is the disparity that exists between the laboratory measurement of ultrasonic pulse velocity (UPV) and CSL field derived velocity data. Specifically, it appears the UPV derived velocity from concrete cylinders to be significantly higher than field measurements of velocity using CSL method so that the entire shaft would be considered flawed. Some of the factors that are thought to be responsible for the differences between laboratory and field measurements include:

1. *Temperature Effects* – As described above, CSL field measured velocities in drilled shafts are obtained at field cured temperatures few days after the concrete placement where a non-linear temperature-dependent process affects velocity. Because the field derived CSL velocities are obtained at much higher temperatures than UPV velocities from laboratory (environmentally controlled) samples, higher UPV velocities are observed.
2. *Velocity Dispersion* - Dispersion refers to changes in sonic velocity as a function of frequency. Typically, CSL measurements are obtained around 40 kHz transducer frequencies. However UPV measurements are typically obtained at 58 kHz (as was done herein in Figures 21 and 22) resulting in higher measured UPV velocities. To correct this, it is recommended that UPV measurements be obtained using lower 40 kHz frequency transducers, which are available from NDT equipment manufacturer.
3. *Scale Factors* – For 1.2 m (4 ft) or larger diameter shafts, usually lower CSL velocities are observed in the perimeter path as compared to longer diagonal paths. One explanation for the difference of velocities with path length can be understood in terms of a self-similar (fractal) distribution of heterogeneities within the material. Therefore, a better averaging of velocities is obtained in long paths.
4. *Tube Effects* – For the perimeter paths, the effect of tube inside diameter (I.D.) and tube bending is more pronounced and must be considered as compared to the diagonal paths.
5. *Dissimilar Concrete Batches* – The field concrete is not always from the same batch proportions as the laboratory samples.

All these factors must be taken into consideration for determining the proper corrective factors that need to be applied to the laboratory data for proper calibration of the CSL/CSLT field derived velocity to concrete strength. However, the most dominant corrective factor is considered to be the temperature effects, which is described next.

4.3 TEMPERATURE MODELING

Concrete samples tested in the laboratory often show higher velocities than those inferred from CSL measurements made on shafts shortly after placement. As previously discussed in Section 4.2, one main reason for this discrepancy is the temperature difference of laboratory samples versus the much warmer concrete in a drilled shaft at the time of CSL testing. However, as described in Section 4.1.3.1, if the CSL data is compared of the same maturity as the cylinders, a better correlation is obtained.

In the next section, the results from computer-based modeling of the radial variations of temperature in drilled shafts are presented. Two-dimensional axisymmetric thermal models are computed for curing concrete shafts and samples, with the goal of understanding if these differences may arise from different thermal and curing states at the time of testing. To summarize, the laboratory samples are found to heat negligibly whereas the shafts remain warm for weeks. The dominant control on the thermal evolution of both small samples and large shafts is the primary curing period of a few days, during which most of the cement's latent heat is released. What little temperature increases can be sustained in the small samples is quickly

erased after this period, whereas the larger shafts require an additional several days to shed the bulk of their heat. Therefore, it is likely that CSL measurements made after several days to a week have elapsed since a shaft is placed will be more compatible with sample measurements. Otherwise, embedded thermocouples must be used to compare shaft velocities to laboratory sample velocities of the same maturity. In Section 4.4, a simple field experiment is described that can determine the minimum time after shaft placement when valid CSL measurements can be obtained, by repeating CSL measurements each day for a period of one week.

4.3.1 Method Used to Determine The Effect of Temperature on Velocity/Strength

The MATLAB 11 Partial Differential Equations Toolbox (Mathworks, 1998) was used to solve the parabolic (heat-flow) equation

$$(k/\rho C_p)\,\nabla^2 T = \partial T/\partial t + Q \qquad (13)$$

where T is the temperature, t is the time, k is the thermal conductivity ρ is the density, C_p is the specific heat at constant pressure, and Q is the volumetric heat production. The assumed physical parameters (adapted from Sims, 1999) are given in Table 2. The quantity κ (= $k/\rho C_p$) in Equation (13) is the thermal diffusivity and for the values selected here is $3\text{x}10^{-7}$ m^2 for concrete and $5\text{x}10^{-7}$ m^2 for earth. Therefore, heat will diffuse somewhat more readily into the ground surrounding a shaft, but not so much so that a distinct thermal boundary will remain between shaft and earth after some time.

Table 2. Material Properties.

Parameter	Concrete	Earth
Thermal conductivity k, W/m-K	1	2
Density ρ, kg/m3	3000	2000
Heat capacity C_p, J-kg/K	1000	2000

The volumetric heat production for concrete was estimated from Figure 3 in Gajda and VanGeem, 2002, for a mixture of 75% Type V cement + 25% Class F fly ash (with a total of 311 kg/m^3 (525 lb/yd^3) of cementitious materials). The adiabatic heating curve (Figure 23) was empirically fit with two linear segments. The slope of the lines is related to the heat production as

$$Q = \rho C_p\, dT/dt \qquad (14)$$

The assumed heat production due to concrete curing is then

$$Q = 675 \text{ W/m}^3,\ t < 2 \text{ days}$$
$$Q = 5.8 \text{ W/m}^3,\ t > 2 \text{ days} \qquad (15)$$

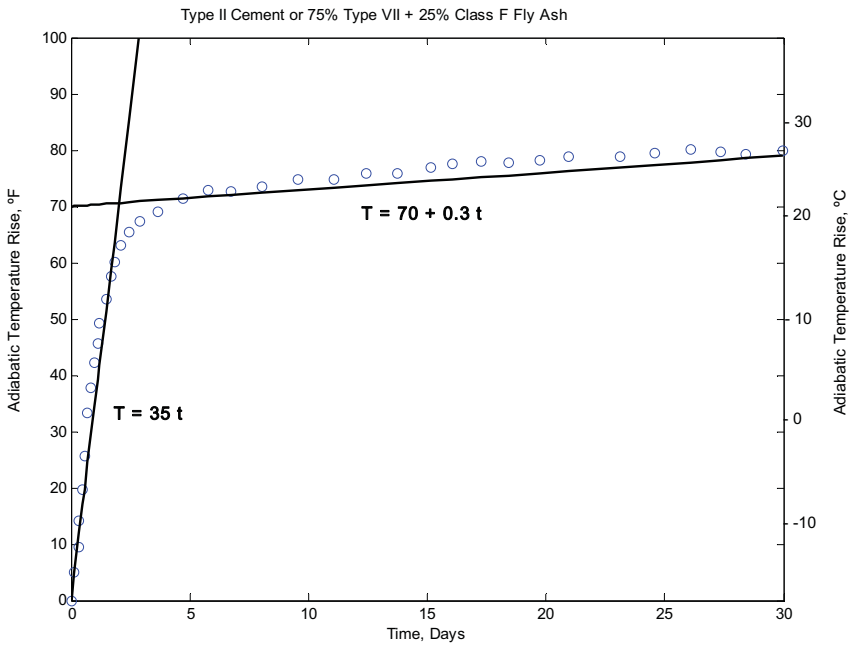

Figure 23. Plot. Adiabatic Temperature Increase vs. Time for Representative Concrete, with Approximate Linear Fits. Note Primary Curing Occurs In 2 Days.

Equation 13 was solved in two-dimensional axisymmetry. The assumed concrete shaft had a diameter of 1.5 m and a length of 10 m (4.9 x 32 ft). The assumed concrete sample had a diameter 15 cm and a length of 30 cm length (6 x 12 in). Both the sample and the shaft had zero heat flux specified across the central axis. For the sample, a film coefficient of 5 W/m^2K—appropriate to convective heat transfer to air (Welty et al., 1984)—was used at the outer boundaries. The air temperature was taken to be 0ºC (32ºF) for convenience. An alternative boundary condition that directly fixes the temperature of the outer wall of the sample at 0ºC (32ºF) is equivalent to an infinite film coefficient. No explicit boundary condition is needed at the shaft wall because it is assumed to be in contact with earth; the outer boundary of the modeled earth is, however, fixed to 0ºC (32ºF).

4.3.2 Temperature Modeling Results

Thermal models for small size concrete samples are shown in Figures 24 and 25 and models for larger size shafts are shown in Figures 26-28. The models for the samples illustrate the differences in boundary-condition assumptions: because the sample is small it has a short thermal response time of minutes to hours (time ~ $radius^2$/thermal diffusivity) and therefore the temperature distribution is strongly controlled by the interaction between internal heating and the boundary conditions. Regardless of which model is chosen, the maximum temperature increases are a few degrees Celsius and the sample cools rapidly after primary curing is completed in a few days.

The larger 1.5 m diameter shaft has a longer thermal response time (a few to several days) which, together with the insulating effect of surrounding earth, permits central peak temperatures in excess of 30ºC (86ºF) and mean temperatures of ~15ºC (59ºF) to develop. Note that the adiabatic temperature increase (i.e., for a perfectly insulated shaft) over the 2-day primary curing

period is ~40ºC (104ºF). Cooling in the shaft is commensurately slow, with temperatures exceeding the maxima observed in the sample (~5ºC (41ºF)) to persist for 3-4 weeks or greater. When curing retardants are added (to impede concrete curing process), the peak temperature is reduced, but the interaction between reduced peak temperature and longer cooling time approximately cancel with regard to the time over which elevated temperatures are observed. In other words, the cooling time to 5ºC (41ºF) is relatively unchanged.

In summary, concrete samples are expected to show only very small temperature increases with prompt cooling after primary curing is completed. For all practical purposes, the interior of concrete samples is therefore at ambient temperature when UPV measurements are performed. Concrete shafts show temperature increases of a few to several tens of degrees Celsius for the first week after concrete is placed, with mean temperatures in excess of the maximum observed in the sample to persist for a month or more. Therefore the shaft is always warm relative to the sample when UPV-CSL measurements are made in the field.

In solid rock—such as sandstone with similar properties as concrete—sound speed varies only slightly with temperature, of order 5%/100ºC (5%/212ºF) (Sheriff and Geldart, 1995). However, the sound speed in rocks saturated with heavy crude oil or tar varies as much as 20%/100ºC (20%/212ºF). For the maximum average temperature differences of a few-to-several tens of degrees Celsius modeled here between samples and shafts, velocity differences of only a few percent would be expected. In practice, mean shaft velocities derived from CSL can be >20% below sample measurements.

It is, therefore, possible that for concrete, there is a nonlinear temperature-dependent process affecting velocity, such as fluid interconnectivity or other strong dependence of elastic constants on curing state. During primary curing there is probably still extensive fluid interconnection. As many CSL measurements are made within a day after placement, concrete may be relatively solid but incompletely cured, and interconnected fluid pathways that persist at elevated temperatures of a few tens of degrees Celsius may reduce mean velocities. If CSL measurements are made after a few thermal response times following primary curing (i.e., ~7 days after placement), then any residual fluid is probably no longer interconnected and velocities are more comparable to those observed in samples. A simple field experiment was conducted and presented in Section 4.4 to examine these characteristics by repeat CSL measurements at intervals of a day and correlation with the temperature profiles.

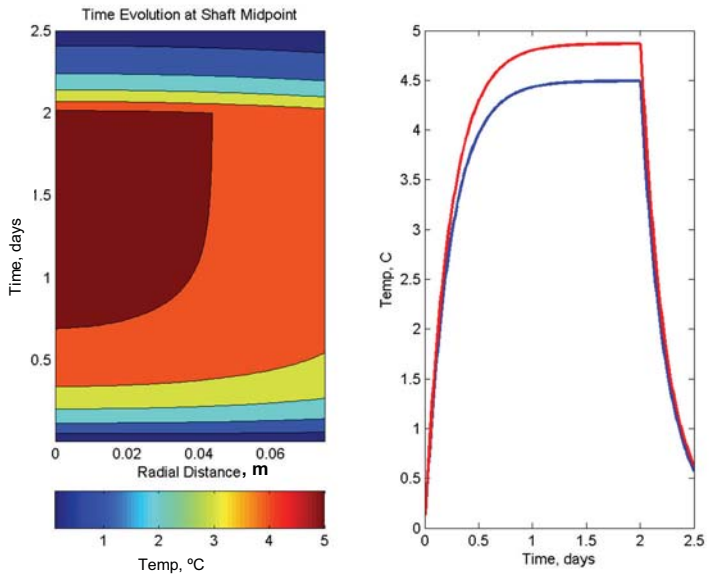

Figure 24. Chart. Thermal Evolution of 15 x 30 cm (6 x 12 in) Concrete Sample under Nominal Convective Cooling to Surrounding Air. Left: Radial Slices at Vertical Midpoint (i.e., at 15 cm (6 in) of 30 cm (12 in) length). Right: Upper Curve (Red) is Shaft Midpoint (Equivalent to Left Vertical Axis on Left-Hand Plot). Lower (Blue) Curve is Average Temperature in the Sample. Curves are Close because Boundary Layer to Convecting Air Effectively Retains Heat. Average Temperature Increase is < 5ºC.

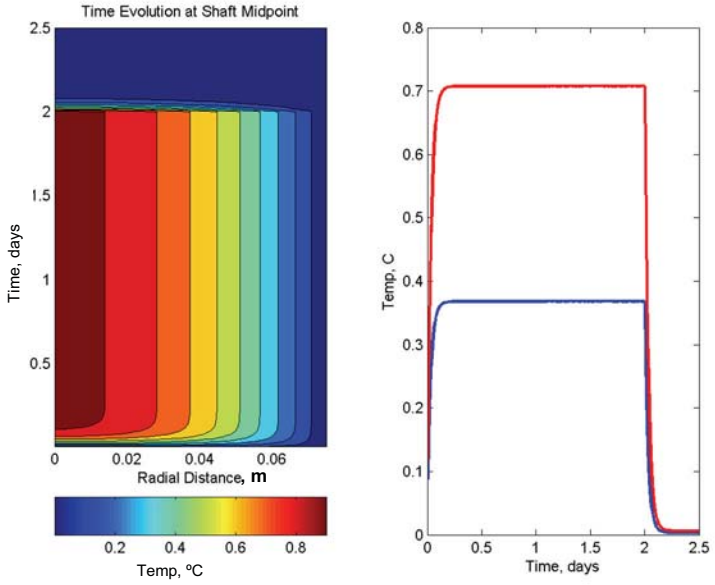

Figure 25. Chart. As Figure 24, but with Constant-Temperature Outer Boundary Condition, Appropriate to Maximally Efficient Convective Cooling to Surrounding Air. Note Strong Radial Temperature Gradients and Large Difference in Central Vs. Mean Temperatures because of Fixed-Temperature Boundary Condition. Maximum Temperature Increase is < 1ºC.

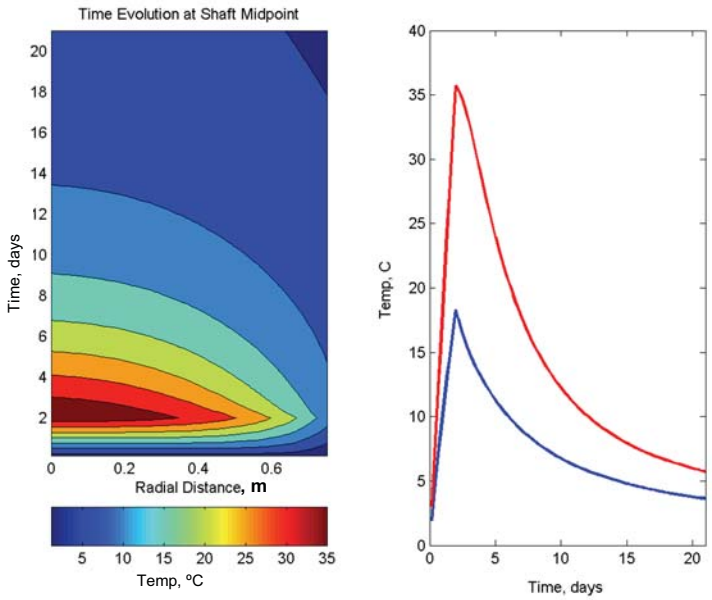

Figure 26. Chart. Thermal Evolution of Nominal Drilled Shaft. Maximum Temperature Increase ~35ºC, Mean Temperature Increase ~18ºC, Temperatures in Excess of Maxima (Peak) in Sample Persist for > 3 Weeks.

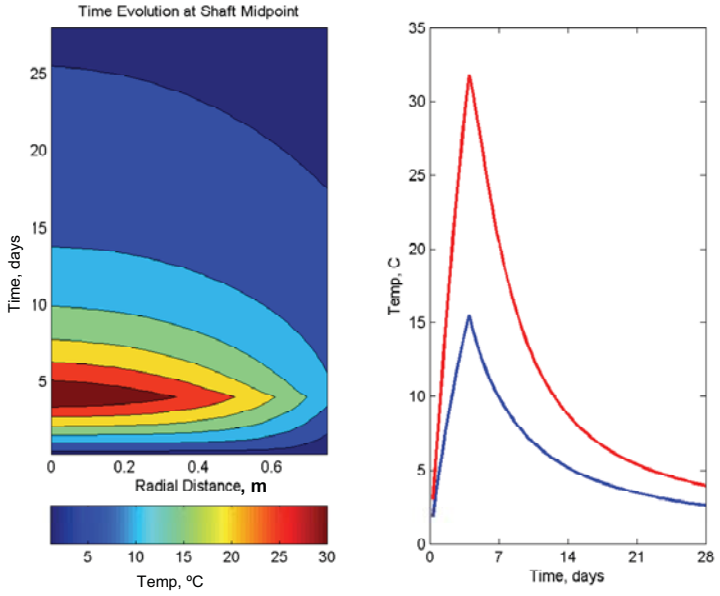

Figure 27. Chart. Thermal Evolution of Nominal Shaft with Curing Retarded by a Factor of 2 (End of First Phase of Curing at 4 Days, with Commensurate Decrease in Heating Rate). Peak Temperatures are Reduced only Slightly because Thermal Response Time of Shaft is still Comparable to Curing Time.

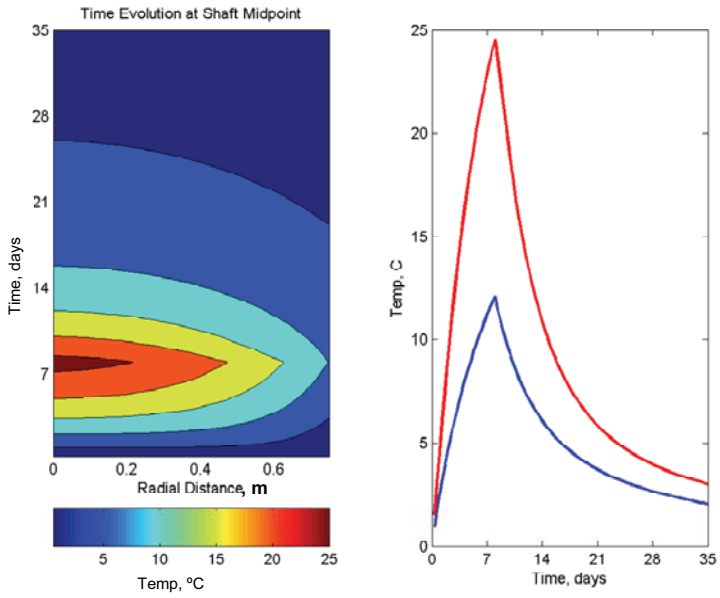

Figure 28. Chart. Thermal Evolution of Nominal Shaft with Curing Retarded by a Factor of 4. Peak Temperatures now Begin to Show Significant Reduction because Shaft Thermal Response Time (a Few Days) is Noticeably Smaller than Primary Curing Period (8 Days). Temperatures in excess of Sample Maxima are Relatively Unaffected, still Remaining High for >3 Weeks.

4.4 CONTINUOUS FIELD MONITORING OF DRILLED SHAFT FOUNDATIONS FOR CHANGES IN TEMPERATURE, VELOCITY, DENSITY, AND MOISTURE

In order to understand the mechanism by which a typical drilled shaft foundation cures under field conditions, two (2) shafts were monitored for up to seven (7) days using four (4) geophysical logging methods at the Hagerman National Wildlife Refuge near Sherman, Texas. The geophysical logging methods used included: 1) temperature logging to monitor changes in shaft's temperature; 2) crosshole sonic logging (CSL) to monitor changes in velocity; 3) gamma-gamma density logging (GDL) to monitor changes in density; and, 4) neutron-moisture logging (NML) to monitor changes in moisture.

4.4.1 Temperature Monitoring Results

Temperature monitoring was performed on two shafts at the Hagerman National Wildlife Refuge using both temperature logging and embedded thermocouples. In addition, one drilled shaft was monitored at the Sevenmile-Gooseberry Project, near Salina, Utah using only thermocouples.

4.4.1.1 *Temperature Monitoring Using Geophysical Temperature Logging*

Two (2) drilled shafts were continuously monitored using temperature logging method at the Hagerman National Wildlife Refuge, TX. These shafts were 0.9-1 m (3-3.5 ft) in diameter, between 13-14.5 m (42.5-47.5 ft) in depth, and were built as part of Harris Creek Bridge Project by the Federal Highway Administration-Central Federal Lands Highway Division. The two-span bridge contained two (2) abutments and one (1) pier line with two (2) shafts per substructure unit. Each shaft contained four 5-cm (2-in) Inside Diameter (I.D.) steel access tubes. Temperature logging was performed at Abutment 1, Shaft 1 and Pier 2, Shaft 2. Thermocouples were also installed in Abutment 2, Shaft 2 to monitor temperature of concrete continuously between August 31 to September 7, 2004. Class A (AE) concrete with required 28-day breaking strength of 27,600 kPa (4,000 psi) placement slump of 25-100 mm (1-4 inch), water/cement ratio of 0.44 (by weight) and air content of 5% was used to construct the drilled shaft.

Abutment 1, Shaft 1

Figure 29 displays the temperature monitoring results from Abutment 1 Shaft 1. The plots show temperature at 6 hours (shown in black), 12 hours (blue), and 24 hours (red) after the concrete placement. An initial rise in the shaft's temperature is observed in the first 24 hours after the concrete placement. In this figure, the temperature logs from four access tubes in the shaft are displayed as a function of depth on the vertical axis. Also presented in the depth axis is the soil profile as reported by the boring logs. The soil profile consisted of a gravel/boulders bed on the top 0.2 m (0.8 ft) followed by sand (mixed with clay) to 6.7 m (22 ft) depth, clay (mixed with sand) to 14 m (46 ft) depth, overlying blue shale bedrock. Groundwater table was at 3.8 m (12.5 ft) depth.

In Figure 30, the temperature logs from the first 24 hours after the concrete placement were combined with other temperature logs from two to six days indicating a gradual decrease in

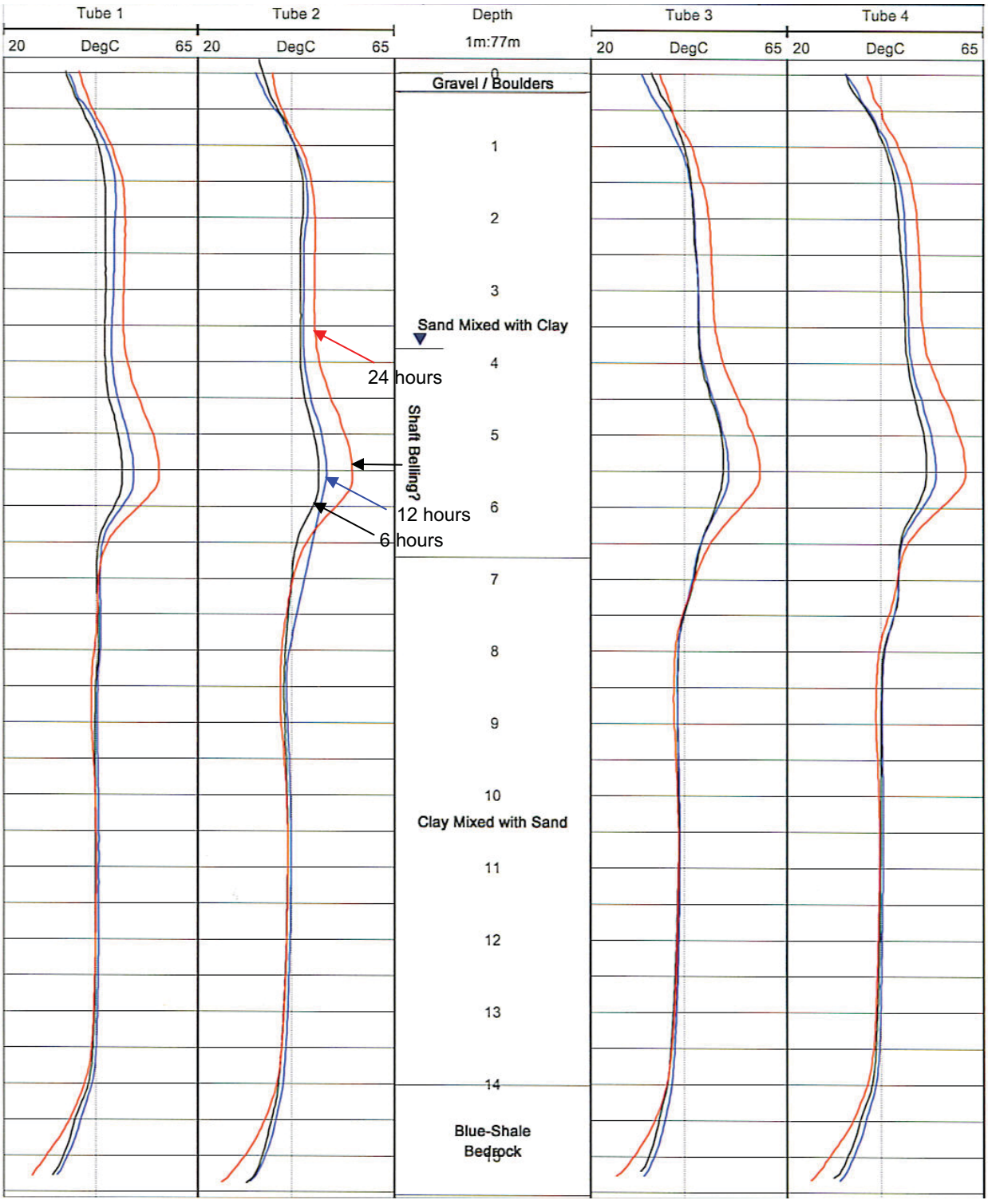

Figure 29. Plot. Temperature Monitoring of Abutment 1 Shaft 1. Hagerman National Wildlife Refuge, TX. Temperature Curves at 6 Hours (Black), 12 Hours (Blue) and 24 Hours (Red) After the Concrete Placement. Vertical Guideline: 41.5 ºC.

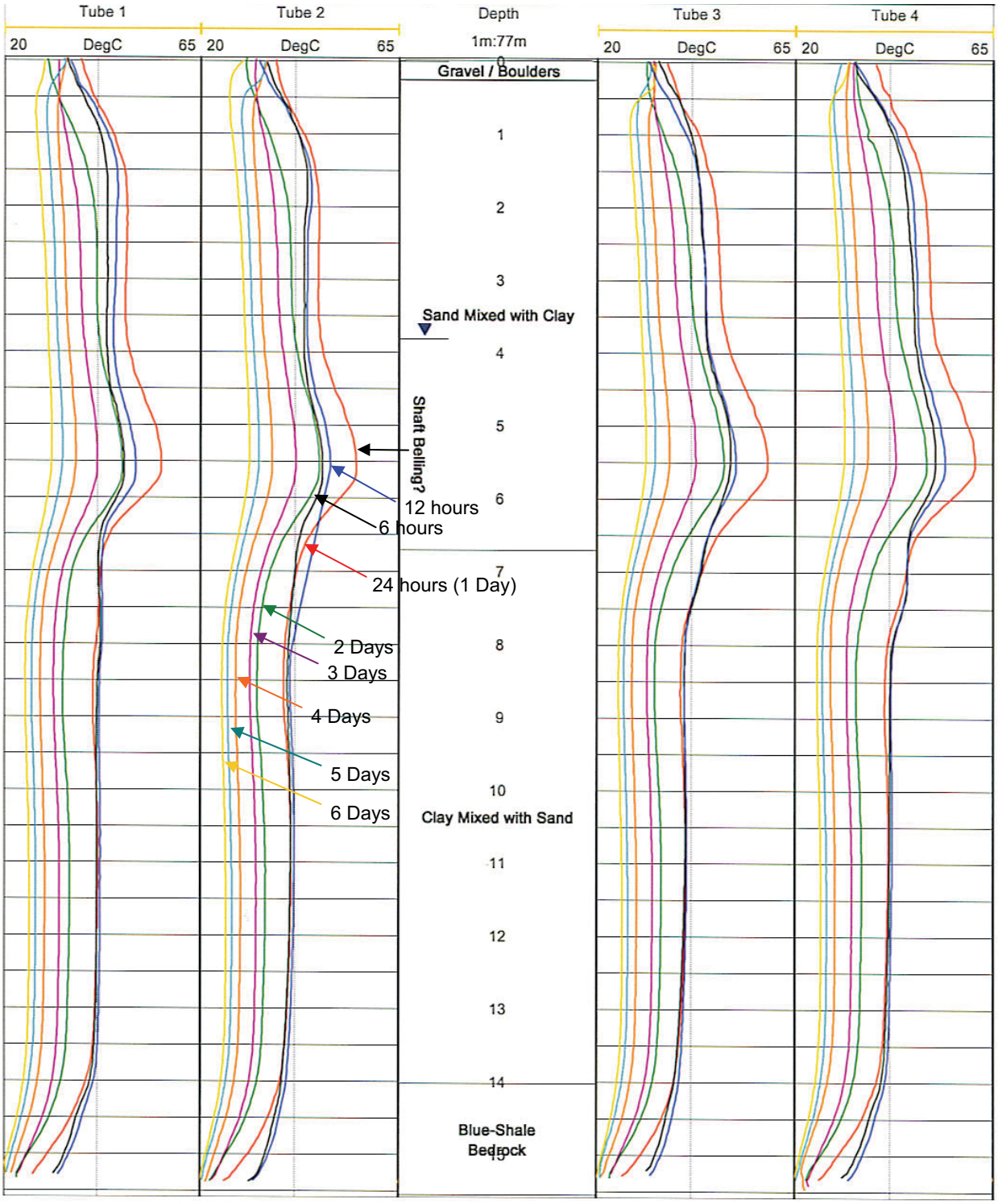

Figure 30. Plot. Temperature Monitoring of Abutment 1 Shaft 1. Hagerman National Wildlife Refuge, TX. Temperature Curves at 6 Hours (Black), 12 Hours (Blue), 24 Hours (1 Day, Red), 2 Days (Green), 3 Days (Purple), 4 Days (Orange), 5 Days (Teal), and 6 Days (Yellow) After the Concrete Placement. Vertical Guideline: 41.5 ºC.

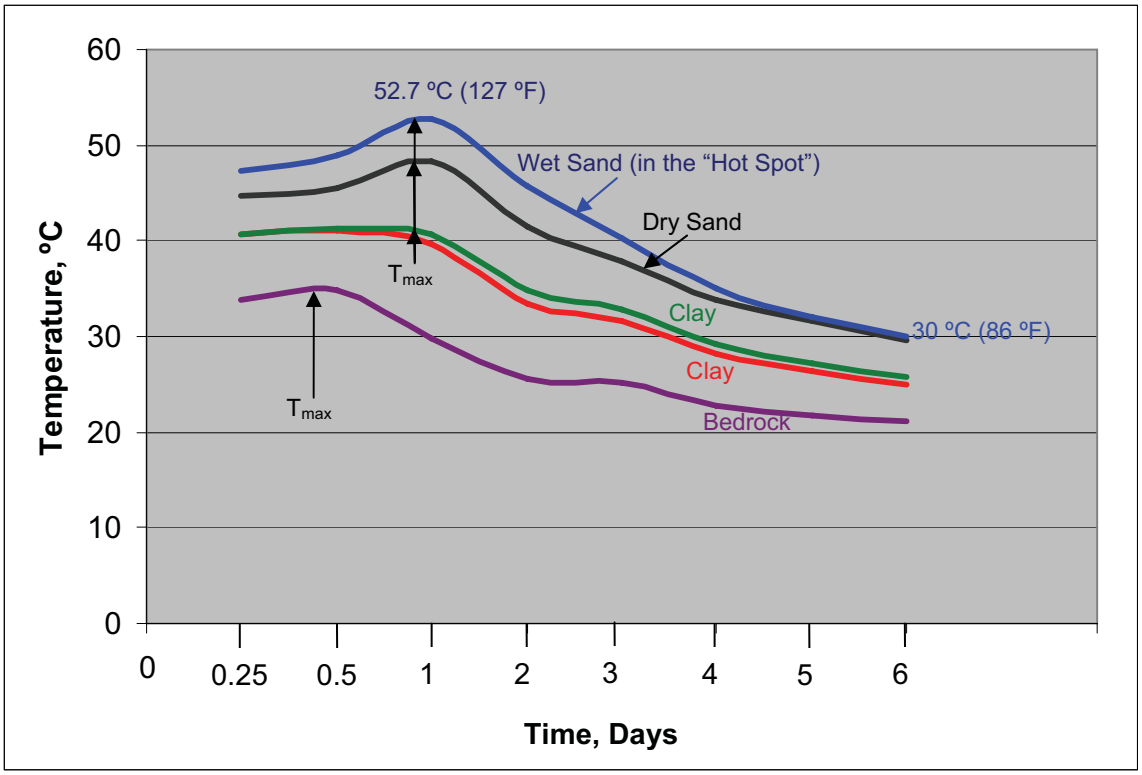

Figure 31. Graph. Temperature Monitoring of Abutment 1 Shaft 1. Hagerman National Wildlife Refuge, TX. Temperature Values are Averaged from the Four Access Tubes at 3m (Black), 6 m (Blue), 9 m (Red), 12 m (Green), and 15 m (Magenta) Depth Points.

temperature after the initial rise. Therefore, in this figure, the complete thermal history of the shaft in the first 6 days after the concrete placement is presented.

Finally, temperature values at five different depth points in Figure 30 are plotted as a function of time in Figure 31. In this figure, the temperature values from the four access tubes are averaged at 3m (in sand above the groundwater table displayed in black); at 6 m (in sand below the groundwater table in blue); at 9 m (clay in red); at 12 m (clay in green); and at 15 m (bed rock in magenta) levels.

The following conclusions can be drawn from the temperature logging studies from this shaft:

1. At a given time period after the concrete placement, the shape of the temperature curve appears to be a function of the thermal conductivity of the soil/rock at the hole. Therefore, in a typical drilled shaft, the shaft's temperature, and its curing rate or age, is non-uniform with depth. In our example, the shaft's temperature was highest (least cure) in the sand/gravel zones, cooler in the clayey zone, and coolest (most cure) at the bedrock level.
2. In the sandy zone, shaft's temperature rises more rapidly than at the clay and bedrock levels. From Figure 31, it is evident that peak temperature was reached about 12 hours after the concrete placement in the clay and bedrock levels as compared to 24 hours in the sand level. Peak temperatures were reached after 12 hours at 9 m, 12 m, and 15 m depths and after 24 hours at 3m and 6 m depths. The maximum temperature reached

was at 52.7 ºC (127 ºF) (at 6 m depth) which was reduced to 30 ºC (86 ºF) after 6 days. Maximum temperature differential in the shaft after 1 day of curing was about 23 ºC (41 ºF). This differential was reduced to 9 ºC (16 ºF) after 6 days of curing making the temperature curve more uniform in shape (compare the shape of the yellow curve (6 days old) to the red curve (1 day old) in Figure 30).

3. A localized "hot spot" was observed in Abutment 1 Shaft 1 as shown in Figures 29 and 30 between the depths of 3.7-7.7 m (12-25 ft). According to the construction records, an additional 6-7.5 m^3 (8-10 $yard^3$) of concrete had to be used at these depths. Therefore, it appears that the higher temperatures can be due to shaft belling at these depths.
4. Near the surface, in the top 1 m (3.3 ft) cooler temperatures were observed due to heat escaping to the air. For Tubes 2 and 3, shaft's temperature actually decreased between 6 to 12 hours before rising in 24 hours (Figure 29). After 24 hours, the temperature decreased except in the top 0.6 m (2 ft) which started to increase again after 3 days (Figure 30). Therefore, high fluctuation in temperature was observed in top 0.6 m (2 ft) of the shaft.

Pier 2, Shaft 2

A second set of temperature monitoring study was conducted in Pier 2, Shaft 2. The results are shown in Figure 32 from 1 hour to 6 days after the concrete placement. The soil profile consisted of a peat gravel on the top 1.22 m (4 ft) followed by clay with organics to 2.3 m (7.5 ft) depth, clay to 11.28 m (37 ft) depth, overlying a blue shale bedrock. Groundwater table was at the ground surface.

In Figure 33, temperature values at five different depth points are plotted as a function of time. In this figure, the temperature values from the four access tubes are averaged at 0.8 m (in gravel displayed in black); at 5 m (in clay in blue); at 10 m (clay in red); and at 12.5 m (shale bedrock in green).

The following conclusions can be drawn from the temperature logging studies from this shaft:

1. At a given time period after the concrete placement, the shape of the temperature curve appears to be a function of the thermal conductivity of the soil/rock at the hole. The shaft's temperature was highest (least cure) in the clay zone, cooler near the surface, and coolest (most cure) in the bedrock. No localized "hot spot" was observed in this dataset.
2. From Figure 33, it is evident that peak temperatures were reached after 24 hours. The maximum temperature reached was at 53 ºC (127 ºF) (at 5 m depth) which was reduced to 35 ºC (95 ºF) after 5 days. Maximum temperature differential in the shaft (at different depth levels) was about 10 ºC (18 ºF) after 6 hours (0.04 days) of curing. This differential was reduced to 3.7 ºC (6.6 ºF) after 5 days of curing making the temperature curve more uniform in shape (compare the shape of the teal curve (5 days old) to the black curve (1 hour old) in Figure 32).
3. Near the surface, in the top 1 m (3.3 ft) cooler temperatures were observed due to heat escaping to the air.

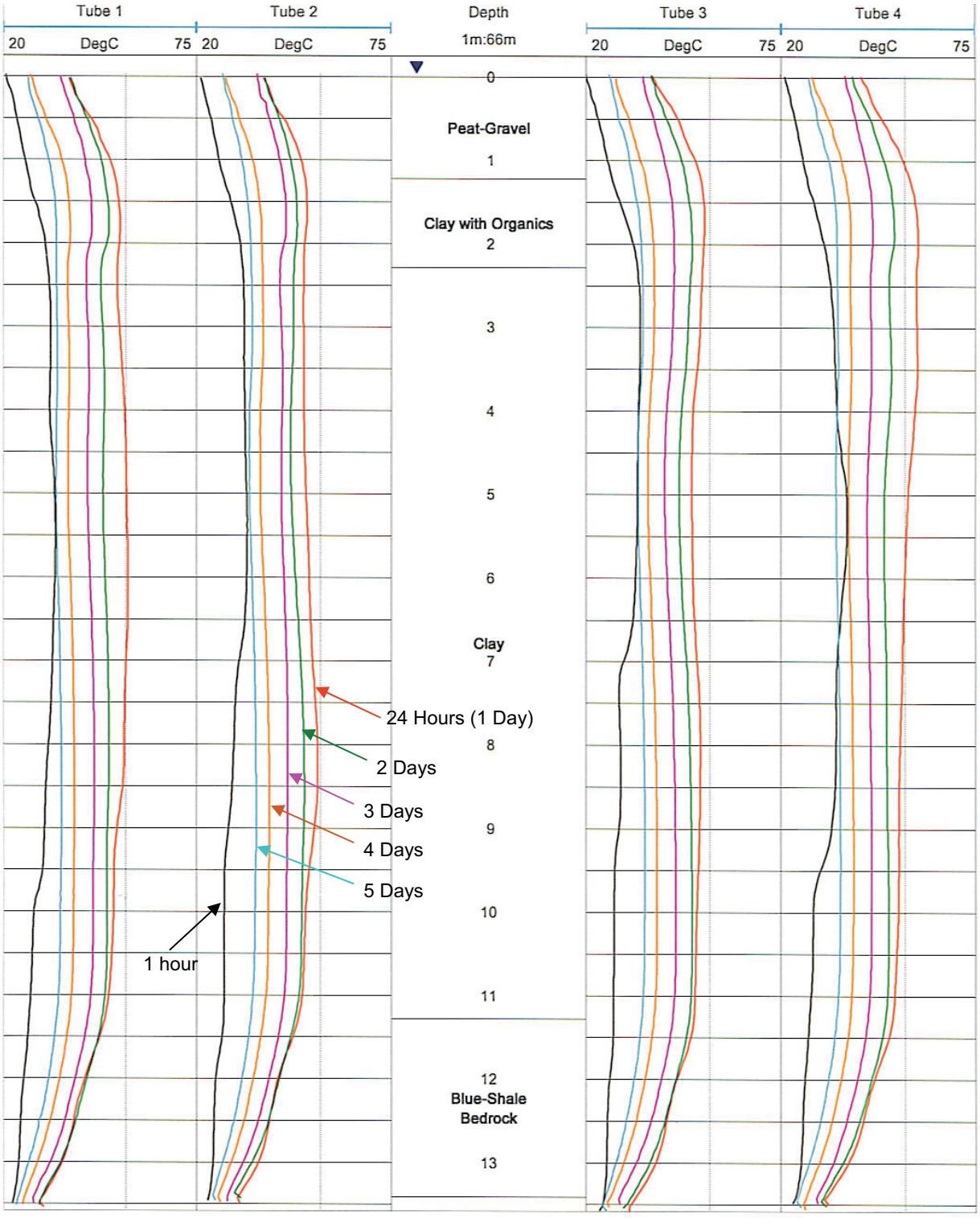

Figure 32. Plot. Temperature Monitoring of Pier 2 Shaft 2. Hagerman National Wildlife Refuge, TX. Temperature Curves at 1 Hour (Black), 24 Hours (1 Day, Red), 2 Days (Green), 3 Days (Purple), 4 Days (Orange), and 5 Days (Teal) After the Concrete Placement. Vertical Guideline: 55 ºC.

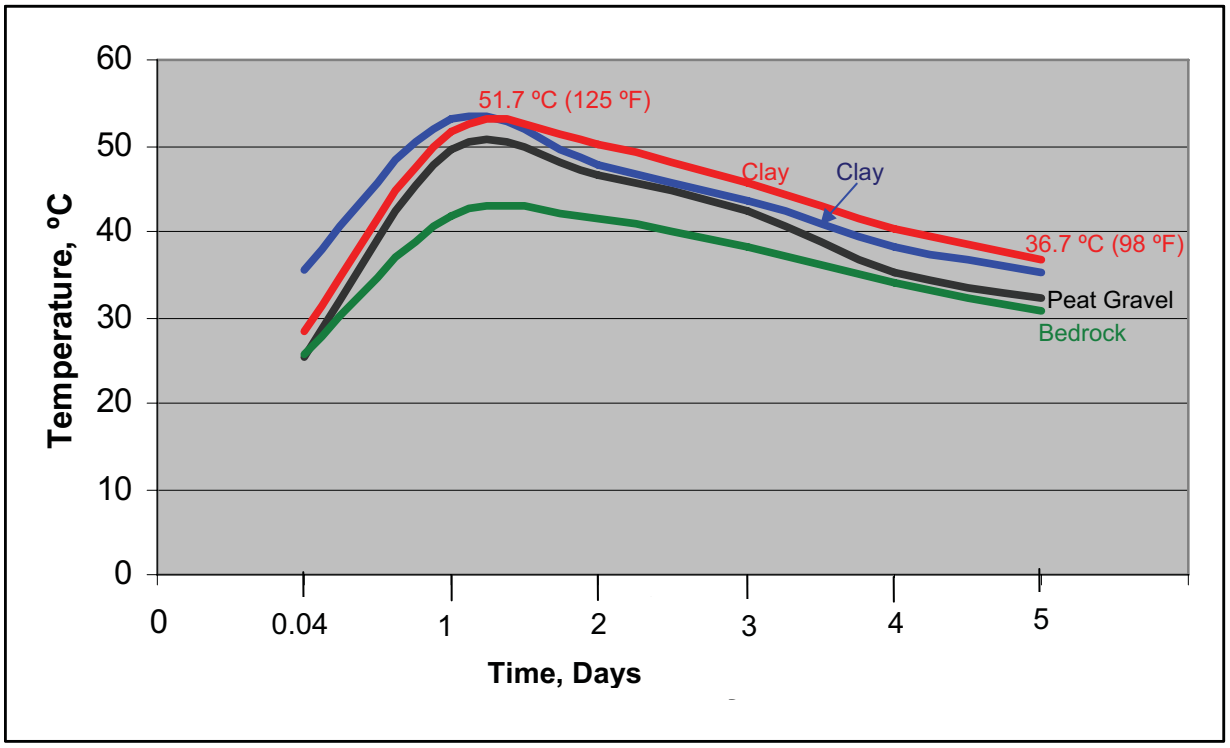

Figure 33. Graph. Temperature Monitoring of Pier 2 Shaft 2. Hagerman National Wildlife Refuge, TX. Temperature Values are Averaged from the Four Access Tubes at 0.8m (Black, Gravel), 5 m (Blue, Clay), 10 m (Red, Clay), and 12.5 m (Green, Shale Bedrock) Depth Points.

4.4.1.2 *Temperature Monitoring Using Embedded Thermocouples*

Embedded thermocouples were used in order to monitor shaft's temperature at two sites, as is described next.

I. Hagerman National Wildlife Refuge Project.

At the Hagerman National Wildlife Refuge Project, a third shaft—Abutment 2, Shaft 2, was monitored with two thermocouples one installed at the *center* and the other attached to the rebar cage (*side*) at 2.4 m (8 ft) depth. The center thermocouple was attached to a single rebar that was pushed in the shaft immediately after the concrete placement. This study was performed to investigate the temperature differential between the center of the shaft and the side of the shaft at the rebar cage level.

As shown in Figure 34, peak temperature was reached after 26 hours both at the center and at the rebar cage in the shaft. The maximum temperature reached was at 68.3 ºC (155 ºF) at the center and 66.1 º C (151 ºF) at the cage. Maximum temperature differential between the center and the side was recorded at 5 ºC (9 ºF) after 29 hours after concrete placement.

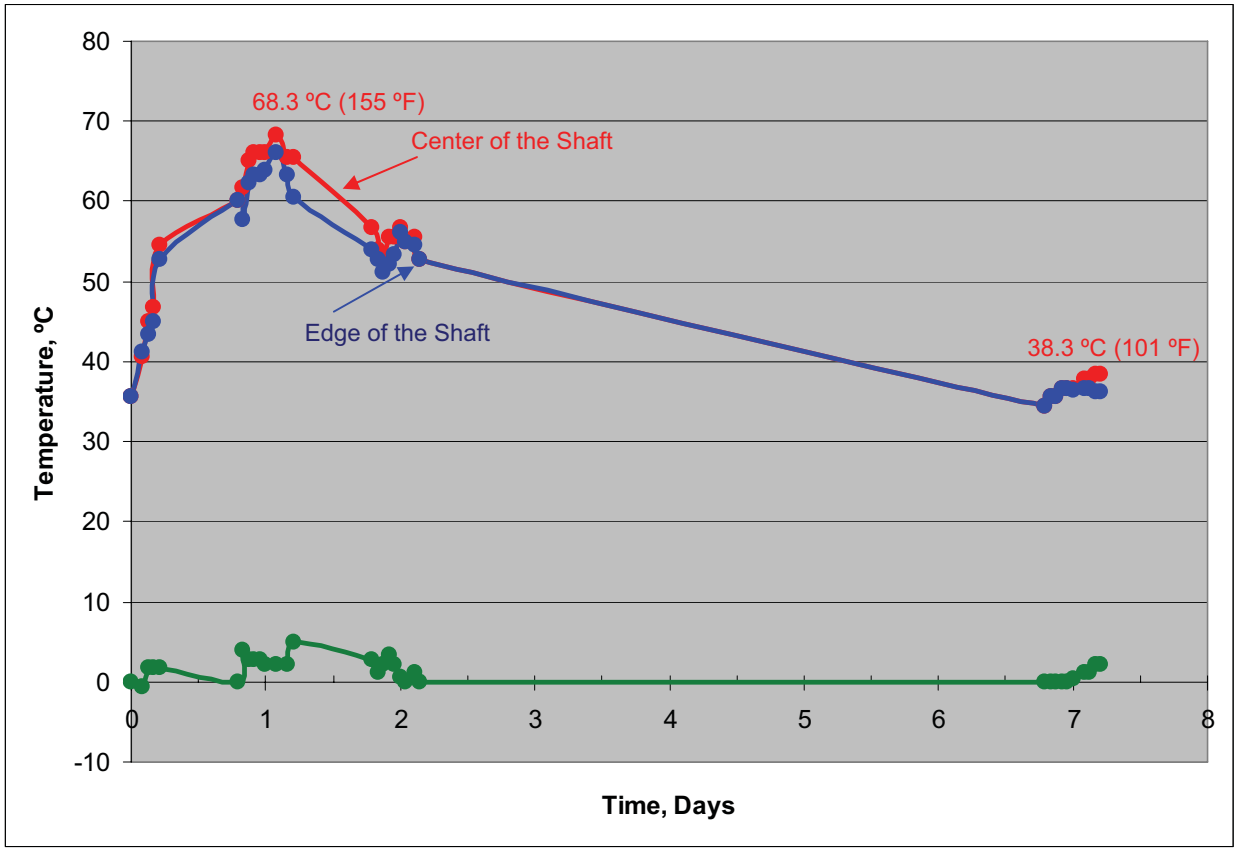

Figure 34. Graph. Temperature Monitoring of Abutment 2 Shaft 2 Using Embedded Thermocouples. The Red Curve Displays the Temperature Readings at the Center of the Shaft at 2.4 m (8 ft), Blue Curve Displays Temperature Reading Near the Rebar Cage at the Same Depth, and the Green Curve Displays the Temperature Differential Between the Two Stations. Hagerman National Wildlife Refuge, TX.

II. Sevenmile-Gooseberry Road Project

At another project, drilled shaft P-3 from the Sevenmile-Gooseberry Road CFLHD Project near Salina, Utah was continuously monitored for a period of 18 days with results shown in Figure 35. Two thermocouple probes were installed outside the rebar cage in approximately two o'clock position (with twelve o' clock representing North) at 3.66 m (12 ft, shown in red) and 12.8 m (42 ft shown in blue) depths. Since the groundwater table was 8.23 m (27 ft), the two probes were located at 4.57 m (15 ft) above and below the groundwater table.

Class A 19-cm (7.5-inch) slump concrete with 6.0% air was used. The concrete temperature at the delivery was 11.1 ºC (52 ºF). Concrete was placed on May 15, 2004 at 12:30 p.m. and the concrete placement was completed at 2 p.m., where the first temperature readings were taken.

As shown in Figure 35, peak temperature was reached after about 20 hours at 41 ºC (106 ºF).

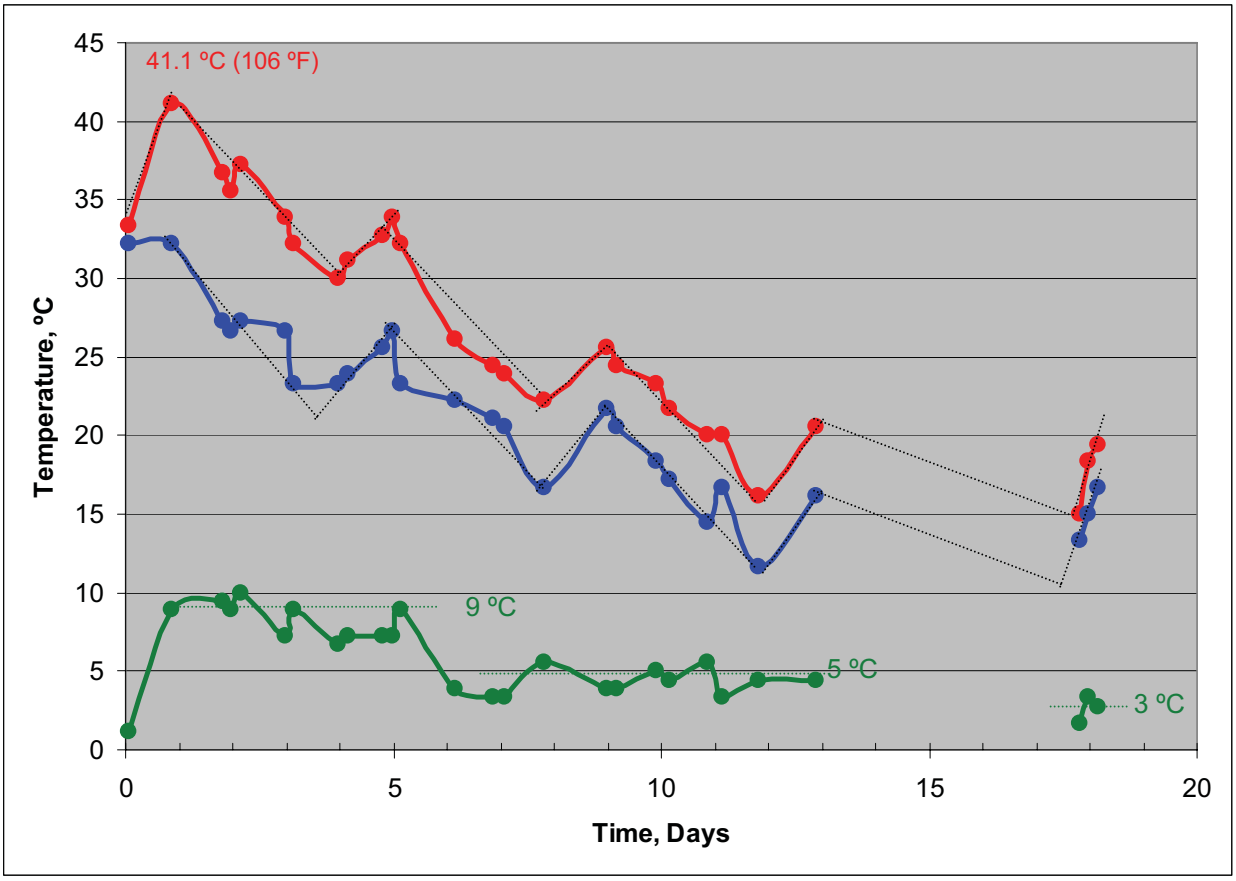

Figure 35. Plot. Temperature Monitoring of Shaft P-3 Using Embedded Thermocouples Near the Rebar Cage. The Red Curve Displays the Temperature Readings at 3.66 m (12 ft) (Above the Groundwater Table), Blue Curve at 12.8 m (42 ft) (Below the Groundwater Table), and the Green Curve Displays the Temperature Differential Between the Two Stations. Gooseberry-Sevenmile Project, UT.

The following conclusions can be drawn from this study:

1. At both measurement depths, the temperature curves are similar in shape and both decrease with time as the shaft is loosing heat as the result of heat of hydration.
2. The shaft temperature measurements at the rebar cage are not uniform with depth. As expected, the groundwater table acted as a heat sink with the thermocouple placed at 4.57 m (15 ft) below the groundwater table measuring lower average temperatures than the one placed at 4.57 m (15 ft) above the groundwater table. Therefore, the shaft is generally hotter (less cured) above the groundwater table.
3. Interestingly, at each measurement location, the temperature curve seems to recover and display distinct temperature jumps at about 4-day intervals.
4. The temperature differential between the two stations decreased with time as the shaft's temperature (or curing rate) becomes more uniform with time. The temperature difference at the two stations is about 9 ºC (16ºF) for the first 1-5 days, decreasing to

about 5ºC (9 ºF) for the next 7 days, and to about 3 ºC (5.4 ºF) after 18 days of measurement.

4.4.1.3 *Conclusions — Temperature Monitoring Studies*

From both the temperature logging and embedded thermocouples studies, the following can be concluded:

- For the small diameter shafts under this study (less than 1 m (3.5 ft) in diameter), peak temperatures of about 41-68 ºC (106-154 ºF) were reached between 12- 26 hours after concrete placement.
- The peak temperatures were reduced to about 23-35 ºC (73-95 ºF) after 6 days and about 12 ºC (54 ºF) after 12 days following concrete placement.
- Shaft's curing rate (or age) is non-uniform as a function of depth in the first 6-7 days. It depends on shaft's diameter, soil properties at the hole, and groundwater table depth.
- After 6-7 days the shafts' temperature curve (and age) appear to reach a more uniform in shape with temperature differential of less than 5ºC (9 ºF) throughout.
- Therefore, if the CSL measurements (or tomographic imaging) are performed before the first 7 days of concrete placement, the sonic velocities (as it relates to concrete strength) will be lower than the lab measurements and non-uniform with depth, unless the concrete strength are based on maturity calculations.
- Temperature logging can be used to observe relative changes in thermal conductivity and possibly infer general soil properties.
- Temperature logging may also be used to detect shaft belling.
- Temperature logging can be used to measure shaft's peak temperature and temperature differential between the center and the edge (with insertion of a thermocouple in the center). This data can be used to mitigate thermal cracking and durability problems in the shaft. According to Gajda and Vangeem (2002), in mass concrete "temperature limits are specified to seemingly arbitrary values of 57ºC (135ºF) for the maximum allowable concrete temperature and 19ºC (35ºF) for the maximum allowable temperature difference between the center and the surface of the mass concrete section". A study is warranted to define these parameters in a drilled shaft environment.

4.4.2 Velocity Monitoring Results

Figure 36 displays the velocity monitoring results from Abutment 1 Shaft 1 at the Hagerman National Wildlife Refuge, TX from 1 day to 6 days after the concrete placement. Six crosshole sonic logs (CSL) were acquired using 4 perimeter logs and 2 diagonal logs. In Figure 36, the static-corrected CSL results are plotted in 6 separate sub-plots from 6 different access-tube pair combinations as indicated on the top label. Depths were measured from the top of the shaft and are shown on the vertical axis. Also presented in the depth axis is the soil profile as reported by the boring logs. In Figure 37, the diagonal CSL Paths 1-3 and 2-4 are plotted in an expanded scale and in Figure 38, the CSL values from four access tubes are averaged at five different depth points and plotted as a function of time.

Unfortunately, large tube bending was observed in top 7.5 m (24.6 ft) of the shaft (particularly note Path 3-4). This made static correction more difficult to apply. Also, it appears that low velocity values were observed in the bottom 1 m (3.3 ft) of the shaft.

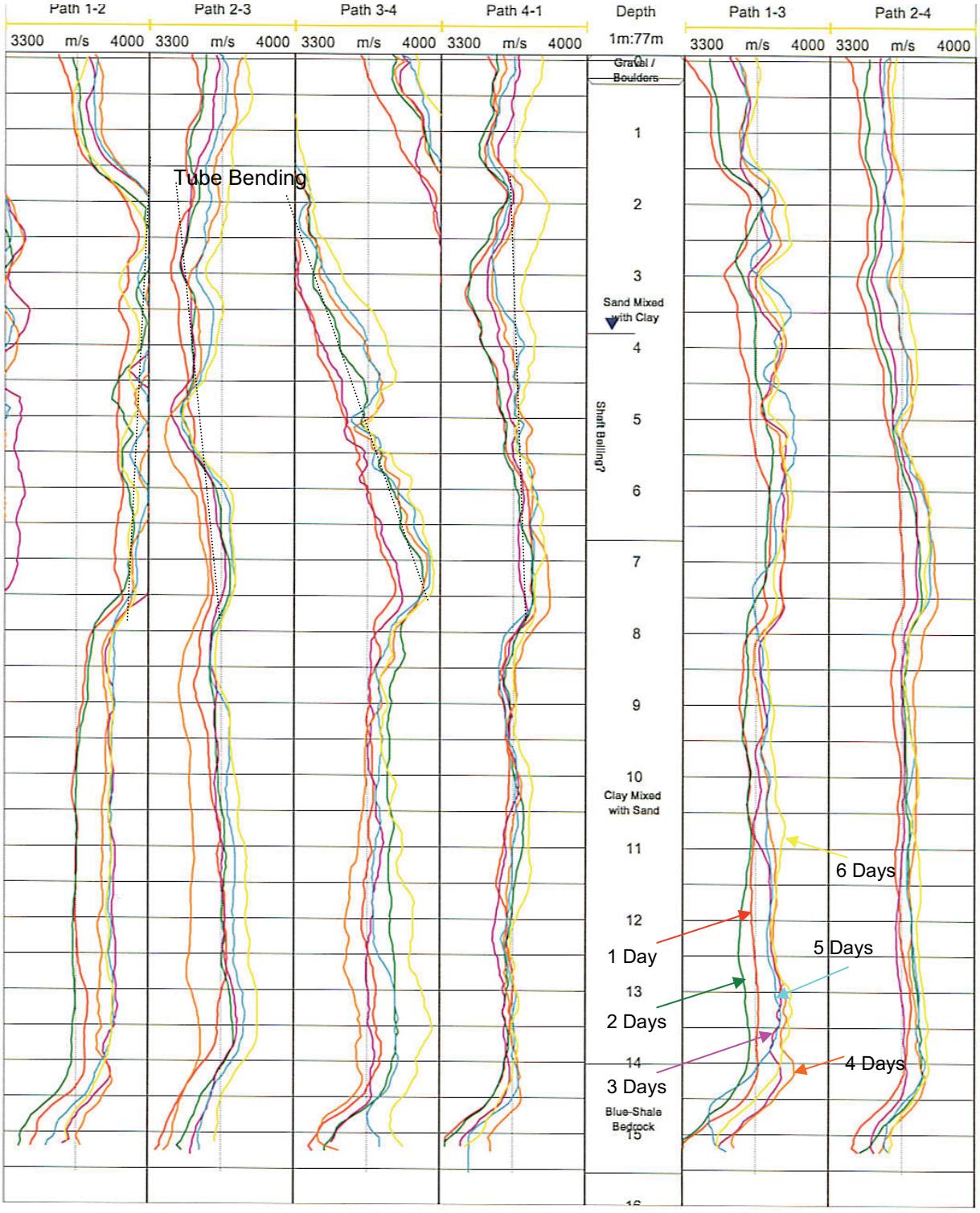

Figure 36. Plot. Velocity Monitoring of Abutment 1 Shaft 1. Hagerman National Wildlife Refuge, TX. CSL Velocity Curves at 1 Day (Red), 2 Days (Green), 3 Days (Purple), 4 Days (Orange), 5 Days (Teal), and 6 Days (Yellow) After the Concrete Placement. Vertical Guideline: 3,650 m/s.

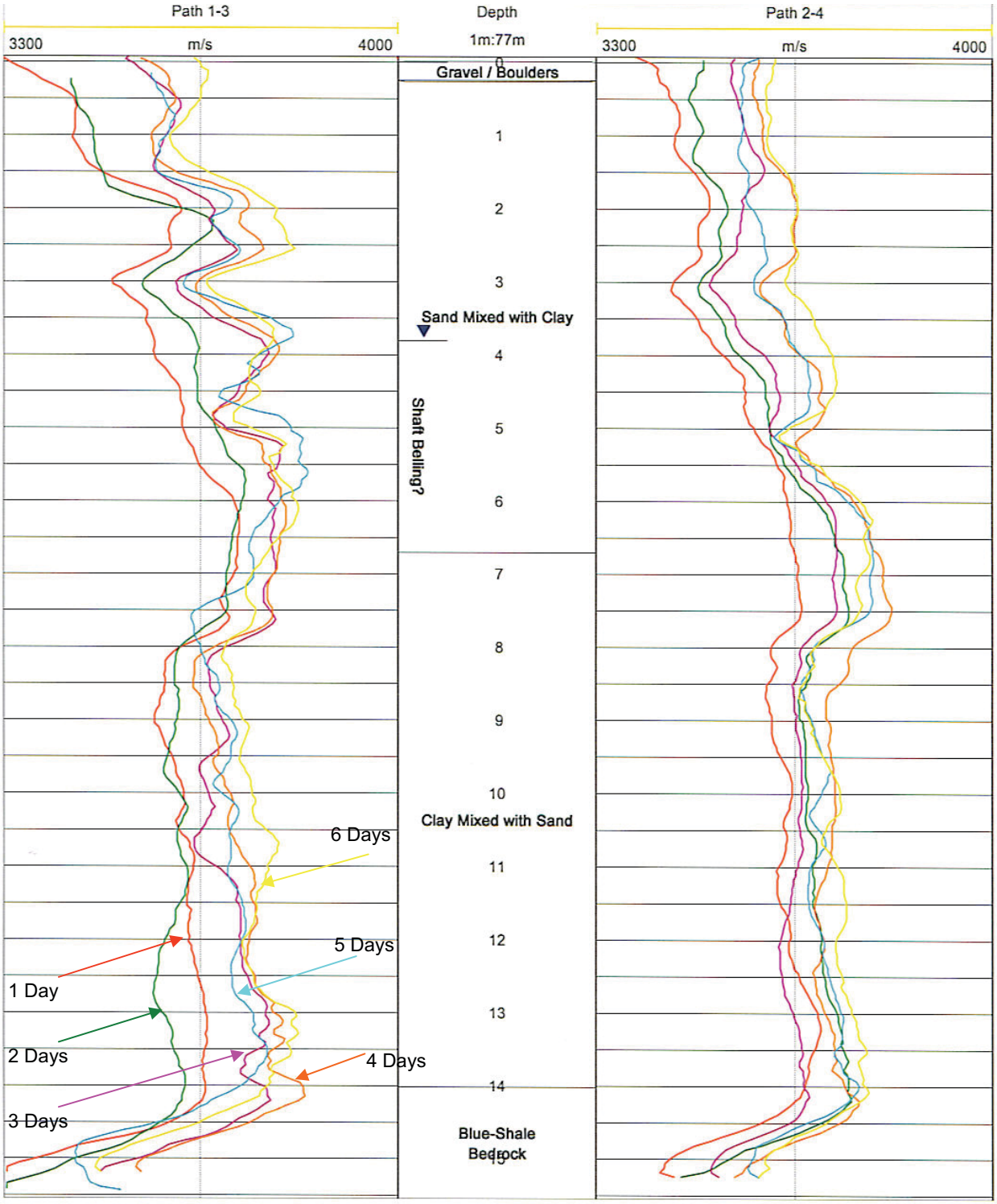

Figure 37. Plot. Velocity Monitoring of Abutment 1 Shaft 1. Hagerman National Wildlife Refuge, TX. CSL Velocity Curves from Tube Paths 1-3 and 2-4 at 1 Day (Red), 2 Days (Green), 3 Days (Purple), 4 Days (Orange), 5 Days (Teal), and 6 Days (Yellow) after Concrete Placement. Vertical Guideline: 3,650 m/s.

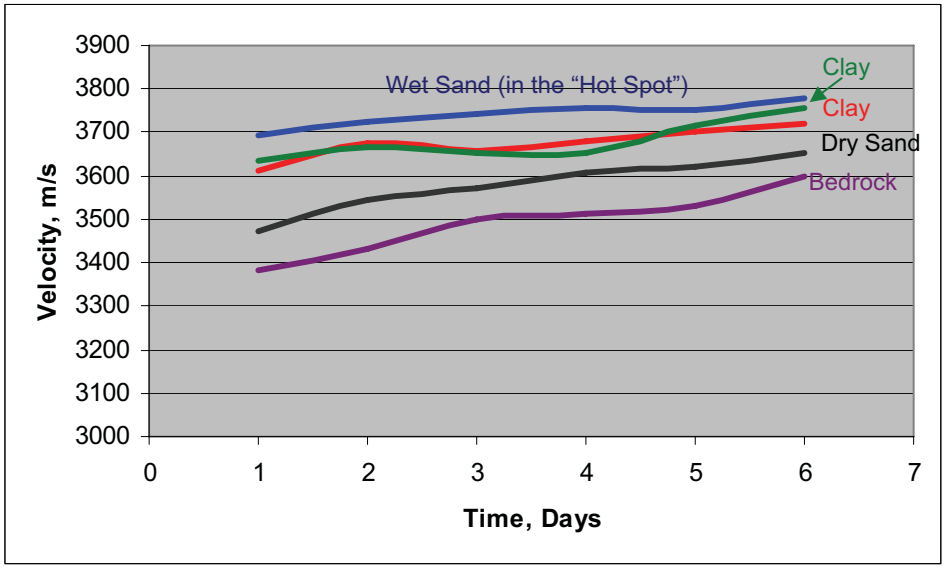

Figure 38. Graph. Velocity Monitoring of Abutment 1 Shaft 1. Hagerman National Wildlife Refuge, TX. Static Corrected Velocity Values are Averaged from the Four Access Tubes (and Six CSL Test Paths) at 3m (Black), 6 m (Blue), 9 m (Red), 12 m (Green), and 15 m (Magenta) Depth Points.

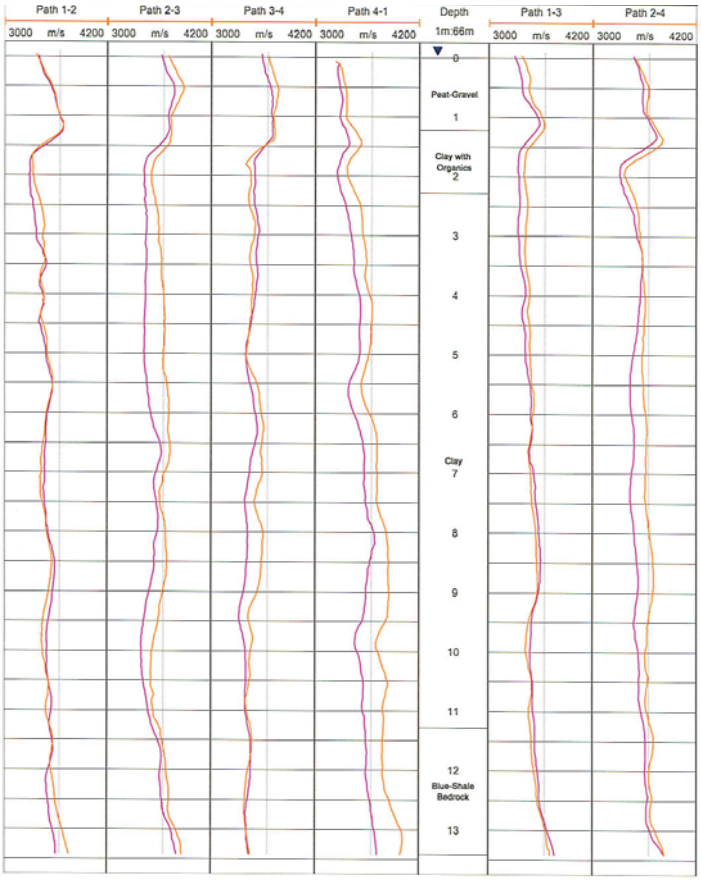

Figure 39. Plot. Velocity Monitoring of Pier 2 Shaft 2. Hagerman National Wildlife Refuge, TX. CSL Velocity Curves at 3 Days (Purple) and 4 Days (Orange) After the Concrete Placement. Vertical Guideline: 3,650 m/s.

Limited CSL monitoring was obtained from Pier 2 Shaft 2 from 3 days and 4 days after the concrete placement. As indicated in Figure 39, a small increase in CSL velocity is observed from 3 and 4 days after the concrete placement.

From this velocity monitoring study, the following conclusions can be drawn:

1. Velocity values appear to increase with time of curing. This well apparent for the Pier 2 Shaft 2 shown in Figure 39. For Abutment 1 Shaft 1 in Figure 36, the CSL curves on the whole were increasing with time; but not continuously. For the long CSL Paths 1-3 and 2-4 plotted in an expanded scale in Figure 37, the velocity increase was more apparent. However, when the CSL values from four access tubes are averaged at five different depth points in Figure 38, a clear increase in velocity is observed.
2. At a given time period, velocity values appear to inversely correlate with shaft's temperature. For Pier 2 Shaft 2, the velocity values in Figure 39 correlated well with the shaft's temperature shown in Figure 33 with clay indicating the lowest velocity (warmest), followed by gravel (cooler), and bedrock indicating highest velocity (coolest temperature). For Abutment 1 Shaft 1, average velocities should have increased from sand (warmest), followed by clay, and bedrock indicating highest velocity (coolest). This trend was generally observed; however, bedrock velocities were anomalously low (possibly due to a defect) and wet sand was anomalously high possibly due to being situated within the tube bending zone.
3. The velocity curves appears to taper off after about 4 days of curing.

4.4.3 Density Monitoring Results

Figure 40 displays the density monitoring results from Abutment 1 Shaft 1 at the Hagerman National Wildlife Refuge, TX from 1 day to 6 days after the concrete placement. In this figure, the GDL results are plotted in 4 separate sub-plots from the tested access tubes. Each individual sub-plot depicts the GDL results from 35.5 cm (14 in) source-detector separation presented in a magnified density scale of 130-200 lbs/ft^3 (2,100-3,200 kg/m^3). Depths were measured from the top of the shaft and are shown on the vertical axis. Also presented in the depth axis is the soil profile as reported by the boring logs. The single-hole GDL results were more uniform than the CSL results as they are not affected by tube bending. In Figure 41, GDL values from four access tubes are averaged at five different depth points and plotted as a function of time.

GDL monitoring was obtained from Pier 2 Shaft 2 from 1 day to 4 days after the concrete placement. As indicated in Figure 42, a steady increase in density values are observed in this dataset.

From this density monitoring study, the following conclusions can be drawn:

1. Density values appear to slightly increase with time of curing. This is well apparent for the Pier 2 Shaft 2 shown in Figure 42 for 1 to 4 days of curing. For Abutment 1 Shaft 1 in Figure 40, the density values also increased steadily from 1 to 4 days after the concrete placement. However, values then decreased after days 5 and 6. The reason is unclear—possibly due to the formation of voids at this time. This decrease in density values are

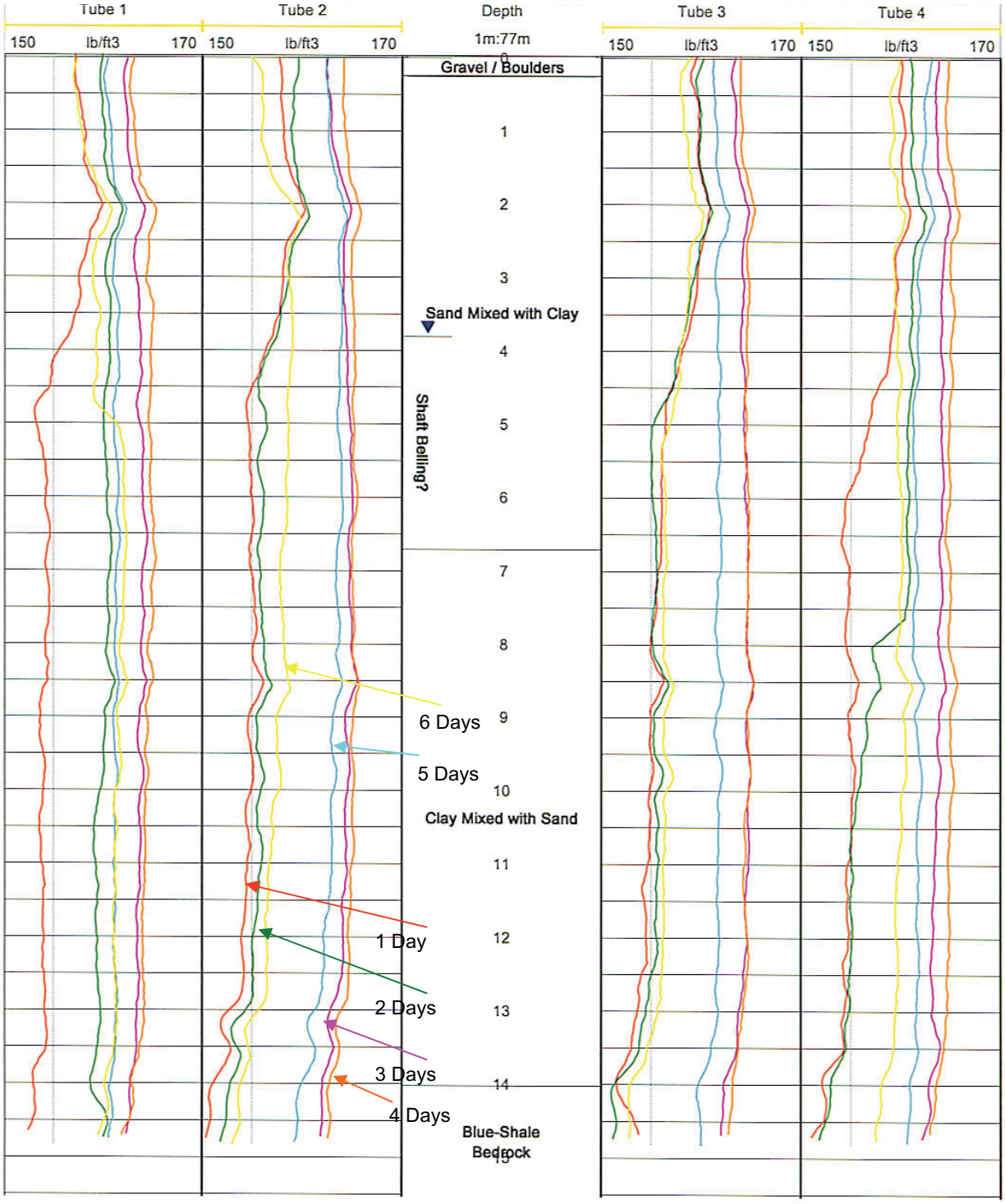

Figure 40. Plot. Density Monitoring of Abutment 1 Shaft 1. Hagerman National Wildlife Refuge, TX. GDL Density Curves with 1 Day (Red), 2 Days (Green), 3 Days (Purple), 4 Days (Orange), 5 Days (Teal), and 6 Days (Yellow) After the Concrete Placement. Vertical Guideline: 155 lb/ft^3.

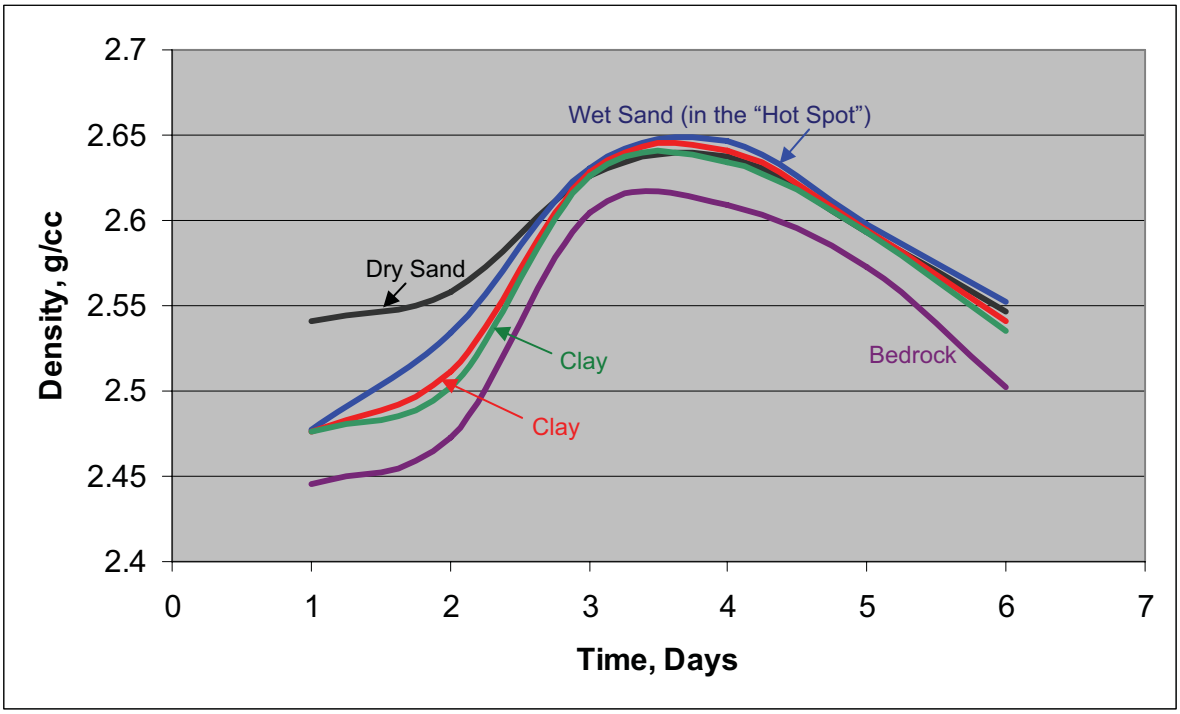

Figure 41. Graph. Density Monitoring of Abutment 1 Shaft 1. Hagerman National Wildlife Refuge, TX. Density Values are Averaged from the Four Access Tubes at 3m (Black), 6 m (Blue), 9 m (Red), 12 m (Green), and 15 m (Magenta) Depth Points.

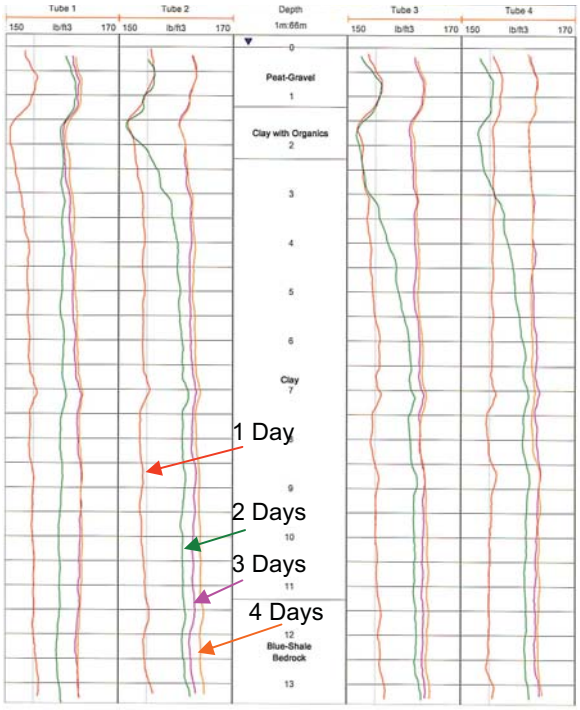

Figure 42. Plot. Density Monitoring of Pier 2 Shaft 2. Hagerman National Wildlife Refuge, TX. GDL Density Curves at 1 Day (Red), 2 Days (Green), 3 Days (Purple), and 4 Days (Orange) After the Concrete Placement. Vertical Guideline: 155 lb/ft^3.

also demonstrated in Figure 41. In this figure, the averaged GDL values are plotted from 3m (in sand above the groundwater table displayed in black); 6 m (in sand below the groundwater table in blue); 9 m (clay in red); 12 m (clay in green); and 15 m (bed rock in magenta) depth levels.

2. At a given time period, the shape of the density (GDL) curves appear to correlate with moisture (NML) curves (Section 4.4.4). For Pier 2 Shaft 2, the density values in Figure 42 correlated well with the shaft's relative moisture levels shown in Figure 45 with gravel (lowest moisture, lowest density), followed by clay and bedrock (highest moisture, highest density). For Abutment 1 Shaft 1, however, an inverse correlation was observed—possibly due to anomalously low densities in the bedrock (due to a probable "defect") and anomalously high densities in the sand (possibly due to erroneous reading in the "hot spot" zone).

4.4.4 Moisture Monitoring Results

Figure 43 displays the neutron monitoring logging (NML) results from Abutment 1 Shaft 1 at the Hagerman National Wildlife Refuge, TX from 1 day to 6 days after the concrete placement. In this figure, the NML results are plotted in 4 separate sub-plots from the tested access tubes. Each individual sub-plot is presented in a magnified scale of 90-170 counts per second (cps). Lower counts denote higher moisture content; therefore, in each sub-plot, moisture content increases from left to right. Depths were measured from the top of the shaft and are shown on the vertical axis. Also presented in the depth axis is the soil profile as reported by the boring logs. In Figure 44, NML values from four access tubes are averaged at five different depth points and plotted as a function of time. A more limited NML monitoring was obtained from Pier 2 Shaft 2 from 2 days to 4 days after the concrete placement and is displayed in Figure 45.

From this neutron-moisture monitoring study, the following conclusions can be drawn:

1. Relatively speaking, the moisture level in Abutment 1 Shaft 1 in Figure 43 was highest at the bedrock followed by clay and sand (lowest). Therefore, for the initial "green" concrete, it appears that the less permeable clay and shale layers allowed less movement of moisture out of the concrete matrix. This trend is also well demonstrated in Figure 44 where the averaged NML values are plotted from 3m (in sand above the groundwater table in black); 6 m (in sand below the groundwater table in blue); 9 m (clay in red); 12 m (clay in green); and 15 m (bedrock in magenta). Similar results were observed in the NML data from Pier 2 Shaft 2 (Figure 45).
2. After 24 hours, moisture values appear to change negligibly with time of curing.

4.4.5 Summary of the Geophysical Monitoring Study

In summary, it appears that the curing strength of the concrete in a drilled shaft is not only a function of time but also a function of the physical properties of the surrounding soil/rock and the depth of the groundwater table. Specifically, two parameters from the soil profile that is noteworthy: thermal conductivity and permeability. Conductivity controls relative changes in temperature and permeability controls small relative changes in the moisture content. These parameters in turn control curing (age) and concrete strength—as it relates to incremental changes in velocity and density.

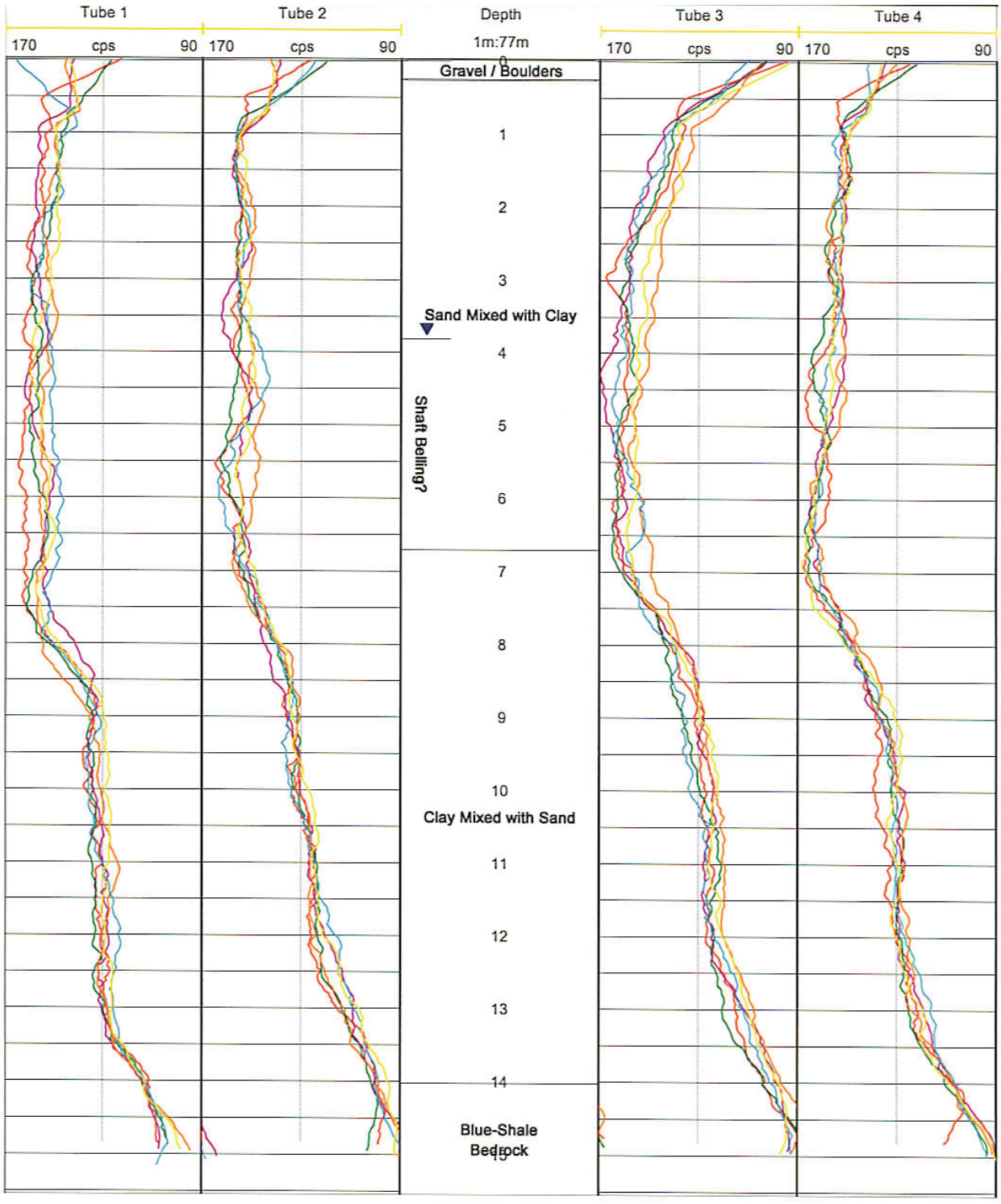

Figure 43. Plot. Moisture Monitoring of Abutment 1 Shaft 1. Hagerman National Wildlife Refuge, TX. NML Moisture Curves at 1 Day (Red), 2 Days (Green), 3 Days (Purple), 4 Days (Orange), 5 Days (Teal), and 6 Days (Yellow) After the Concrete Placement. Vertical Guideline: 130 cps.

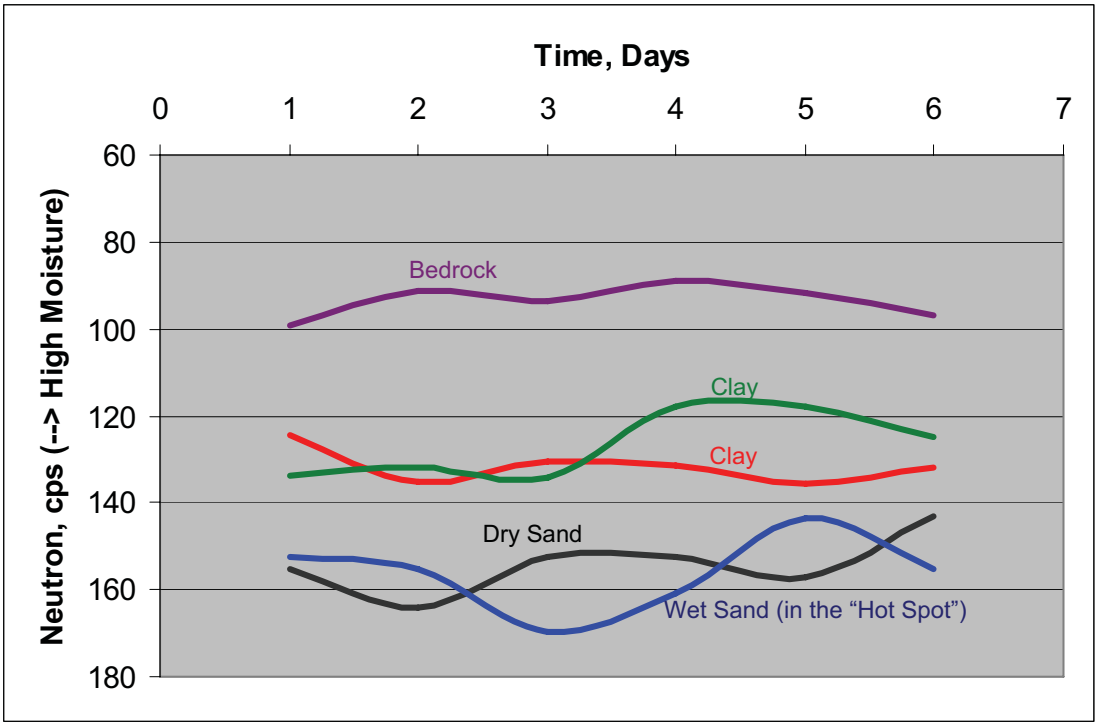

Figure 44. Graph. Moisture Monitoring of Abutment 1 Shaft 1. Hagerman National Wildlife Refuge, TX. Temperature Values are Averaged from the Four Access Tubes at 3m (Black), 6 m (Blue), 9 m (Red), 12 m (Green), and 15 m (Magenta) Depth Points.

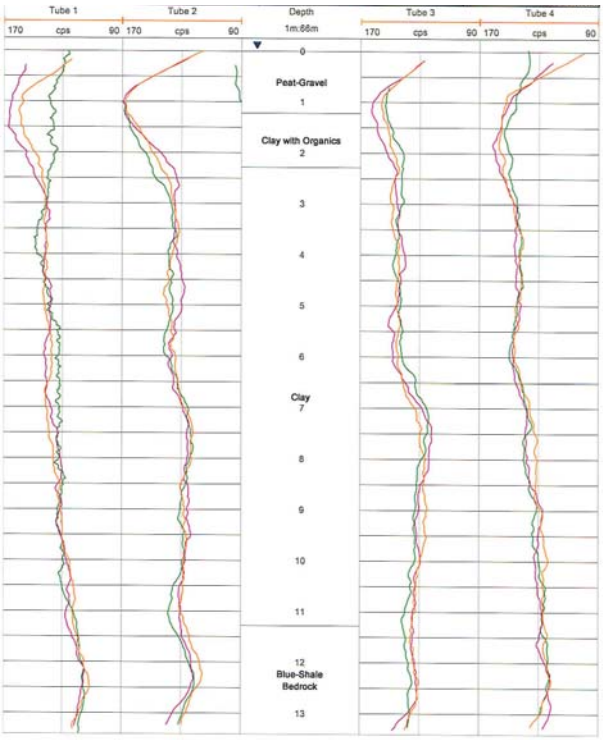

Figure 45. Plot. Moisture Monitoring of Pier 2 Shaft 2. Hagerman National Wildlife Refuge, TX. NML Moisture Curves at 2 Days (Green), 3 Days (Purple), and 4 Days (Orange) After the Concrete Placement. Vertical Guideline: 130 cps.

CHAPTER 5 – EXAMINATION OF FIELD DATA

As part of this study, several NDT dataset from different project sites are used for analyses and tomographic imaging. These data are used in developing strength images according to the methodologies described in Chapter 2-4. The data were obtained from twenty (20) different drilled shaft foundations from three (3) different project sites, including:

- *Existing* dataset from two (2) test drilled shafts with planned defects from NGES, Amherst, Massachusetts;
- *Existing* dataset from twelve (12) production shafts (shafts used in a bridge project with unplanned defects) from Jim Camp Bridge Project, Arizona;
- *New* dataset from four (4) production shafts from Sevenmile Gooseberry Project, Utah.

5.1 STANDARDIZED PRESENTATION OF THE DEFECT CHARACTERIZATION AND IMAGING RESULTS

In this chapter, the NDT results from twenty (20) drilled shafts discussed above are presented in a standardized template display format for comparison. The assumptions and definitions of terms used in the analysis and imaging of the results are explained next.

5.1.1 Standardized Template Format for the Display of Imaging Results

As mentioned in Chapters 2 to 4, a three-step approach for integrity assessment of drilled shafts is developed. This three-step approach is presented herein in a standardized template display. Each standardized template displays, from top to bottom, four distinct sub-templates in the following order:

1. *Current Practice* – This sub-template display standard zero-offset CSL data (velocity/picked time vs. depth) and velocity tomograms **without** velocity equalization applied, which represents current state of practice[5].
2. *Step 1: Anomaly Identification (and independent verification, if dual CSL/GDL testing was performed)* – This sub-template displays the three-dimensional tomograms **after** velocity equalization applied for comparison. Also included is the "roughness model" which measure the spatial derivative (or curvature) of the velocity field.
3. *Step 2: Defect Definition* – Displays velocity histograms and Gaussian curve fits for various defect zones. For multiple levels of defects, velocity distribution curves for different depth levels are examined. The purpose of these curves is to identify cut-off velocities used to define defect volumes.
4. *Step 3: Defect Characterization and Imaging* –In this sub-template, velocity images are presented in unit of strength. Velocity cut-off values for each defect are used to give

[5] For the most part, in the U.S., the "current practice" consists of crosshole sonic logging (CSL). In our displays, the 3-D tomographic inversion without velocity equalization is included under "current practice" even though this is presently an advancement used only on a limited basis in the field.

final volumetric strength images of defects. Empirical fourth power strength to velocity relation (Equation 7) is used. Areas identified as artifacts are not imaged; therefore, the "strength model" and volumetric images represents the final interpretation of shaft condition for the engineer for shaft integrity assessment.

5.1.2 Different Tomographic Inversion Methods

Crosshole sonic data can be acquired using "zero-offset" geometry (standard CSL) with no separation between the source and receiver probe (or in near horizontal plane). Alternatively, sonic data can be acquired using "offset logs" where continuous log measurements are performed with the source or the receiver offset in depth (by some nonzero angle). Therefore tomographic inversion can be performed using zero-offset logs or multi-offset logs.

In addition, tomographic reconstruction can be performed using 2-D or 3-D inversion methods. In 2-D inversion, each test panel is inverted independently. In 3-D inversion, travel time picks from all test panels are inverted simultaneously.

In this study, a velocity equalization procedure is introduced as an important tomography pre-processing quality control (QC) step. Velocity equalization is a process performed prior to tomography that equalizes all offset CSL logs to the same median velocity by applying constant static shifts to the individual logs. Median velocity is calculated using zero-offset CSL logs. It is considered to be a better representative of background shaft velocity than mean (average) velocity because it is less affected by the low velocity anomalies that may be present. The median velocities are indicated as vertical green lines in the "standard zero-offset" CSL logs in the "Current Practice" sub-template. CSL logs are presented in units of velocity versus depth.

In this report, 3-D tomographic inversion results are presented before and after velocity equalization. Only the Amherst-NGES dataset was multi-offset. Dataset from the Jim Camp and Sevenmile Gooseberry Projects were all zero-offset. The 3-D tomographic inversion results are displayed in 3-D, or in other words, in cross-sectional side-by-side view or by a contoured velocity image of a defect volume indicating the shaft condition inside the rebar cage.

5.1.3 Tomographic Processing Parameters

In each figure, processing parameters used in tomographic inversion are tabulated. "Smooth" refers to the smoothing factor used for tomographic data inversion. The higher the number, the smoother the image boundaries become. Low smoothing results in courser and grainier looking images that are suitable for distinguishing subtle anomalies. Tomography inversion is performed for five iterations and the final RMS (root mean square) error is calculated. At each iteration, the RMS value should progressively decrease indicating stable inversion. RMS represents the degree of fit of the observed data to the imaged results (final model). The smoothing and RMS error are provided for the tomography results before and after velocity equalization for comparison.

Equalized median or background "shaft" velocities are also provided in another table for the velocity field before performing tomography (from the offset CSL logs) and after tomography.

These values are provided to examine changes in background velocity as a result of the tomographic inversion.

5.1.4 Anomaly Versus Defect

In this study and in the figures presented in this chapter, "anomaly" refers to a deviation from uniformity in a concrete structure. No determination is yet made regarding its exact size or extent; just identification has been made in a CSL or GDL record (Step 1 above). Ideally, an independent verification (using another logging method like GDL) is needed to determine if the anomaly is not a false positive. Three-dimensional tomographic imaging (CSLT) is performed for imaging these anomalies. Therefore, the term "anomaly" refers to a suspected zone in a CSL, GDL, or CSLT data without determination for its size or extent.

Once a suspected (blue color) "anomaly" zone is identified in a CSLT data, statistical analysis is performed to separate velocity distribution of sound concrete from anomalous concrete (Step 2). With this analysis, a cut-off velocity is obtained that separates the two velocity distributions. Statistical analysis can be performed for multiple depth "zones", which sometimes are overlapping.

Sometimes, no clear distinction between velocity distributions of sound concrete versus velocity distribution of anomalous concrete can be made. In addition, for some shafts a cut-off velocity is obtained that is close to the shaft median velocity (representing sound concrete velocity). In these cases, it is concluded that the "anomaly" is not statistically significant and the shaft is sound at those depths.

For those anomalies that a clear distinction between sound and anomalous concrete can be made, cut-off velocity is used to define a "defect" as the volume of concrete with a velocity lower than the cut-off velocity. Note that, within a given depth zone, none or several defects can be indicated. Therefore, the number of interpreted defects or depth zones used in statistical analysis may not equal to the number of suspected anomalies.

For engineering analysis, defect values are presented in units of strength using velocity to strength empirical relationships. Sound concrete (velocities above the cut-off velocity) is presented at concrete compressive strength, which is assumed as 27,600 kPa (4,000 psi). Velocity contouring is performed to obtain "volumetric imaging of defect" plots at 27,600 kPa (4,000 psi) and at 16,500 kPa (2,400 psi) representing 60% strength. The blue color defects that are indicated in the "strength model" and the imaged defect volumes represent the final interpretation of the data. Whether these defects are structurally significant, however, depends on location, size, and design factors to be determined by modeling by the engineer (integrity assessment).

5.1.5 Artifacts and the Roughness Model

In tomographic images where no velocity equalization is performed, often the final images contain artifacts. Artifacts are erroneous values produced by the tomographic matrix inversion which is non-linear and non-unique. Non-uniqueness in geophysical interpretation and

mathematical modeling refer to a problem for which two or more models satisfy the data equally well. Artifacts can also be a result of inadequate scanning (ray coverage) of the test volume and inaccuracies in travel time picking. These artifacts mostly occur near the image boundaries.

The final 3-D tomography results are presented side by side with an interpretational tool called the "Roughness Model". In the roughness model, the roughness value at a given cell point, is calculated by computing changes in velocity from its six neighboring points (or spatial derivative) and it represents the curvature (or roughness) of the velocity field. It identifies regions where a large change in velocity values has taken place. It is included in the figures as a means of assessing the stability of the tomographic inversion process (along with the RMS error and smoothing factors used) and as an interpretational tool for distinguishing anomalies from artifacts, which typically exhibit high localized roughness.

5.1.6 Narrative Description of Each Figure

For each dataset, the field results are described using similar standardized logic. First, from each figure, the suspected "anomalies" are identified from the CSL data as low velocities zones. The anomalies are numbered sequentially. Next, the same anomalies are examined in the three-dimensional tomographic inversion CSLT images before and after velocity equalization, noting inversion artifacts and the roughness model. Statistical analysis is analyzed to define cut-off velocities as compared to median velocities. This analysis is examined separately for different anomalies at different depth zones. The number of depth zones may not correspond to the number of anomalies as a depth zone may contain several anomalies. Finally, the strength model is explained which presents the interpreted blue color "defects'. Defects are referenced using the same numbering system used in defining anomalies. Velocity contouring is described for imaging interpreted defect volume at 27,600 kPa (4,000 psi), representing breaking strength of assumed sound concrete; and, as an example, 16,500 kPa (2,400 psi) for 60% strength concrete.

5.2 AMHERST NGES RESULTS

Six drilled shafts were constructed at the NGES site during March and April, 2000. The shafts contained both built-in and unplanned defects (Iskander, et al., 2000). Built-in defects include necking, voids, caving, and soft bottoms.

CSL/CSLT data for the original NGES study was collected by InfraSeis, Inc.. Although the data was collected about one year from the shaft construction, no tube debonding was indicated.

In the next section, CSL and CSLT results from two of the Amherst-NGES drilled shaft study (Shaft 1 and Shaft 4) are presented. Both shafts had a diameter of 0.9 m and a length of about 15.2 m (50 feet). Four CSL steel access tubes were attached to the rebar cage in an approximately symmetrical pattern. Therefore, field data was collected from six separate CSL paths (or panel combinations) consisting of four perimeter paths and two diagonal paths.

For each test panel, seven offset CSL logs were produced: zero offset; three positive offset; and, three negative offsets. In these panels, 0º CSL logs was combined with approximately ±26º, ±45º, and ±60º offset logs. Therefore, for each shaft, the acquisition geometry included a total of 42 offset CSL logs (=6 panel combinations x 7 offset logs).

Results from the Amherst test site are summarized below.

5.2.1 Amherst NGES, Shaft 1 (Figure 46)

1. *Current Practice* – Standard CSL (velocity vs. depth) indicates three suspected "anomalies":
   Anomaly 1: 2-3 m depth and mostly between Tubes 1 and 2;
   Anomaly 2: 8-8.5 m depth and mostly between Tubes 2 and 3;
   Anomaly 3: 14-15 m depth and mostly between Tubes 2, 3, and 4.
   Multi-offset (7-offsets) 3-D CSLT tomography, with no velocity equalization, images CSL Anomalies 1 and 3 but not Anomaly 2.
2. *Anomaly Identification* – Multi-offset CSLT with velocity equalization better resolves Anomalies 1 and 3. Slight indication for Anomaly 2 is now indicated in both the CSLT image and the roughness model. Also, a small anomaly (0-0.5 m) near the shaft surface is indicated (Anomaly 0).
3. *Defect Definition* – Three depth zones are selected (to examine the four Anomalies 0-3) and velocity cut-off values are indicated using 2 and 3 Gaussian fits to the velocity histogram.
4. *Defect Characterization and Imaging* – Four blue color "defects" zones are interpreted in the strength model. Volumetric images indicate only Defects 0, 1, and 3 between 0-0.5 m, 2-3 m, and 14-15 m depths, respectively are of low strength (<16,500 kPa (2,400 psi)).

Comments. Next to the strength model, a cross-section is provided indicating actual locations of planned defects and a description of the defects. Six defects were pre-planned with only two defects (planned Defects D and F) were located inside the rebar cage. Tomography clearly imaged the planned defects D and F as well as planned Defect A. The planned Defect A was a plastic bucket located outside the cage which is clearly imaged by CSLT. Again note a slight indication of an unplanned low velocity defect near the surface (0-0.5 m) close to Tube 3.

5.2.2 Amherst NGES, Shaft 4 (Figure 47)

1. *Current Practice* – Standard CSL indicates four suspected "anomalies":
   Anomaly 1: 2.5-3 m depth and mostly between Tubes 3 and 4;
   Anomaly 2: 5-6 m depth and mostly between Tubes 3 and 4;
   Anomaly 3: 9.2-9.8 m depth and mostly between Tubes 3 and 4;
   Anomaly 4: 14.5-15 m depth and mostly between Tubes 2, 3, and 4.
   Multi-offset tomography (CSLT), with no velocity equalization, images Anomalies 1 and 2 but not Anomalies 3 and 4 (only a slight indication is observed).
2. *Anomaly Identification* – Multi-offset CSLT with velocity equalization better resolves Anomalies 1, 2 and 4. Slight indication for Anomaly 3 is indicated in both the CSLT image and the roughness model.

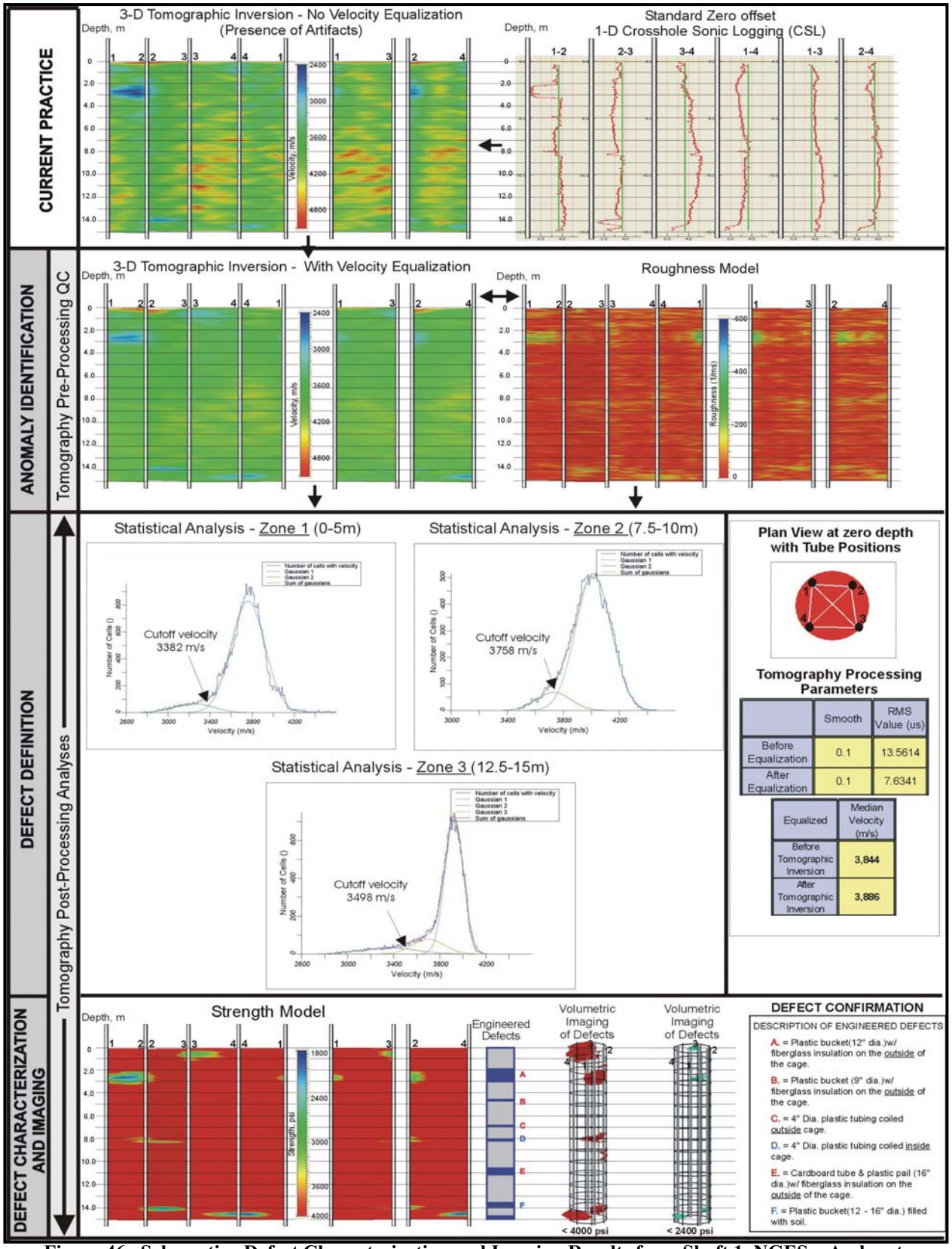

Figure 46. Schmeatic. Defect Characterization and Imaging Results from Shaft 1, NGES – Amherst.

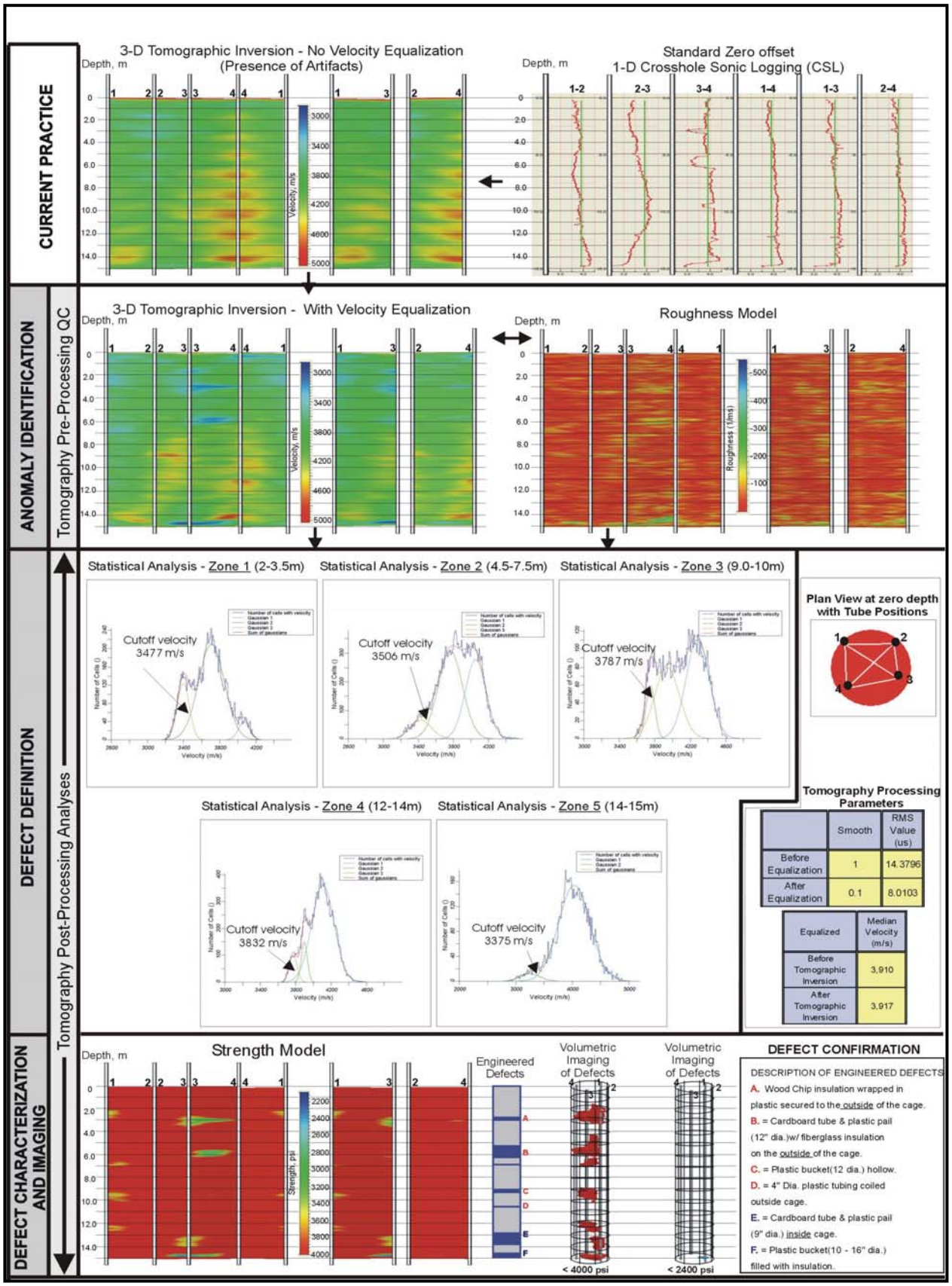

Figure 47. Schematic. Defect Characterization and Imaging Results from Shaft 4, NGES – Amherst.

3. *Defect Definition* – Five depth zones are selected and velocity cut-off values are indicated using 2 and 3 Gaussian fits to the velocity histogram. Anomalies 3 and 4 have a cut-off velocities close to median velocity (3,917 m/s) and; therefore, not statistically significant.
4. *Defect Characterization and Imaging* – Three (3) green-blue color "defects" zones are interpreted in the strength model (Defects 1, 2, and 4). Other minor defects are indicated by yellow-orange colors. Volumetric images indicate only Defect 4, between 14.5-15 m depth, is of low strength (<16,500 kPa (2,400 psi)).

Comments. Next to the strength model, a cross-section is provided indicating actual locations of planned defects and a description of the defects. Six defects were pre-planned with only two defects (planned Defects E and F) were located inside the rebar cage. Tomography clearly imaged the planned Defect F as well as exterior planned Defects A and B. Minor indication of exterior planned Defects C and E are also observed (yellow color).

5.3 JIM CAMP BRIDGE RESULTS

Jim Camp Wash Bridge project site was located on the Petrified Forest National Park, east of Holbrook, Arizona. Jim Camp Bridge was designed using two (2) abutments and four (4) pier lines each supported by two (2) drilled shafts. Each drilled shaft had a diameter of 0.76 m (2.5 ft) and each contained three (3) 50.8 mm (2 in) I.D. steel access tubes.

As indicated in Figure 48, all shafts were tested during February – March, 2002 using only zero offset CSL. CSL data was collected by EarthSpectives, Inc. In addition to standard CSL, subsequently gamma-gamma density logging (GDL) data was collected by AMEC, Inc for Pier 2, Shaft B. The GDL logs were acquired to evaluate if the concrete integrity was jeopardized by problems that occurred during shaft construction.

5.3.1 Description of UPV Testing Results Overview

Ultrasonic Pulse Velocity (UPV) test was performed prior to the CSL field work. Table 3 presents the UPV test results for concrete samples obtained from the original mix between 2 to 7

Table 3. UPV Testing Results on Concrete Cylinders.

	Day # 2 Velocity (m/s)	Day # 3 Velocity (m/s)	Day # 4 Velocity (m/s)	Day # 5 Velocity (m/s)	Day # 6 Velocity (m/s)	Day # 7 Velocity (m/s)
Center	4158.7	4336.7	4299.9	4355.3	4399.4	4269.7
L. side	4158.7	4234.0	4269.7	4330.5	4374.1	4299.9
R. side	4210.5	4170.1	4228.1	4216.4	4257.7	4281.7
Average	4175.97	4346.93	4265.90	4300.73	4343.73	4283.77
Center	4124.8					4318.2
L. side	4222.2					4263.7
R. side	4141.7					4305.9
Average	4162.90					4295.93
Average Velocity	4169.43	4346.93	4265.90	4300.73	4343.73	4289.85

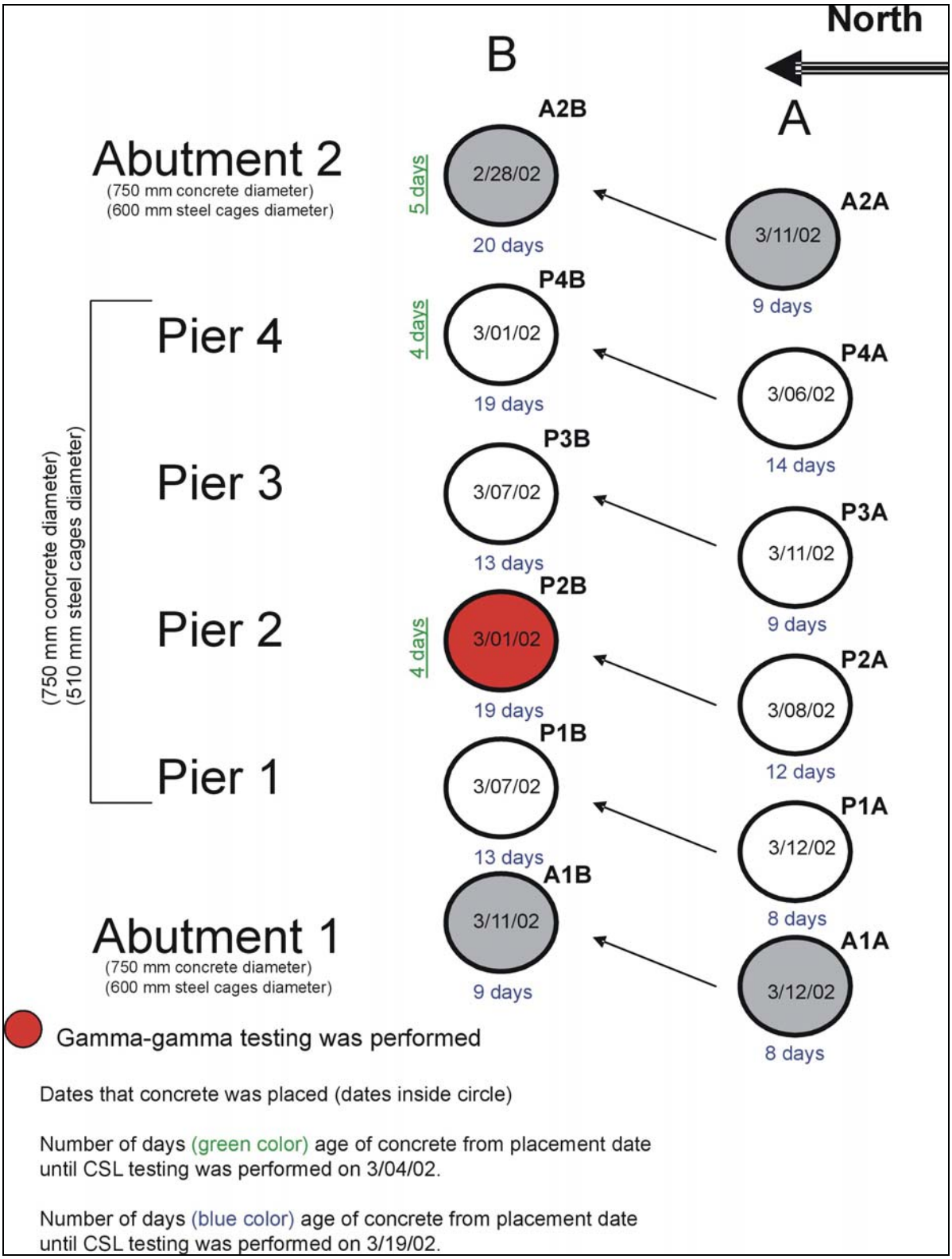

Figure 48. Schematic. Plan View of the Drilled Shafts at the Jim Camp Bridge, AZ.

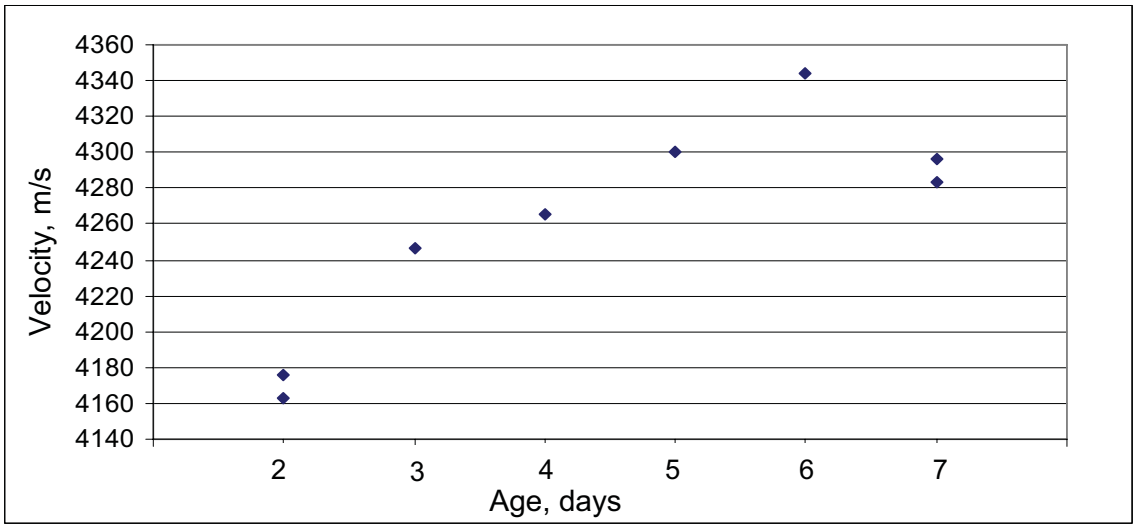

Figure 49. Graph. UPV Velocities Versus Age.

days of age. The velocities were measured on the concrete cylinders of 0.1524 x 0.3048 m (6 x 12 in) in size. Three measurements were taken from each cylinder: at the center, and from the left and right sides with the results presented in Figure 49. An average UPV velocity of 4,280 m/s is indicated for the laboratory samples. CSL testing was performed with more than 7 days of concrete age. However, CSL velocities from the drilled shafts indicated average velocity values less than the average 7-day UPV velocity of 4,280 m/s (please refer to section 4.2).

CSL results from the Jim Camp Bridge site are summarized below:

5.3.2 Jim Camp Bridge, Shaft A1A (Figure 50)

1. *Current Practice* – Standard CSL indicates no anomalies, just irregular CSL dataset. Zero-offset tomography (CSLT), with no velocity equalization, indicates un-balanced velocity panels with artifacts in the CSLT images, probably due to errors in measuring tube offsets in the field.
2. *Anomaly Identification* – Zero-offset CSLT with velocity equalization balances the velocity panels. A low velocity zone is indicated between 0.2-1 m around Tube 3.
3. *Defect Definition* – No single cut-off velocity can be defined. Shaft is sound.
4. *Defect Characterization and Imaging* – No defects are indicated.

5.3.3 Jim Camp Bridge, Shaft A1B (Figure 51)

1. *Current Practice* – Standard CSL indicates no anomalies, just irregular CSL dataset. Zero-offset tomography (CSLT), with no velocity equalization, indicates un-balanced velocity panels with artifacts in the CSLT images, probably due to errors in measuring tube offsets in the field.
2. *Anomaly Identification* – Zero-offset CSLT with velocity equalization balances the velocity panels. A low velocity zone is indicated between 0.2-0.7 m around Tube 2 with slight indication in the roughness model.

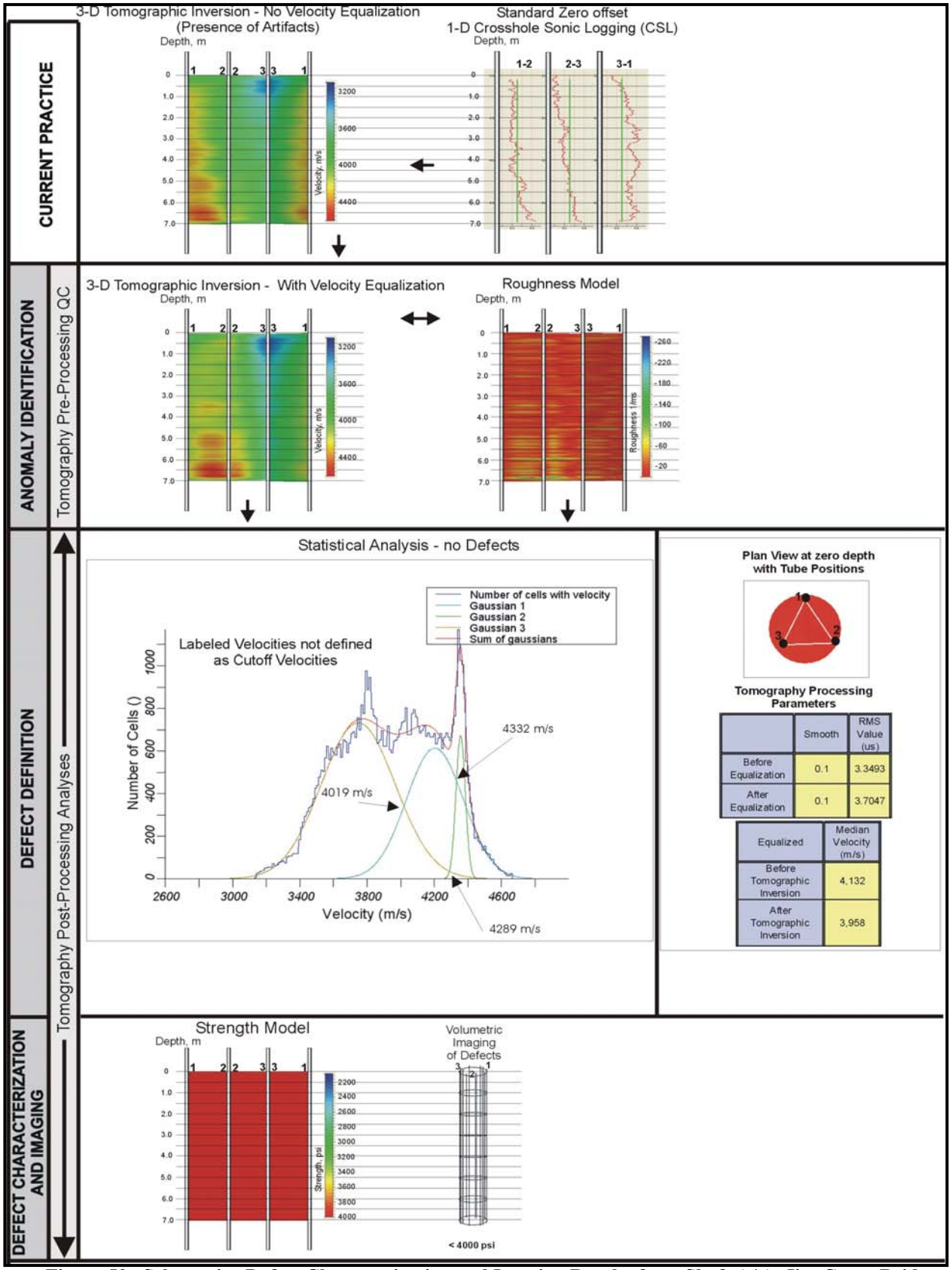

Figure 50. Schematic. Defect Characterization and Imaging Results from Shaft A1A, Jim Camp Bridge.

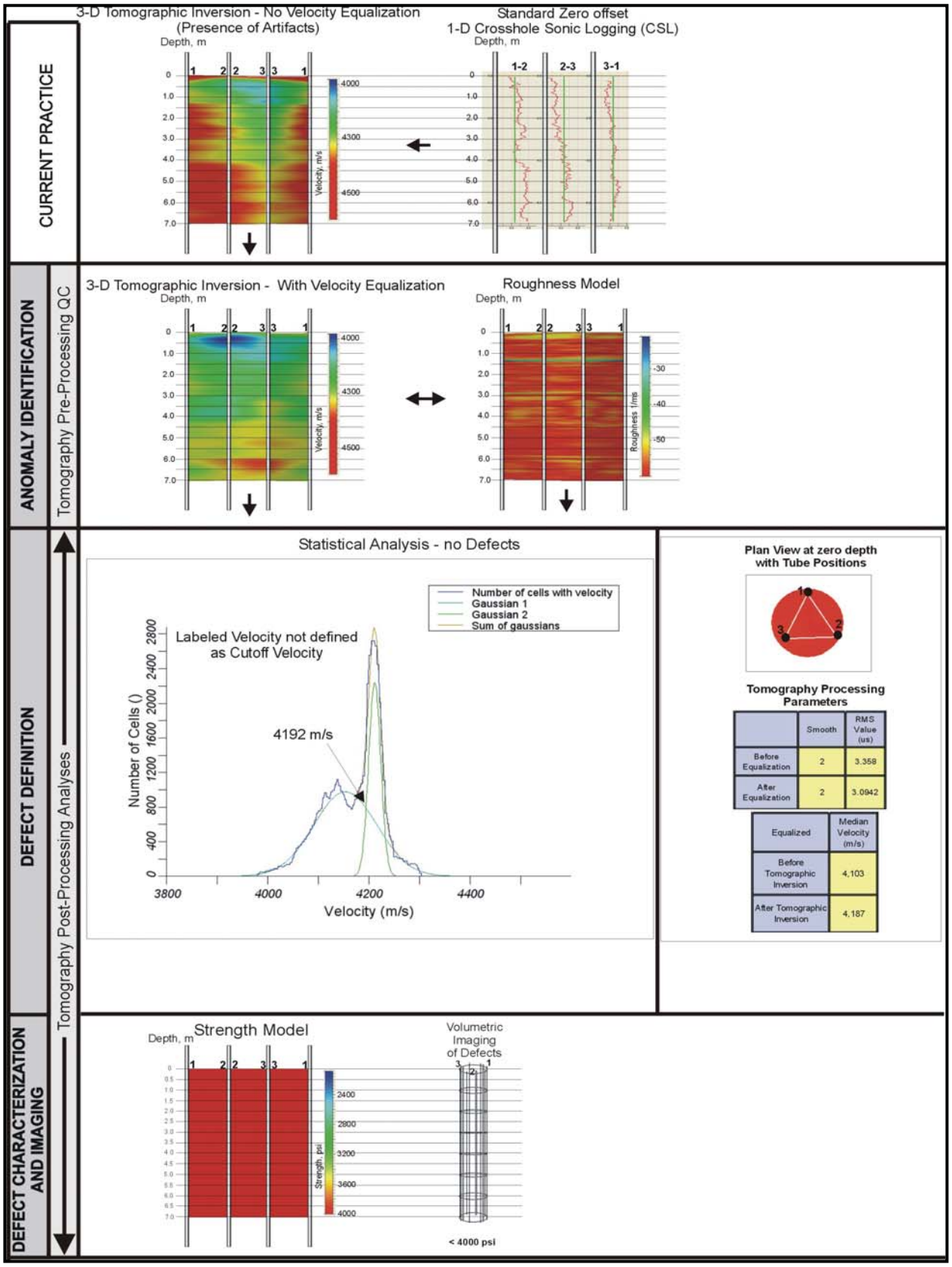

Figure 51. Schematic. Defect Characterization and Imaging Results from Shaft A1B, Jim Camp Bridge.

3. *Defect Definition* – A single cut-off velocity of 4,192 m/s is obtained for the whole shaft which is close to the shaft median velocity (4,187 m/s).
4. *Defect Characterization and Imaging* – No defects are indicated.

5.3.4 Jim Camp Bridge, Shaft A2A (Figure 52)

1. *Current Practice* – Standard CSL indicates no anomalies, just irregular CSL dataset. Zero-offset tomography (CSLT), with no velocity equalization, indicates un-balanced velocity panels with artifacts in the CSLT images, probably due to errors in measuring tube offsets in the field.
2. *Anomaly Identification* – Zero-offset CSLT with velocity equalization balances the velocity panels.
3. *Defect Definition* – Two zones are selected and velocity cut-off values are indicated using 2 and 3 Gaussian fits to the velocity histogram. One anomaly between 0-3 m in depth has a cut-off velocity 3,836 m/s close to median velocity of 4,150 m/s, and; therefore, may not be statistically significant.
4. *Defect Characterization and Imaging* – One small defect between 0.2-0.5 m near Tube 1 is indicated. Volumetric images indicate that this defect is of high relative strength (>16,500 kPa (2,400 psi)).

5.3.5 Jim Camp Bridge, Shaft A2B (Figure 53)

1. *Current Practice* – Standard CSL indicates no anomalies, just irregular CSL dataset. Zero-offset tomography (CSLT), with no velocity equalization, indicates a low velocity zone between Tubes 1 and 2.
2. *Anomaly Identification* – Zero-offset CSLT with velocity equalization balances the velocity panels and also confirms the low velocity zone between 0.2-1 m with slight indication in the roughness model.
3. *Defect Definition* – Two zones are selected and velocity cut-off values are obtained close to median velocity using 2 and 3 Gaussian fits to the velocity histogram.
4. *Defect Characterization and Imaging* – No defects are indicated.

5.3.6 Jim Camp Bridge, Shaft P1A (Figure 54)

1. *Current Practice* – Standard CSL indicates no anomalies, just irregular CSL dataset. Zero-offset tomography (CSLT), with no velocity equalization, indicates a low velocity zone between Tubes 2 and 3.
2. *Anomaly Identification* – Zero-offset CSLT with velocity equalization balances the velocity panels also confirms the low velocity zone between 0.5-1 m with slight indication in the roughness model.
3. *Defect Definition* – A single cut-off velocity of 4,401 m/s is obtained for the whole shaft which is close to shaft median velocity (4,428 m/s).
4. *Defect Characterization and Imaging* – No defects are indicated.

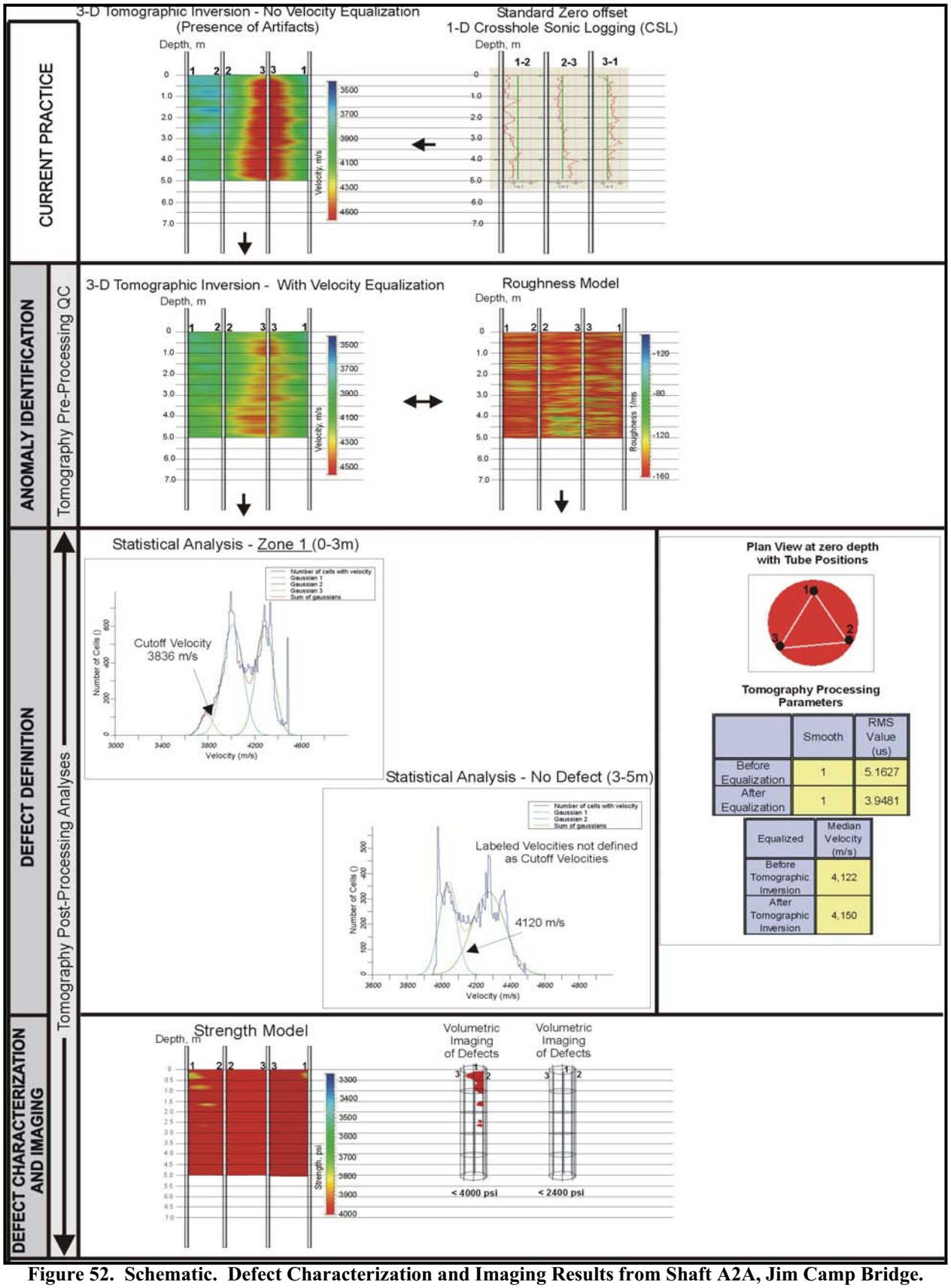

Figure 52. Schematic. Defect Characterization and Imaging Results from Shaft A2A, Jim Camp Bridge.

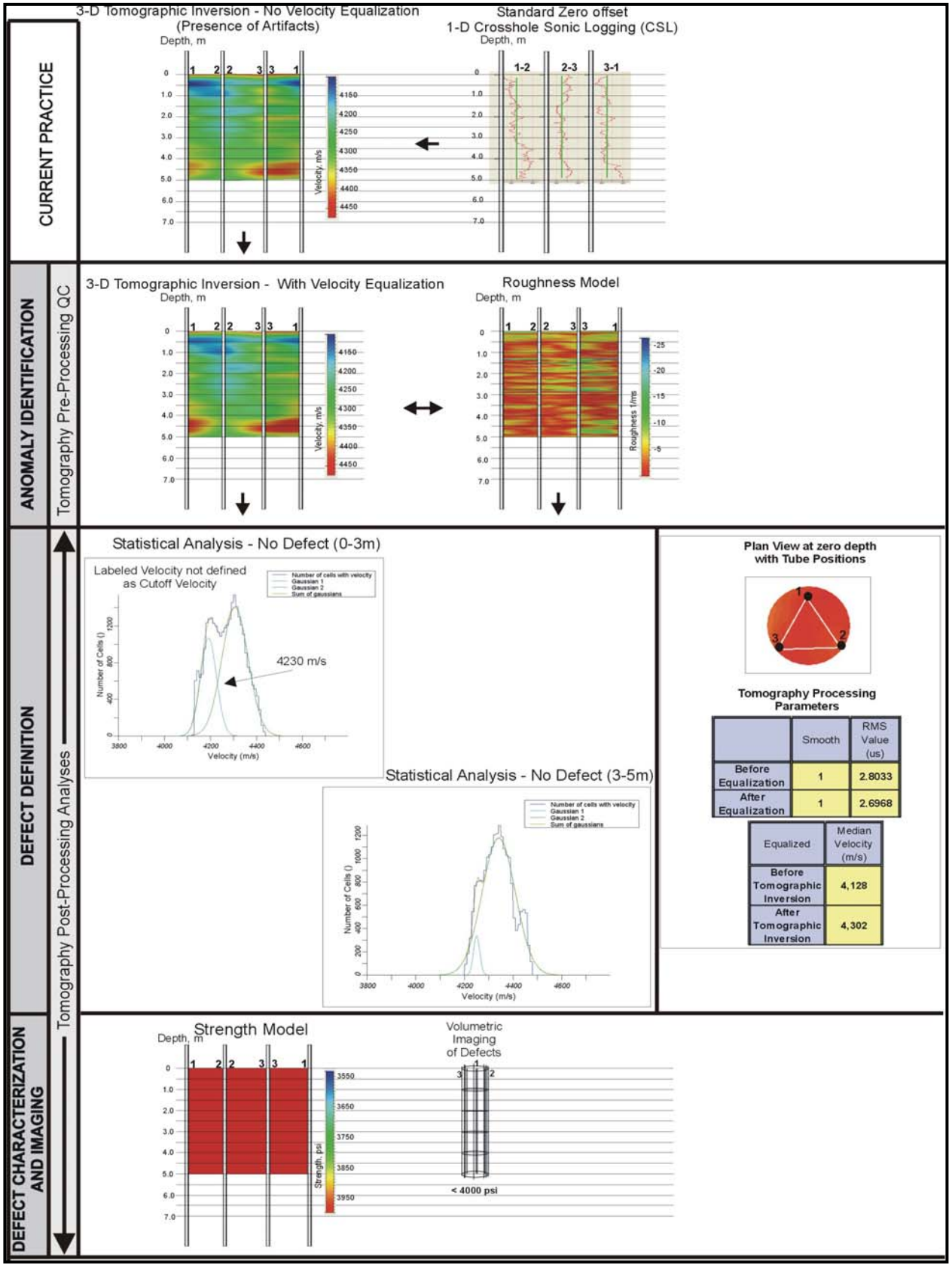

Figure 53. Schematic. Defect Characterization and Imaging Results from Shaft A2B, Jim Camp Bridge.

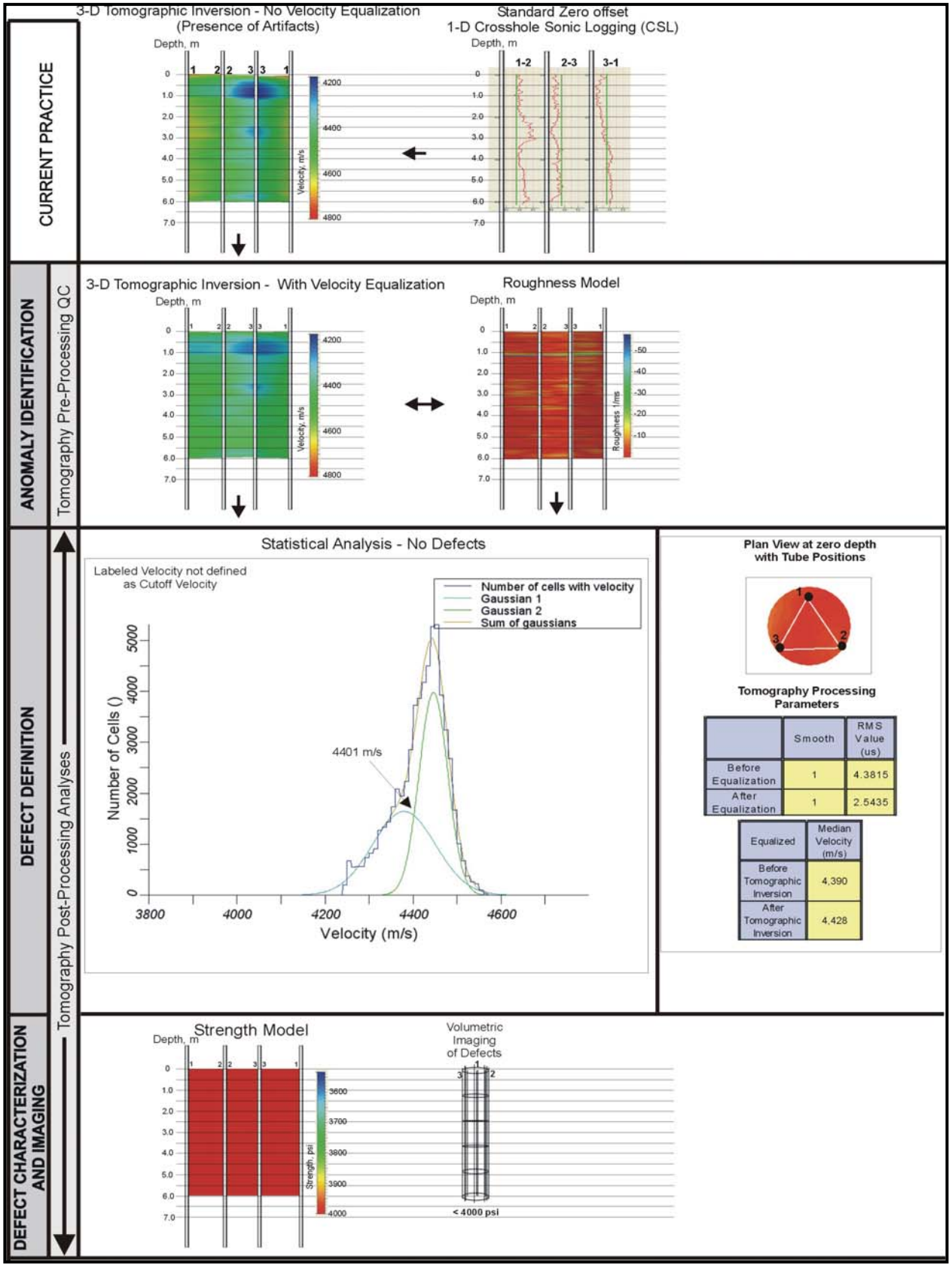

Figure 54. Schematic. Defect Characterization and Imaging Results from Shaft P1A, Jim Camp Bridge.

5.3.7 Jim Camp Bridge, Shaft P1B (Figure 55)

1. *Current Practice* – Standard CSL indicates no anomalies, just irregular CSL dataset. Zero-offset tomography (CSLT), with no velocity equalization, indicates a low velocity zone near Tube 2.
2. *Anomaly Identification* – Zero-offset CSLT with velocity equalization balances the velocity panels also confirms the low velocity zone between 0.5-1 m with slight indication in the roughness model.
3. *Defect Definition* – A single cut-off velocity of 4,293 m/s is obtained for the whole shaft which is close to shaft median velocity (4,410 m/s).
4. *Defect Characterization and Imaging* – One small defect between 0.2-1 m near Tube 2 is indicated. Volumetric images indicate that this defect is of high relative strength (>16,500 kPa (2,400 psi)).

5.3.8 Jim Camp Bridge, Shaft P2A (Figure 56)

1. *Current Practice* – Standard CSL indicates no anomalies.
   Zero-offset tomography (CSLT), with no velocity equalization, indicates two low velocity zones between Tubes 2 and 3 between 0.5-0.8 m and 5-5.5 m.
2. *Anomaly Identification* – Zero-offset CSLT with velocity equalization balances the velocity panels and the apparent low velocity zones.
3. *Defect Definition* – No single cut-off velocity could be obtained for the whole shaft.
4. *Defect Characterization and Imaging* – No defects are indicated.

5.3.9 Jim Camp Bridge, Shaft P2B (Figure 57)

1. *Current Practice* – Standard CSL indicates no anomalies.
   Zero-offset tomography (CSLT), with no velocity equalization, indicates a low velocity zone near Tube 3 between 0-1 m.
2. *Anomaly Identification* – Zero-offset CSLT with velocity equalization balances the velocity panels and the apparent low velocity zone.
3. *Defect Definition* – A single cut-off velocity of 4,130 m/s is obtained for the whole shaft which is close to the shaft median velocity (4,238 m/s).
4. *Defect Characterization and Imaging* – No defects are indicated.

5.3.10 Jim Camp Bridge, Shaft P3A (Figure 58)

1. *Current Practice* – Standard CSL indicates no anomalies.
   Zero-offset tomography (CSLT), with no velocity equalization, indicates un-balanced velocity panels in the CSLT images, probably due to the tube positioning errors.
2. *Anomaly Identification* – Zero-offset CSLT with velocity equalization balances the velocity panels and an apparent low velocity anomaly is indicated between 0.2-1.0 m depths.
3. *Defect Definition* – A single cut-off velocity of 4,102 m/s is obtained for the whole shaft which is close to the shaft median velocity (4,240 m/s).
4. *Defect Characterization and Imaging* – No defects are indicated.

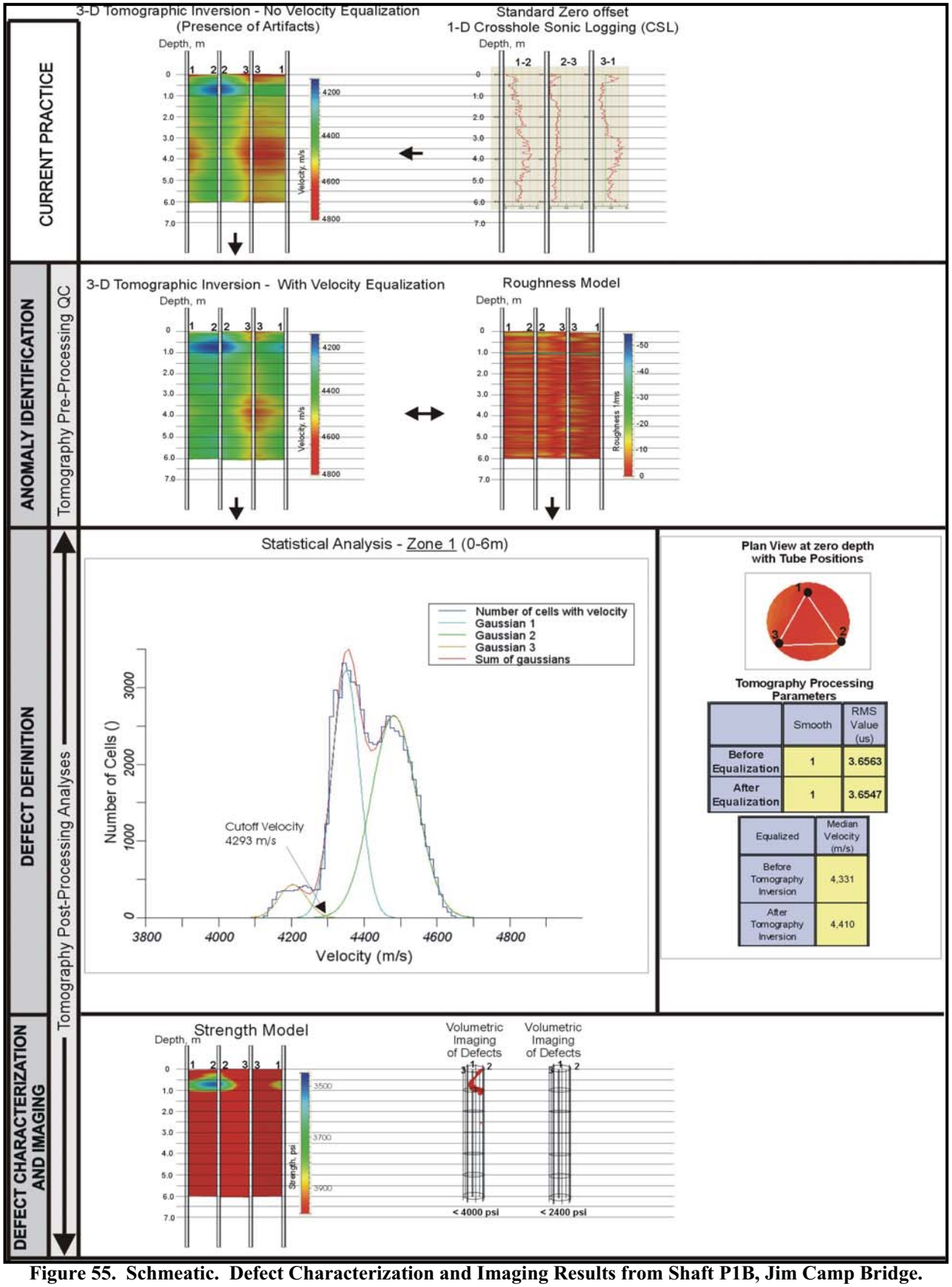

Figure 55. Schmeatic. Defect Characterization and Imaging Results from Shaft P1B, Jim Camp Bridge.

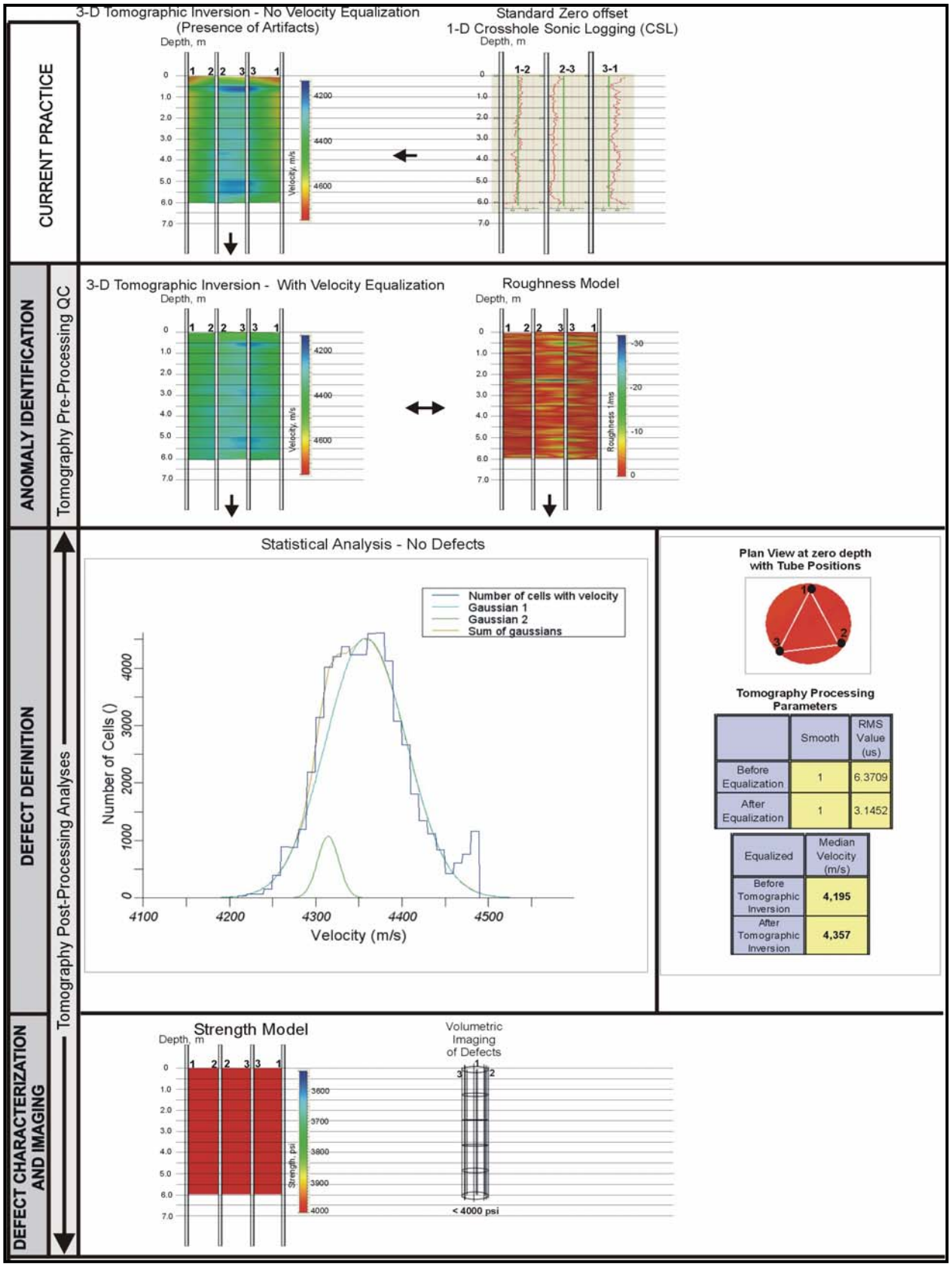

Figure 56. Schematic. Defect Characterization and Imaging Results from Shaft P2A, Jim Camp Bridge.

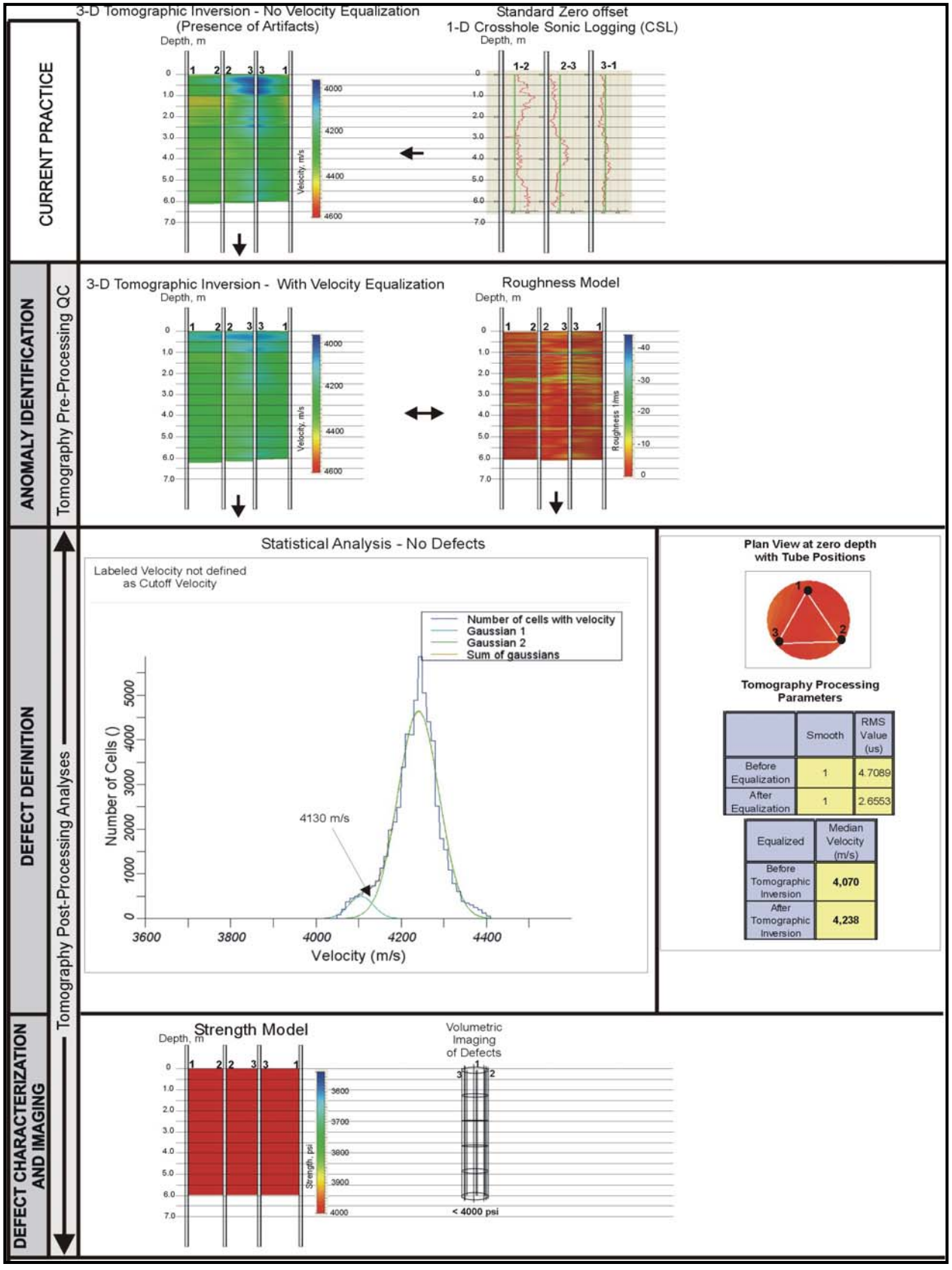

Figure 57. Schematic. Defect Characterization and Imaging Results from Shaft P2B, Jim Camp Bridge.

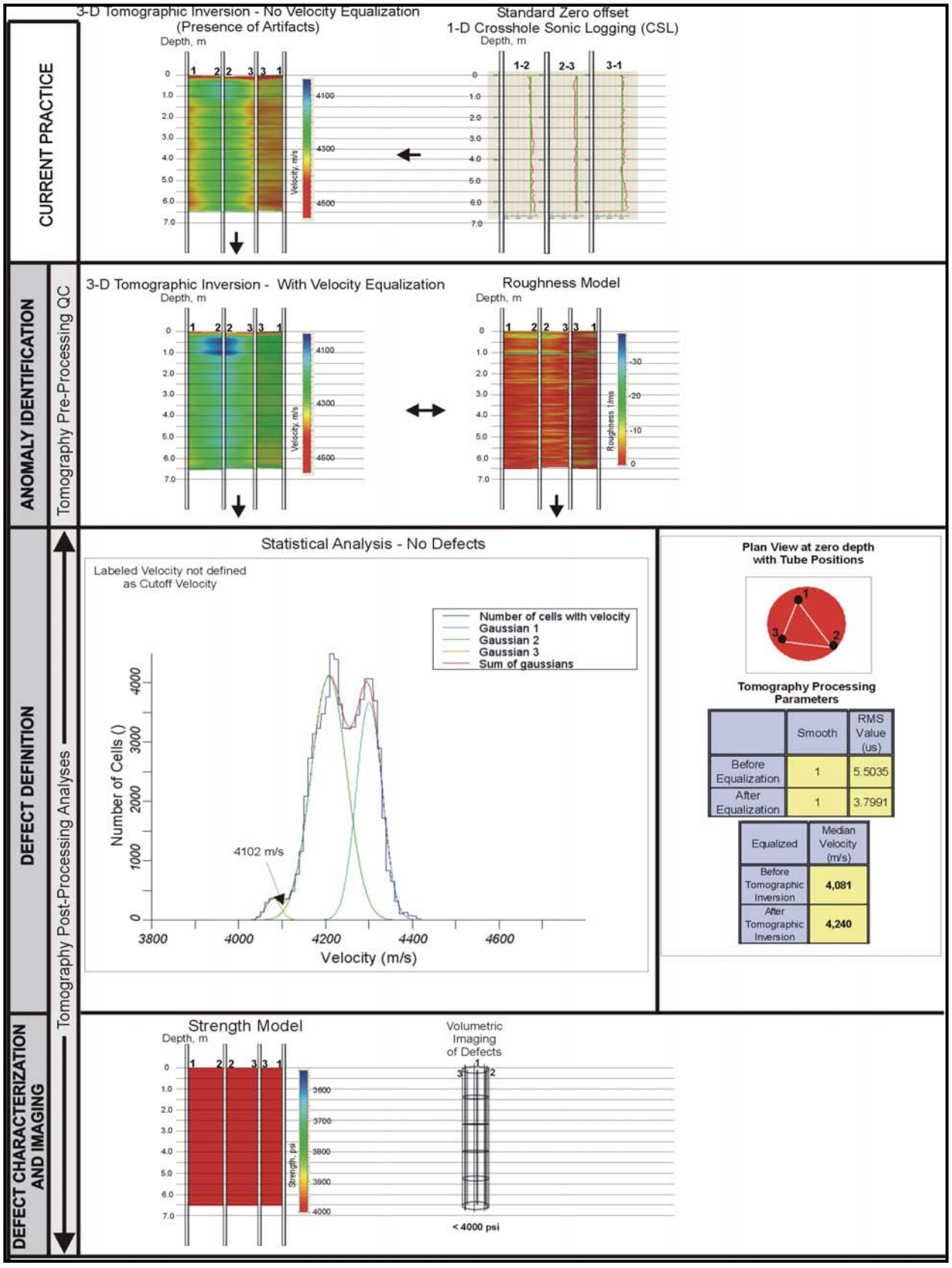

Figure 58. Schematic. Defect Characterization and Imaging Results from Shaft P3A, Jim Camp Bridge.

5.3.11 Jim Camp Bridge, Shaft P3B (Figure 59)

1. *Current Practice* – Standard CSL indicates no anomalies.
   Zero-offset tomography (CSLT), with no velocity equalization, indicates slightly un-balanced velocity panels in the CSLT images.
2. *Anomaly Identification* – Zero-offset CSLT with velocity equalization balances the velocity panels and an apparent low velocity zone indicated between 0.3-1.0 m depths.
3. *Defect Definition* – A single cut-off velocity of 4,400 m/s is obtained for the whole shaft which is about equal to the shaft median velocity (4,428 m/s).
4. *Defect Characterization and Imaging* – No defects are indicated.

5.3.12 Jim Camp Bridge, Shaft P4A (Figure 60)

1. *Current Practice* – Standard CSL indicates no anomalies, just irregular CSL dataset.
   Zero-offset tomography (CSLT), with no velocity equalization, indicates a low velocity zone between 0.5-1 m.
2. *Anomaly Identification* – Zero-offset CSLT with velocity equalization balances the velocity panels also confirms the low velocity zone near Tube 2 with slight indication in the roughness model.
3. *Defect Definition* – Two zones are selected and velocity cut-off values are indicated using 2 and 3 Gaussian fits to the velocity histogram. Anomaly 1 (0-2 m) has a cut-off velocity of 3,800 m/s, which is close to shaft median velocity of 4,067 m/s.
4. *Defect Characterization and Imaging* – One small defect between 0.2-1 m near Tube 2 is indicated. Volumetric images indicate that this defect is of high relative strength (~27,600 kPa (4,000 psi)).

5.3.13 Jim Camp Bridge, Shaft P4B (Figure 61)

1. *Current Practice* – Standard CSL indicates no anomalies.
   Zero-offset tomography (CSLT), with no velocity equalization, indicates un-balanced velocity panels in the CSLT images.
2. *Anomaly Identification* – Zero-offset CSLT with velocity equalization balances the velocity panels.
3. *Defect Definition* – A single cut-off velocity of 4,128 m/s is obtained for the whole shaft which is close to the shaft median velocity (4,299 m/s).
4. *Defect Characterization and Imaging* – No defects are indicated.

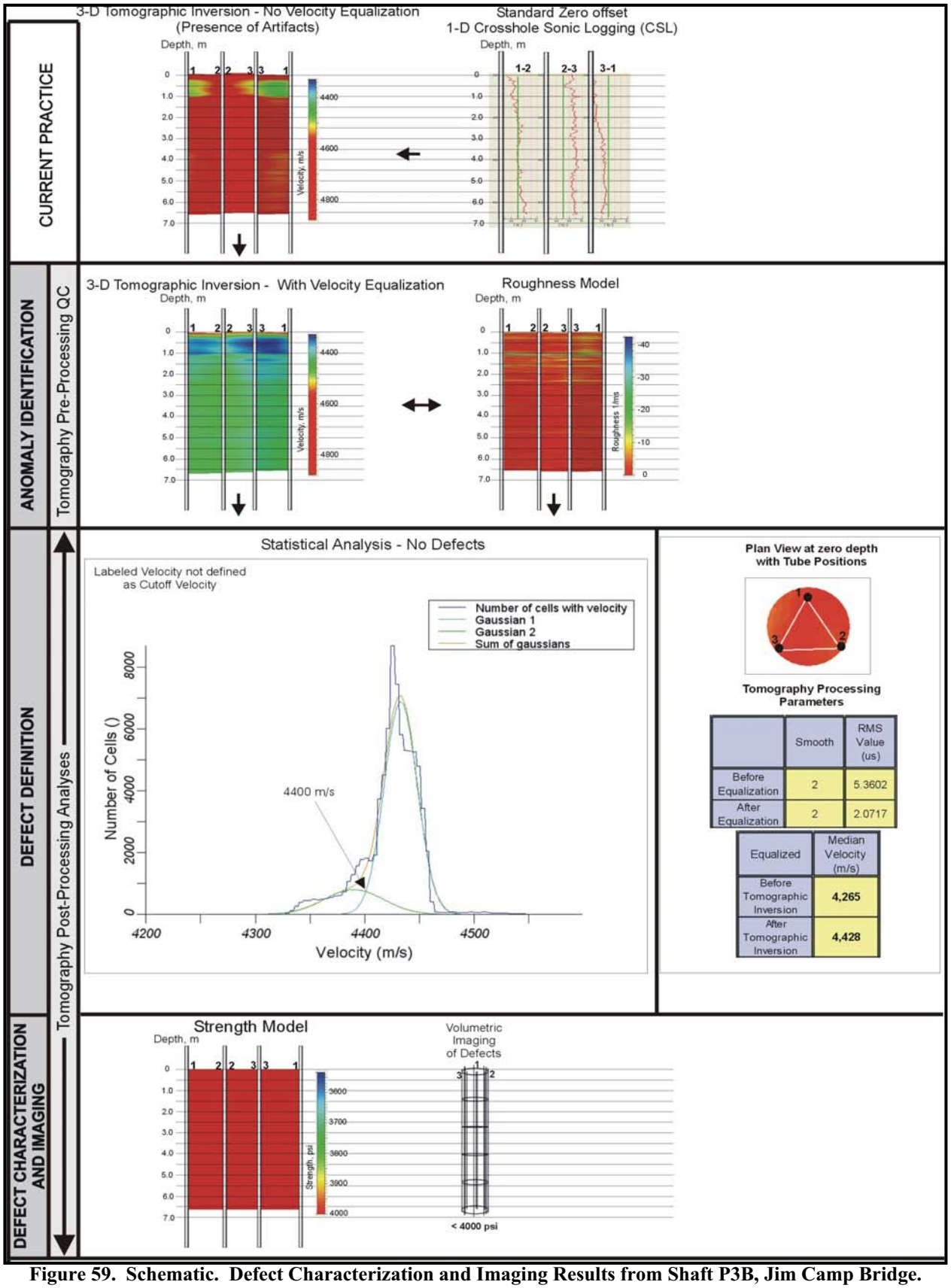

Figure 59. Schematic. Defect Characterization and Imaging Results from Shaft P3B, Jim Camp Bridge.

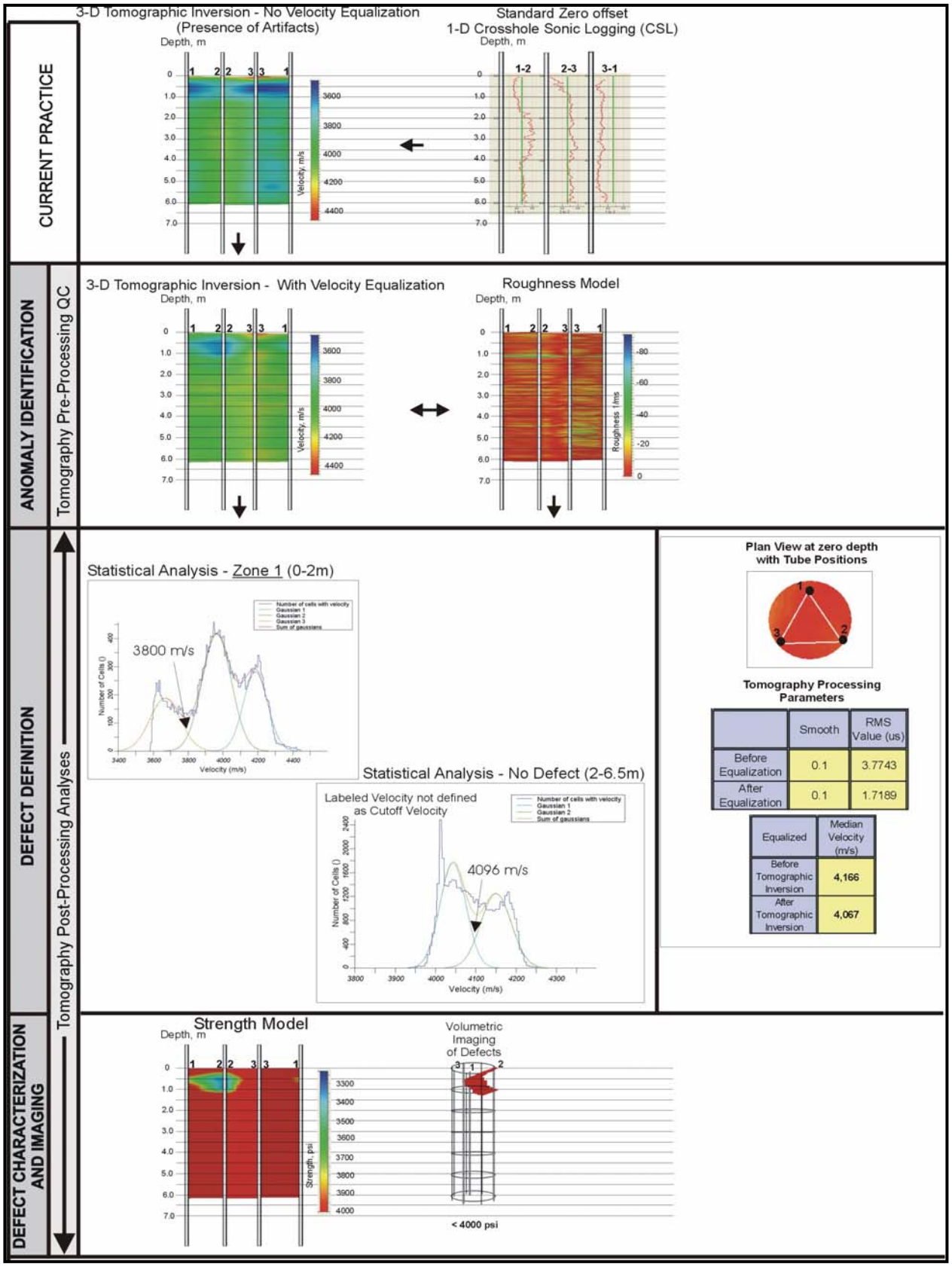

Figure 60. Schematic. Defect Characterization and Imaging Results from Shaft P4A, Jim Camp Bridge.

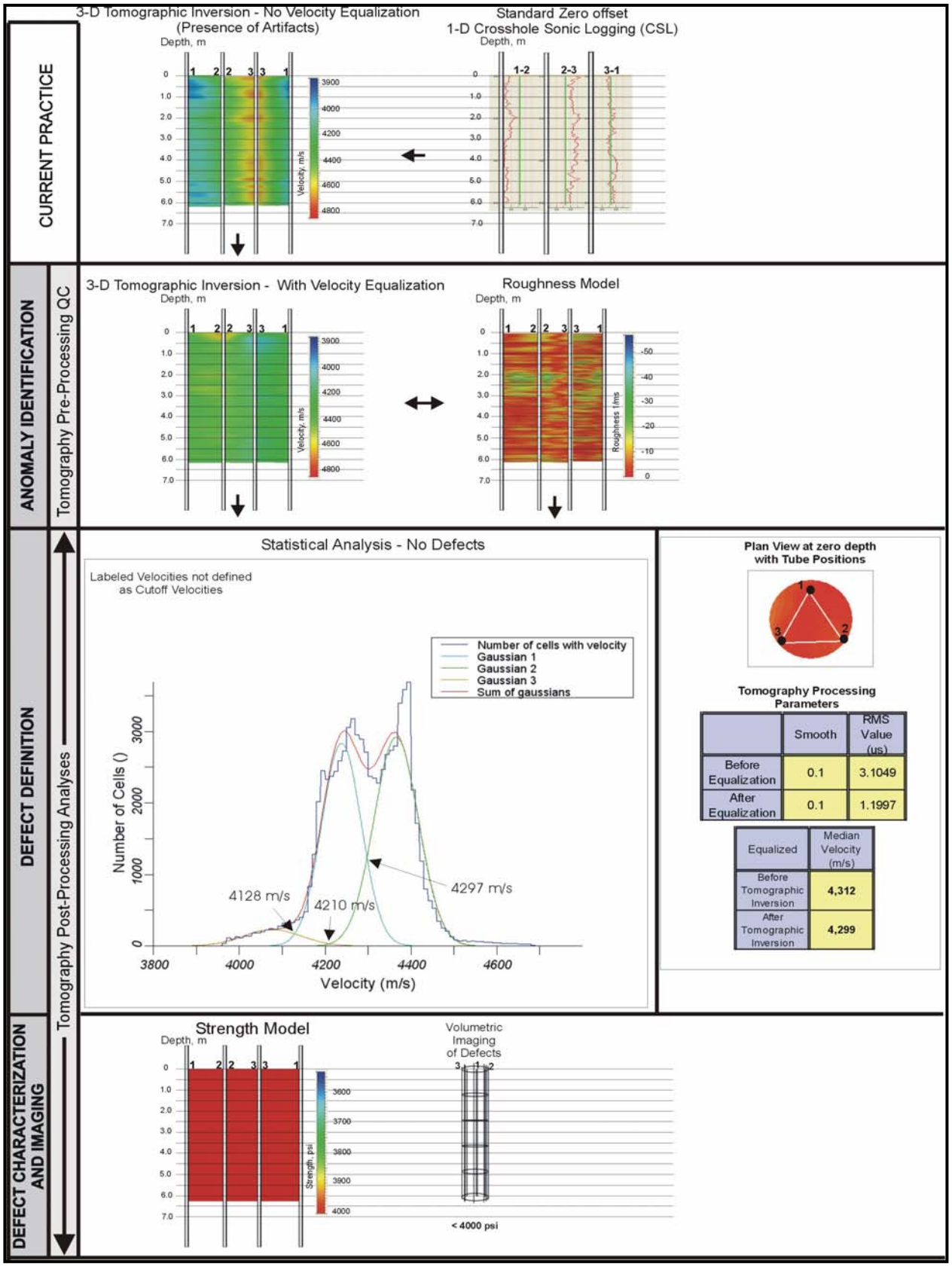

Figure 61. Schematic. Defect Characterization and Imaging Results from Shaft P4B, Jim Camp Bridge.

5.4 SEVENMILE-GOOSBERRY ROAD BRIDGE RESULTS

The Sevenmile-Gooseberry Road Project is located at Fishlake National Forest, near Salina, Utah. Six (6) existing shafts were tested using standard crosshole sonic logging by Olson engineering. Each drilled shaft had a diameter of 0.91 m (3 ft) and each contained three (3) 50.8 mm (2 in) I.D. schedule-40 steel access tubes.

In summary, CSL results indicated five (5) shafts out of a total of six (6) shafts to exhibit a soft bottom condition at the bottom 0.5 – 1 m (1-3 ft). The defective shafts were Abutment 2: Shafts 8, 9,10, 11, and 12. Subsequently, gamma-gamma density (GDL) and neutron-moisture logging (NML) was performed by Blackhawk GeoServices which confirmed the CSL soft bottoms for independent verification of anomalies. In addition, as reported in Section 4.1.3.1, laboratory ultrasonic pulse velocity (UPV) testing was performed at 4, 7, 14, 21, and 28 day intervals to obtain strength information.

Results from the Sevenmile-Gooseberry test site are summarized below:

5.4.1 Sevenmile-Gooseberry, Shaft 7 (Figure 62)

1. *Current Practice* – Standard CSL indicates no anomalies.
   Zero-offset tomography (CSLT), with no velocity equalization, is highly un-balanced, probably due to the tube positioning errors in the field.
2. *Anomaly Identification and Verification* – Zero-offset CSLT with velocity equalization indicates no anomalies. GDL data indicates no anomalies. (In our presentation format, GDL data is shown along with mean, 2, and 3 standard deviations from mean indicated in green, blue, and red vertical lines, respectively).
3. *Defect Definition* – No single low cut-off velocity can be determined for the sound shaft.
4. *Defect Characterization and Imaging* – No anomalies are detected in the shaft.

5.4.2 Sevenmile-Gooseberry, Shaft 8 (Figure 63)

1. *Current Practice* – Standard CSL indicates a soft bottom between 17-17.5 m.
   Zero-offset tomography (CSLT), with no velocity equalization, images the soft bottom.
2. *Anomaly Identification and Verification* – Zero-offset CSLT with velocity equalization better resolves the soft bottom with slight indication in the roughness model. GDL (shown in black) indicates no anomalies; therefore, the anomaly is located in the interior portion of the shaft. Note, however, that NML (shown in red) indicates that a high moisture zone exists in the bottom of the shaft.
3. *Defect Definition* – A single low cut-off velocity of 2,807 m/s is obtained for the whole shaft, which is less than the shaft median velocity (3,344 m/s).
4. *Defect Characterization and Imaging* – The soft bottom is clearly imaged in the strength model. Volumetric imaging indicates the soft bottom to be structurally significant (<16,500 kPa (2,400 psi)).

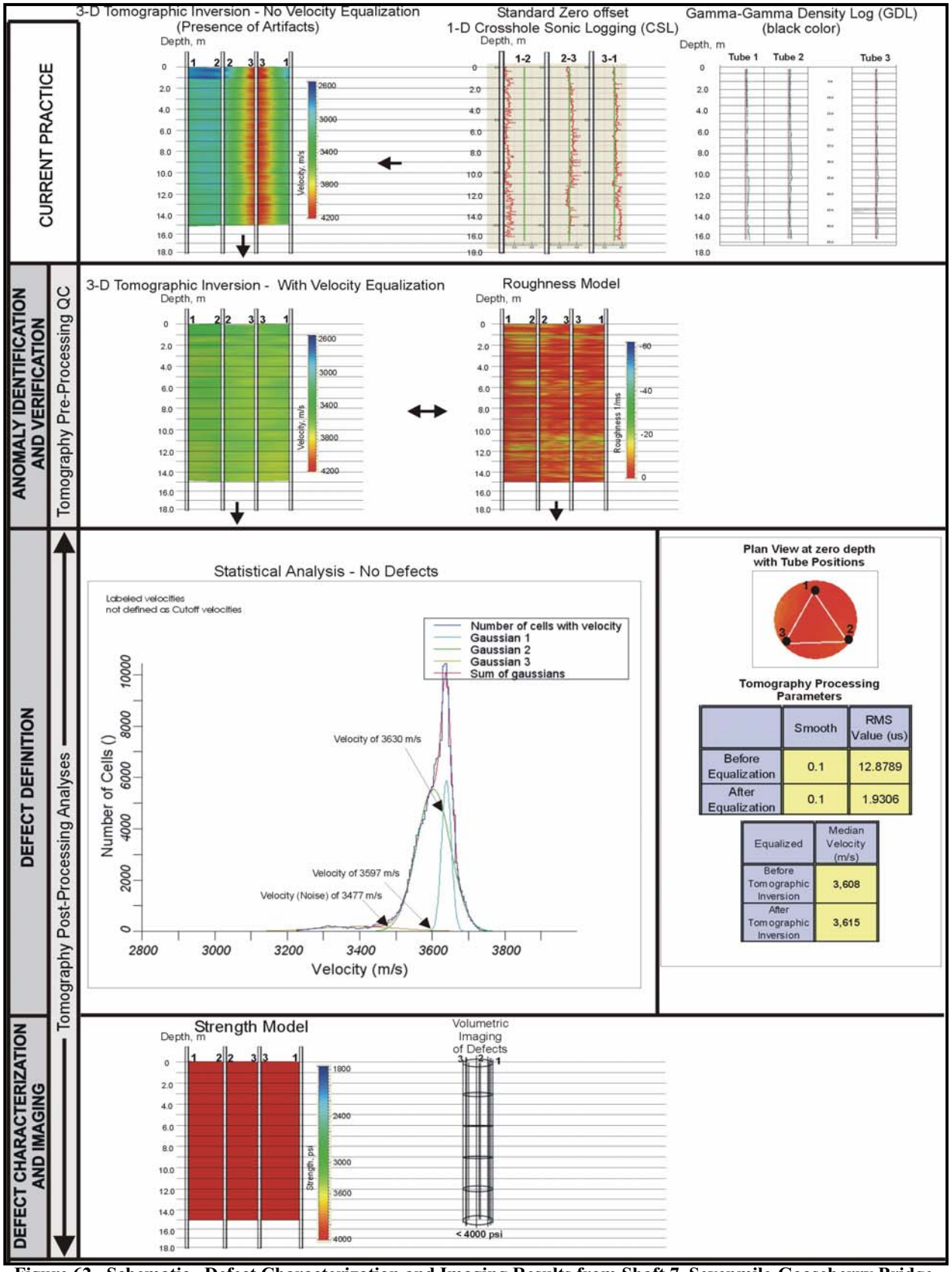

Figure 62. Schematic. Defect Characterization and Imaging Results from Shaft 7, Sevenmile-Gooseberry Bridge.

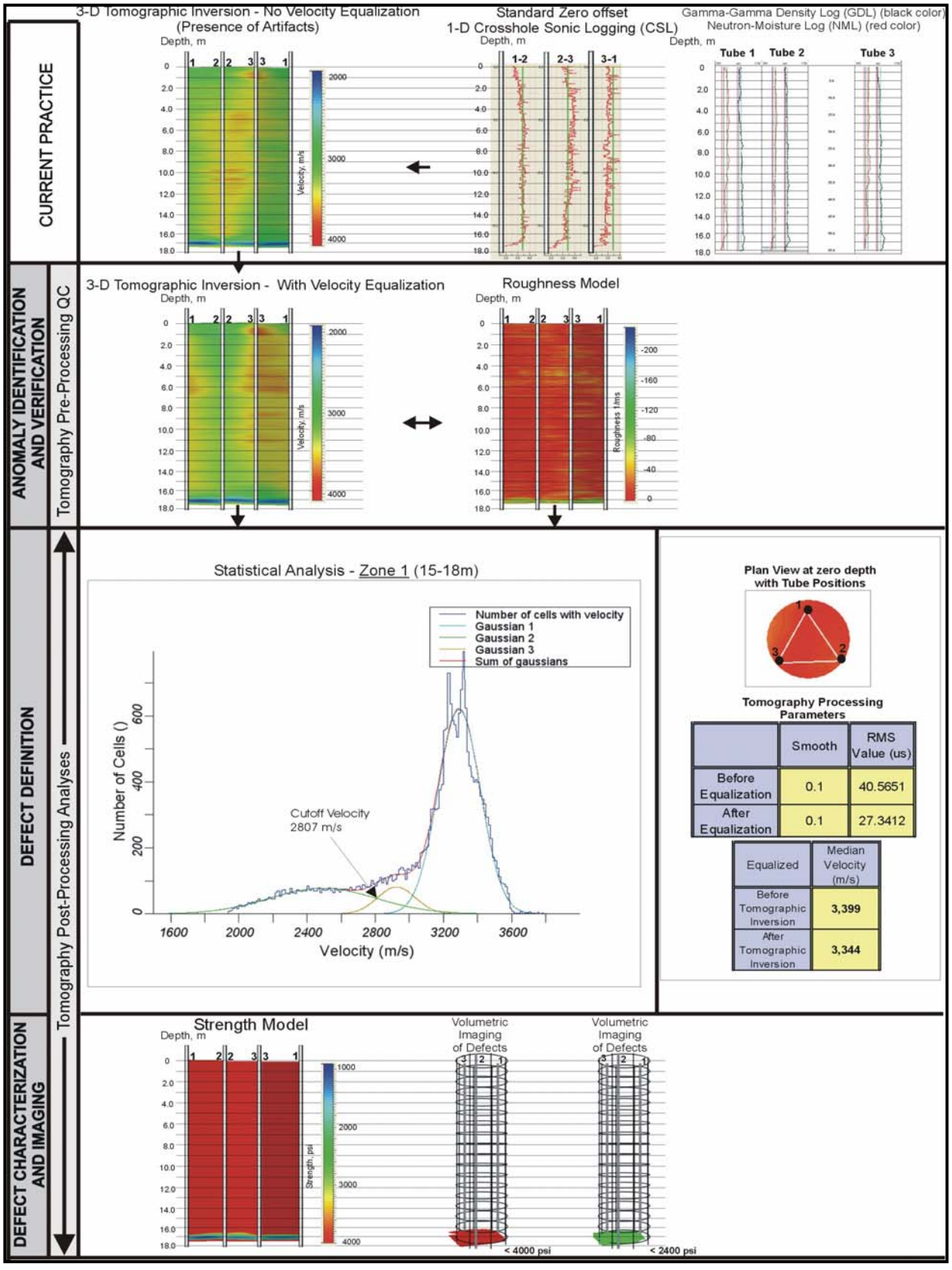

Figure 63. Schematic. Defect Characterization and Imaging Results from Shaft 8, Sevenmile-Gooseberry Bridge.

5.4.3 Sevenmile-Gooseberry, Shaft 9 (Figure 64)

1. *Current Practice* – Standard CSL indicates a soft bottom between 17-17.5 m. Zero-offset tomography (CSLT), with no velocity equalization, images the soft bottom.
2. *Anomaly Identification and Verification* – Zero-offset CSLT with velocity equalization slightly better resolves the soft bottom with slight indication in the roughness model. GDL (shown in black) and NML (shown in red) confirm the soft bottom anomaly.
3. *Defect Definition* – A single low cut-off velocity of 2,634 m/s is obtained for the whole shaft.
4. *Defect Characterization and Imaging* – The soft bottom is clearly imaged in the strength model. Volumetric imaging indicates the soft bottom to be structurally significant.

5.4.4 Sevenmile-Gooseberry, Shaft 10 (Figure 65)

1. *Current Practice* – Standard CSL indicates a soft bottom between 16-16.5 m near Tube 2. Zero-offset tomography (CSLT), with no velocity equalization, images the soft bottom.
2. *Anomaly Identification and Verification* – Zero-offset CSLT with velocity equalization better resolves the soft bottom with good indication in the roughness model. GDL indicates only a small drop in density in Tube 2; therefore, the anomaly is situated in the inside of the shaft just missing Tubes 1 and 3.
3. *Defect Definition* – A single low cut-off velocity of 3,455 m/s is obtained for the whole shaft.
4. *Defect Characterization and Imaging* – The soft bottom is clearly imaged in the strength model. Volumetric imaging indicates the soft bottom to be structurally significant (<16,500 kPa (2,400 psi)).

5.4.5 Sevenmile-Gooseberry, Shaft 11 (Figure 66)

1. *Current Practice* – Standard CSL indicates a soft bottom between 17-17.5 m. Zero-offset tomography (CSLT), with no velocity equalization, images the soft bottom.
2. *Anomaly Identification and Verification* – Zero-offset CSLT with velocity equalization better resolves the soft bottom with slight indication in the roughness model. GDL indicates an anomaly only in Tube 3; therefore, the anomaly extends to the interior portion of the shaft just missing Tubes 1 and 2.
3. *Defect Definition* – A single low cut-off velocity of 2,831 m/s is obtained for the whole shaft.
4. *Defect Characterization and Imaging* – The soft bottom is clearly imaged in the strength model. Volumetric imaging indicates the soft bottom to be structurally significant (<16,500 kPa (2,400 psi)).

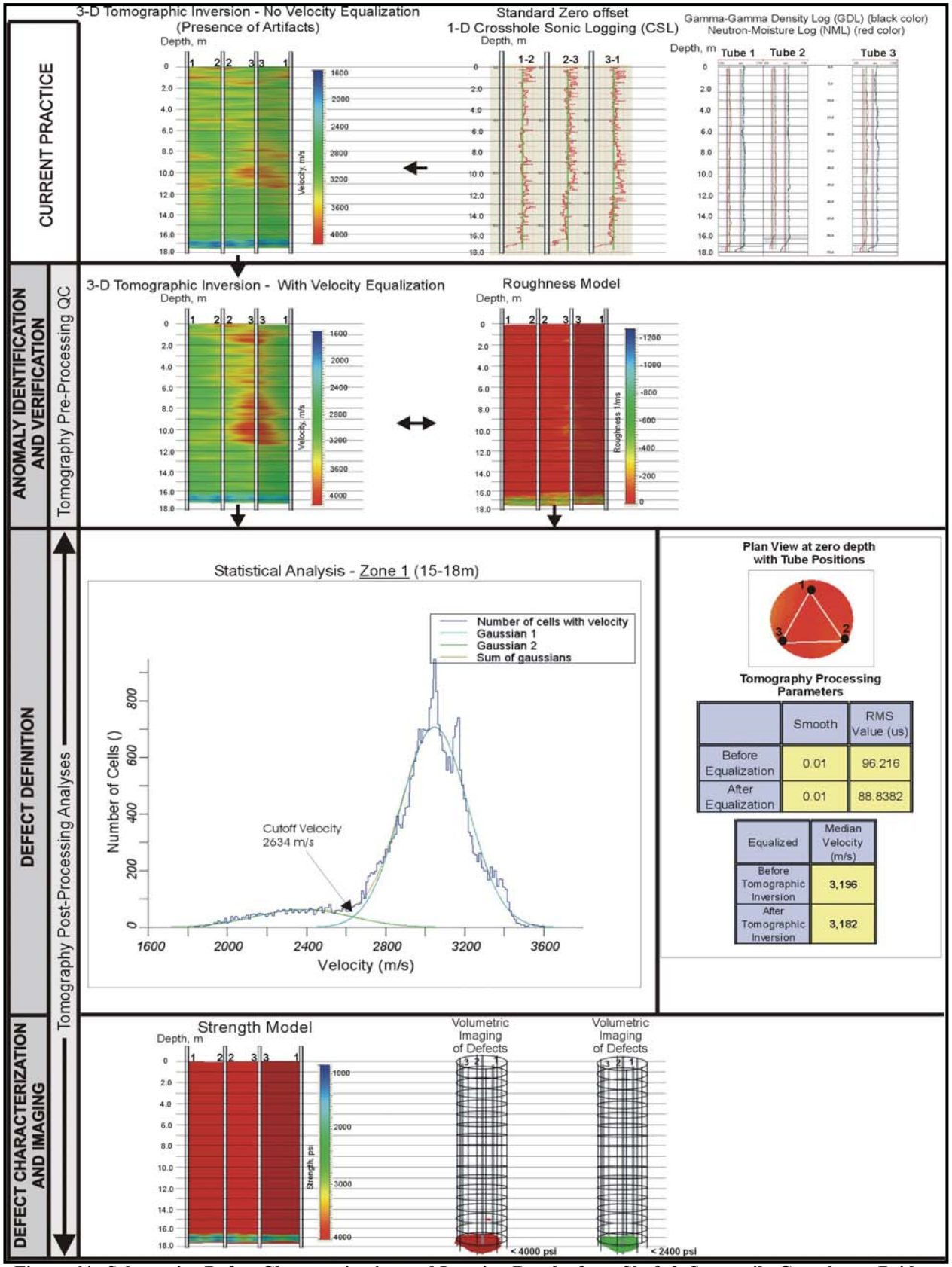

Figure 64. Schematic. Defect Characterization and Imaging Results from Shaft 9, Sevenmile-Gooseberry Bridge.

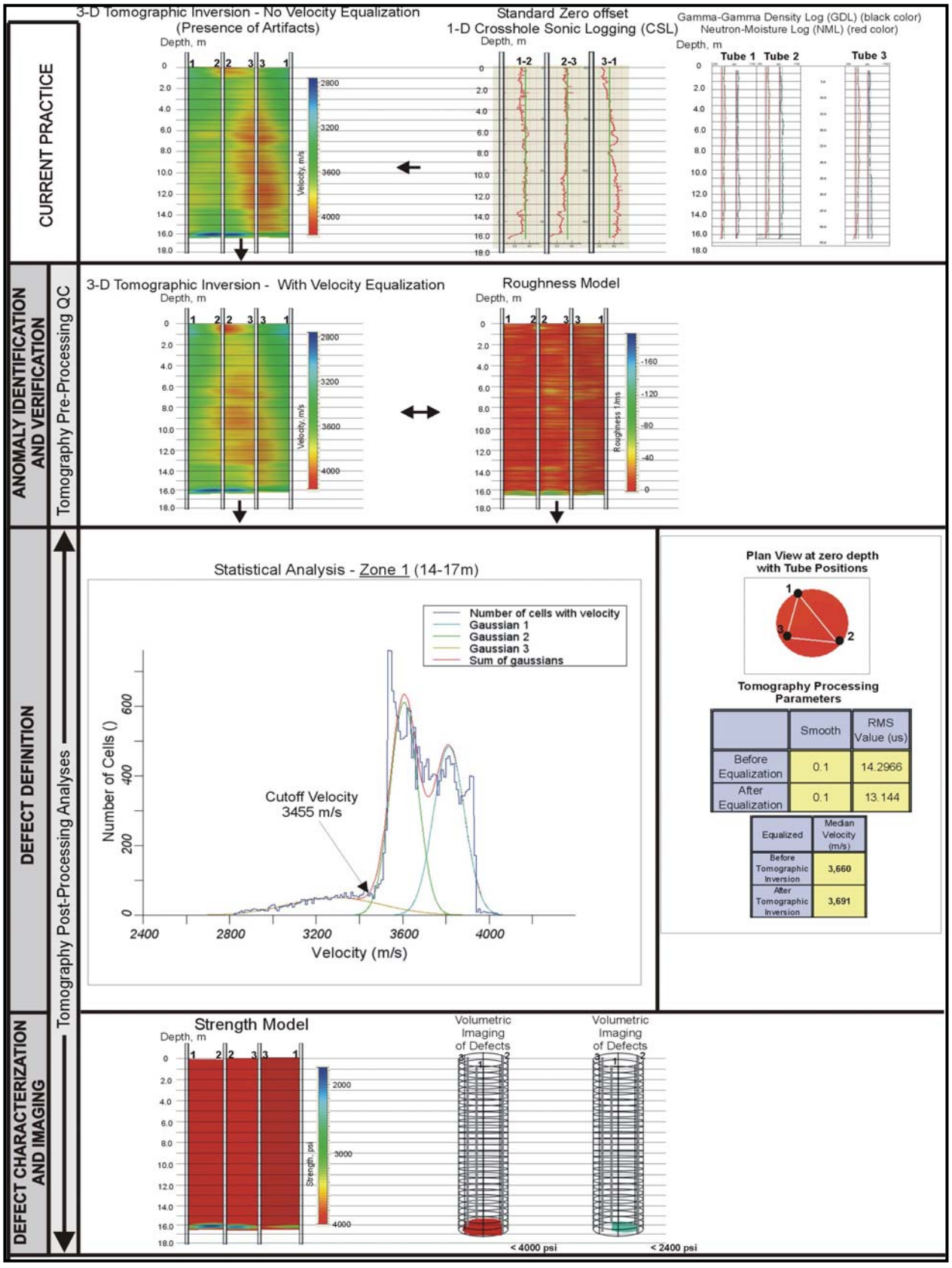

Figure 65. Schematic. Defect Characterization and Imaging Results from Shaft 10, Sevenmile-Gooseberry Bridge.

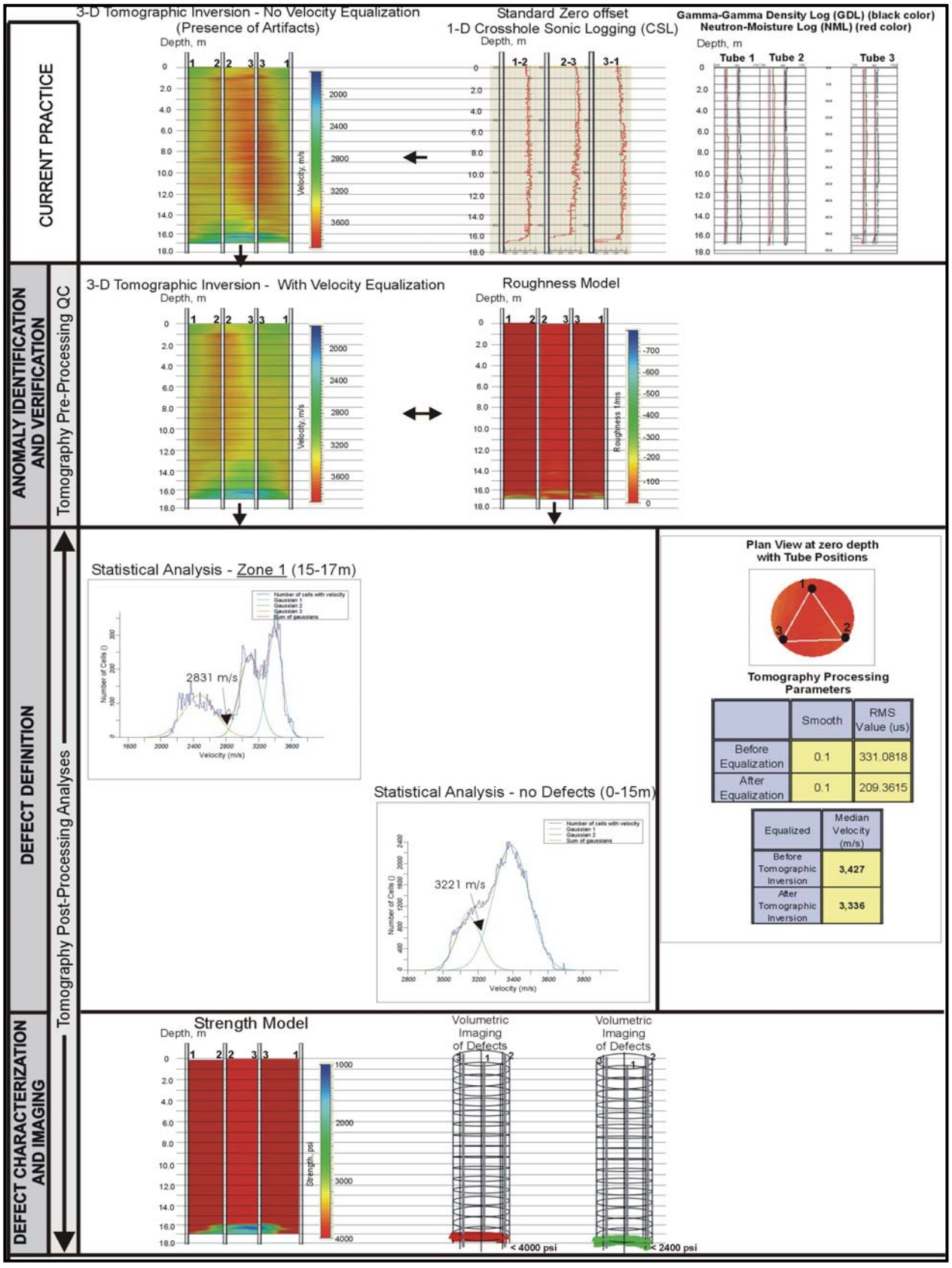

Figure 66. Schematic. Characterization and Imaging Results from Shaft 11, Sevenmile-Gooseberry Bridge.

5.4.6 Sevenmile-Gooseberry, Shaft 12 (Figure 67)

1. *Current Practice* – Standard CSL indicates no anomalies.
   Zero-offset tomography (CSLT), with no velocity equalization, is highly un-balanced, probably due to the tube positioning errors in the field.
2. *Anomaly Identification and Verification* – Zero-offset CSLT with velocity equalization indicates a small anomaly between 14-16 m. GDL also indicates no anomalies.
3. *Defect Definition* – A single low cut-off velocity of 2,596 m/s is obtained for the whole shaft.
4. *Defect Characterization and Imaging* – One small defect between 13-16 m near Tubes 2 and 3 is indicated. Volumetric images indicate that this defect is not structurally significant (>16,500 kPa (2,400 psi)).

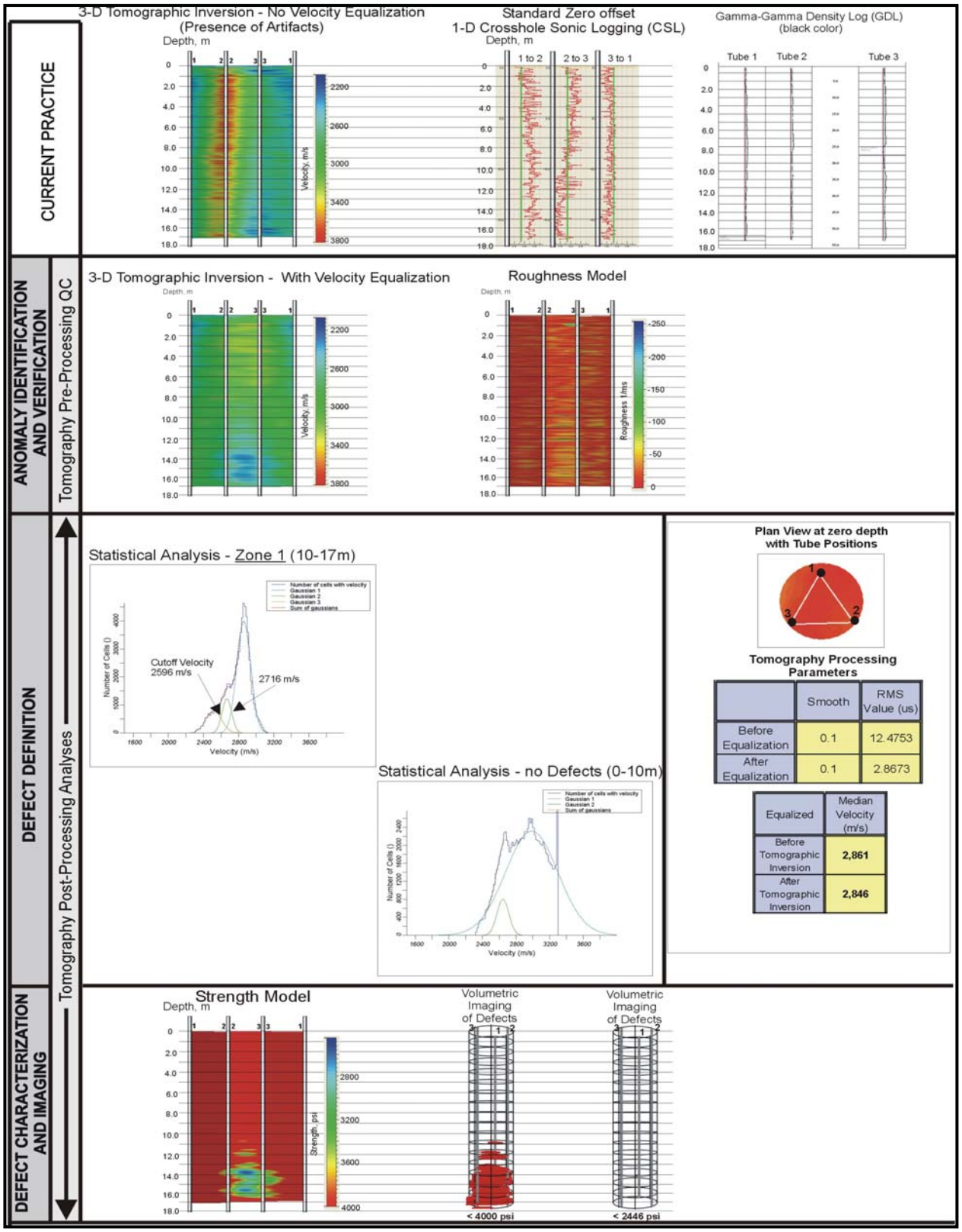

Figure 67. Schematic. Characterization and Imaging Results from Shaft 12, Sevenmile-Gooseberry Bridge.

CHAPTER 6 – SUMMARY, CONCLUSIONS, AND RECOMMENDATIONS

6.1 SUMMARY

In this study, a three-step approach was developed for integrity assessment of drilled shaft foundation that contains access tubes, according to:

1. *Anomaly Identification and Independent Verification* - The first step addressed how to correctly identify and independently verify anomalies in a drilled shaft. A dual testing approaches using crosshole sonic logging (CSL) and gamma-gamma density logging (GDL) methods was used. For proper imaging of shaft's interior, a three-dimensional crosshole sonic logging tomography (CSLT) inversion technique was utilized.
2. *Defect Definition* – Once a suspected "anomaly" zone was identified in a CSLT data, the second part of this study used a statistical analysis to separate velocity distribution of sound concrete from anomalous concrete. With this analysis, a cut-off velocity was obtained that separated the two velocity distributions. The cut-off velocity was used to volumetrically image (contour) a "defect".
3. *Defect Characterization and Imaging* - The third part of this study related changes in velocity values in the defect volume to changes in concrete strength and a 3-D strength image was developed for the integrity assessment by the engineer.

6.2 CONCLUSIONS

The report conclusions are as follows:

- *Anomaly Identification and Verification* – It was demonstrated that a dual CSL/GDL testing must be used to correctly identify anomalies. CSL did not record anomalies outside the rebar cage; GDL did not record anomalies in the interior portion of the shaft and did not distinguish between isolated anomalies located outside the cage from those that extend inside the cage but do not intercept the tubes. Dual testing approach also eliminated CSL and GDL false positives.
- *Shaft Velocity Imaging* – Two and three- dimensional crosshole sonic logging tomography (CSLT) was used for imaging the shaft's interior. It was found that for best results, a tomographic inversion package must be used that employs true 3-D inversion followed by 3-D display of the data. 2-D inversion of data followed by 3-D display sometimes created unacceptable velocity gradients between 2-D panels.
- *CSLT Pre-Processing (Velocity Equalization)* - CSLT requires the use of a true 3-D tomographic inversion package which entails the critical pre-processing step for velocity equalization. It was demonstrated that velocity equalization significantly reduced boundary artifacts and resolved anomalies better—especially for the 3-D inversion.
- *Defect Definition* - In this study, a statistical approach was used to determine cut-off velocities by fitting multiple Gaussian distribution curves to the CSLT velocity histogram. The curve fitting approach was applied separately for several levels of defects. For defective shafts, two to three Gaussian fit adequately resolved for a cut-

off velocity. For shafts without a defect, either a single Gaussian fit to the velocity histogram or a two Gaussian fit was obtained with a cut-off velocity close or higher than the median velocity. It was demonstrated that the cut-off velocity defines the defect volume in a velocity tomogram.

- *Defect Imaging (Velocity)* – Using the cut-off velocities, volumetric images of the defect was obtained (velocity contouring). It was demonstrated that tomography slightly over sizes defects but underestimates their velocities.
- *Defect Imaging (Strength)* – Finally, an empirical method was used to correlate velocity to strength and defect images were obtained in units of strength. A procedure was described for developing a shaft-specific velocity to strength correlation using laboratory concrete cylinders with the same design mix as the shaft and measuring their maturity. In developing the strength models, the edge artifacts present in tomograms were excluded; therefore, the strength tomograms represented the final interpretation for integrity assessment by the engineer. Strength tomograms sometimes resolved for small defects which were not readily observed in velocity tomograms using a separate cut-off velocity in that zone.
- *Shaft Monitoring Results* - It appeared that the strength of the concrete in a drilled shaft was not only a function of time but also a function of the physical properties of the surrounding soil/rock and the depth of the groundwater table (boundary condition). Two parameters from the soil profile were noted: the thermal conductivity and the permeability. Conductivity controls relative changes in temperature and permeability controls small relative changes in the moisture content. These parameters in turn control curing (age) and concrete strength—as it relates to incremental changes in velocity and density.

Therefore, in this study, a more compelling basis was created for the foundation engineer in deciding to accept, correct (remediate), or reject a given drilled shaft or a wall structure.

6.2.1 Benefits of Tomographic Imaging

For the anomalies that extend inside the rebar cage, the CSLT method is an indispensable tool for volumetric imaging of defects. CSLT also images horizontally elongated defects (such as cold joints) missed by both CSL and GDL methods. Therefore, three (3) main benefits of tomographic imaging can be identified:

1. Tomographic imaging provides better spatial resolution of defects for confirmation through coring followed by remedial action (if necessary);
2. Tomographic images provides a more accurate correlation between percentage drop in velocity with percentage drop in concrete strength for shaft acceptance criteria; and,
3. Two and three dimensional tomography, when performed routinely, will provide engineers in the owner agencies a tool for assessing the integrity of drilled shaft foundations without further costly delays to construction.

6.3 RECOMMENDATION FOR FUTURE STUDY

For future study, it is recommended to construct a test drilled shaft (preferably at a federal or state test site) of diameter of 1.8 m (6 ft) or larger containing both PVC and steel access tube with engineered defects. Accordingly, the following investigations are recommended:

- *Field Monitoring of The Shaft during Curing Cycle* – A second temperature monitoring study needs to be conducted at a larger diameter shaft of at least 1.8 m (6 ft)—as compared to the present study of 0.9 m (3 ft) diameter shaft—to better understand mass concrete behavior in drilled shafts. A continuous monitoring of temperature must be performed using both maturity meters and continuous geophysical temperature logging method. Along with temperature monitoring above, continuous crosshole sonic logging, gamma-gamma density, and neutron-moisture log measurements must be obtained on at least a 7-day period to examine changes in velocity, density, and moisture content versus time (or curing of the mass concrete).
- *Laboratory Testing and Monitoring* – Standard size concrete cylinders and beams must be placed using the same mix proportions used in the construction of the test drilled shaft. The specimens, equipped with thermocouples, must be connected to a maturity meter for a period of 28 days. Shortly before a specimen is subjected to strength test, ultrasonic pulse velocity measurement must be performed with 40 kHz frequency transducers. Standard compression or three point bending tests must be performed on at least 3 cylinders or beams at ages of 1, 4, 7, 14, 21, and 28 days. Next, a plot between the average compressive or flexural strengths and average maturity values at corresponding times must be made and a best-fit curve is drawn through the plot. The curve is then used for estimating the strength of concrete based on maturity. Similarly, a plot between the average compressive or flexural strengths and average velocity must be developed.
- *Permanent Test Site for the Calibration of Gamma-Gamma Density Probes* – The shaft must be constructed using three different concrete mixes (for instance, by changing water-cement ratio) at three different depth intervals. In this way, this shaft will serve as a much-desired permanent test site for GDL probe calibration under realistic field conditions with different tube types, and presence of the rebar cage. The three batches can be created using different densities; for example, at 1.6 g/cm^3 (100 lb/ft^3), 2.4 g/ cm^3 (150 lb/ft^3), and 3.2 g/cm^3 (200 lb/ft^3). In addition, velocity strength information must be obtained using each different concrete batch.
- *Defect Study* – The shaft must be constructed using engineered defects both inside and outside the rebar cage. The defects will be used in a defect study comparing the capabilities of all geophysical logging methods. In addition, defect definition by GDL method will be compared using PVC versus steel pipes. The carefully designed defects can be used for calibrating the radius of investigation of GDL probes. Special care must be taken in constructing the defects so that they do not collapse during construction.
- *Velocity to Strength Correction Factors* - Tomography tends to slightly over size defects and underestimates their velocities. Therefore, a corrective factor needs to be determined to apply to defect velocities for accurate correlation to strength. More extensive modeling study, similar to tomography modeling in Section 2.2.3, needs to be performed. Other correction factors include terms to correct for the effect of temperature, as

discussed above, and those discussed in Section 4.2. Using these correction factors, shaft-specific strength models must be developed.

- *Integrity Assessment* – The final goal of this study is to input strength models described in this study into a drilled shaft design modeling program (such as Florida Pier and PLAXIS finite element programs). Procedures for doing this task using commonly used shaft design programs needs to be described. These programs may also incorporate the soil profile as well as other drilled shafts in a shaft group. In this way, the effect of a defective shaft to the load capacity of the entire designed structure can be assessed and final evaluation of shaft integrity and serviceability can be analyzed by the engineer more quantitatively than the present practice.
- *Development of New Guidelines* – Finally, a new testing guideline needs to be written to address the steps required to identify, verify, image and assess the integrity of drilled shafts, as is described in the next section. This guideline must also include a detailed description of remediation methods and discuss each method's advantages and limitations.
- *Refine the Design Procedures* – Given the assumption that the drilled shafts are constructed properly without defects, the design procedures and factors of safety need to be refined for an improved cost efficiency and design life.

6.4 PROPOSED NEW GUIDELINES FOR NDE TESTING PROGRAM OF DRILLED SHAFT FOUNDATIONS

Ultimately, this focused effort will be directed by the FHWA-FLH in developing new guidelines and specifications for the foundation engineers in defining potentially defective concrete drilled shaft foundations and retaining walls. The guideline will close the decision making loop so that integrity evaluation are made within days of field testing rather than within weeks/months which is the current practice. A clear methodology or "road map" must be laid out for the engineers in the owner agencies as how to relate observed anomalies in CSL/CSLT data to possible defect definition, whether those defects are structurally significant, and what effective corrective measures are available for immediate remedial solutions. Ultimately, the new guidelines and specifications will eliminate uncertainty in integrity assessment of drilled shaft foundations, will result in project savings, and reduces costly project delays.

A brief example of the NDT testing guidelines are described herein. Based on the results of this study, it is recommended that the NDT testing program of the owner agencies to consist of the following three phases:

Phase I. Anomaly Identification (and Verification) – In this phase, the testing agency initially performs dual CSL and GDL testing at any time after 1.5-2 days after concrete placement to *screen*—as a whole—between sound and anomalous shafts and independently verify their existence. Dual testing is required to assess shaft integrity both inside ("core" of the shaft) and outside the rebar cage (cage "cover" and rebar's exposure to soil/moisture). Dual testing is also required to independently verify anomalies and discern false positives (or false negatives) of a particular test method (please refer to Appendix A case histories for examples).

Phase II. Strength Imaging of Defects – Only for the shafts suspected to be defective in the first phase, tomographic imaging is performed at least 7 days after the concrete placement. In this way, the sonic velocities in the tomogram will be similar to the laboratory measurements and a more realistic velocity-strength correlation is obtained in developing the final strength images.

Alternative Approach - Combined Phase I and II. CSLT testing is done at the same time as CSL/GDL testing and less than 7 days after the concrete placement. A total of 2-3 shafts must be instrumented with thermocouples at each soil, rock, and ground water boundary and continuously logged using maturity meters. In this way, CSLT velocities of the same maturity will be compared to the cylinder strength data. Otherwise, the less accurate fourth-power velocity to strength empirical relationships must be used.

In either approach, three-dimensional tomographic imaging software must be used and all CSL velocity curves must be equalized prior to the tomographic inversion. Statistical analysis must be used to analyze post-tomography images for determining cut-off velocity between sound and defective concrete.

Phase III. Shaft Integrity Evaluation and Remediation – In this phase, the strength image is input into the original shaft design program to determine if the shaft is still serviceable, can be repaired by remediation, or unacceptable. In this way, a final integrity (and pay-factor) is assessed by the engineer more quantitatively than the present practice.

Based on the results of modeling and the effects of size and location of a defect in relation to the load capacity of the designed structure, the engineer may recommend remediation. Some important criteria include the location of the maximum moment or the shaft's vulnerability to rebar corrosion when the cage cover is lost due to soil intrusion. For shallow defects, the shaft is usually excavated and patched in place. For deeper defects, the most common remediation method used is coring followed by pressure grouting using micro-fine cement. Other techniques used for deeper defects include compaction grouting (with about 2.5 cm (1" slump)) and jet grouting. CSLT tomography can be used post-remediation to check the effectiveness of remediation.

In the medical field, the first phase is analogous to the initial examination and diagnosis by the general practitioner. The second phase is analogous to the imaging of an unhealthy member. The third phase is analogous to conducting external or internal remedies by the specialist.

Laboratory and Field Support. In support of the NDE testing program above, standard size cylinders or beams must be placed using the same mix proportions used in the construction of the test drilled shaft. Shortly before a specimen is subjected to strength test, ultrasonic pulse velocity measurement (or equivalent test) must be performed using transducers with similar center frequency than the CSL system. Standard compression or three point bending tests must be performed on at least 3 cylinders or beams at ages of 1, 4, 7, 14, 21, and 28 days and a plot between the average compressive or flexural strengths and average velocity must be developed.

If the combined Phase I and II is used, the concrete cylinders must be equipped with thermocouples and be connected to a maturity meter for a period of 28 days. A plot between the

average compressive or flexural strengths and average maturity values at corresponding times must be made and a best-fit curve is drawn through the plot. The curve is then used for estimating the strength of concrete based on maturity. Similarly, a plot between the average compressive or flexural strengths and average velocity must be developed. In the field, the temperature history of each drilled shaft must be recorded from placement to the time CSLT measurements are performed. Using the maturity index, the strength at that maturity is estimated by comparing to the laboratory measurements.

If a separate Phase I and Phase II approach is used, it is *recommended* to equip 1-2 test cylinders with thermocouples and connect to a maturity meter for a period of 28 days. In the field, one test drilled shaft must be embedded with thermocouples near the rebar cage and at the center of the shaft and be monitored for about 10 days. The purpose of this study is to: 1) assess the maximum temperature reached in the shaft; 2) examine maximum temperature differential between the center and the side of the shaft; and, 3) determine the required time for tomographic testing by comparing maturity indexes from the field to the laboratory samples.

REFERENCES

ASTM C597-83 “Standard Test Method for Pulse Velocity through Concrete,” Annual Book of ASTM Standards, Vol 04.02, Philadelphia.

ASTM C1074-93 “Standard Practice for Estimating Concrete Strength by the Maturity Method”, Annual Book of ASTM Standards, Vol 4.02 Concrete and Aggregates.

Chung, H.W. (1978) “Effect of Embedded Steel Bars upon Ultrasonic Testing of Concrete” Magazine of Concrete Research, London, 30(102), 19.

DiMaggio, J. (2004), “Developments in Deep Foundation Highway Practice – The Last Quarter Century” *Foundation Drilling Magazine - The International Association of Foundation Drilling (ADSC)*, Vol 24, No. 2, pp. 16-22.

Dines, K. A., Lytle, R. J. (1979) "Computerized Geophysical Tomography" *Proc. IEEE*, Vol 67, pp. 1065-1073.

Ealy, C., M. Iskander, M. Justason, D. Winters, and G. Mullins (2002) “Comparison Between Statnamic and Static Load Testing of Drilled Shafts in Varved Clay” *Proc.* 9’th International Conference on Piling and Deep Foundations, Nice, June 3-5, 2002.

Gajda, J., VanGeem, M (2002) “Controlling Temperatures in Mass Concrete,” *Concrete International*, pp. 59-61.

Herman, G. T. (1980) “Image Reconstruction from Projections, the Fundamentals of Computerized Tomography” (Academic Press, Inc.).

Ivansson, S. (1986) "Seismic Borehole Tomography- Theory and Computation Methods" *Proc. IEEE*, Vol 74, pp. 328-338.

Iskander M., Roy, D., Ealy, C., Kelley, S.. (2000) “Class-A Prediction of Construction Defects in Drilled Shafts”. Submitted to TRB 2001 Session on Drilled Shaft Capacity & Defects in Varved Clay.

Jones, R. (1954) “Testing of Concrete by an Ultrasonic Pulse Technique” RILEM International Symposium on Nondestructive Testing of Materials and Structures. Paris, Vol 1, Paper no. A-17, 137. RILEM Bull. No. 19, 2nd part, November.

Jones, R., Facaoaru, I. (1969) “Recommendations for Testing Concrete by the Ultrasonic Pulse Method” Materials and Structures Research and Testing (Paris), 2(19), 275.

MATLAB 11 (1998) Partial Differential Equations Toolbox. Mathworks, Inc., Natick, MA.

Nilson, A. H., Winter G., (1986), Design of Concrete Structures, McGraw-Hill Book Company, p.35

Nolet, G. (1987) “Seismic Wave Propagation and Seismic Tomography”, in *Seismic Tomography with Applications in Global Seismology and Exploration Geophysics*, ed. G. Nolet (D. Reidal Publishing Co.), pp. 1-23.

O’Neil, W. M., Reese, C. L. (1999). Drilled Shafts: Construction Procedures and Design Methods. Publication No. FHWA-IF-99-025.

Saul A.G.A. (1951) “Principles Underlying the Steam Curing of Concrete at Atmospheric Pressure” Magazine of Concrete Research, 2(6), 127.

Scales, J. A. (1987) "Tomographic Inversion via the Conjugate Gradient Method" *Geophysics*, Vol 52, pp. 179-185.

Sheriff, R.E., Geldart, L.P. (1995) *Exploration Seismology*, 2nd ed., Cambridge.

Sims, F. *Engineering Formulas*, Industrial Press, 1999.

Welty, J., Wicks, C.E., Wilson, R.E., Rorrer, G.L. (1984) *Fundamentals of Mass, Momentum, and Heat Transfer*, 3rd ed., Wiley and Sons.

Yuan, D., Nazarian, S., Medichetti, A, (2003) “A Methodology for Optimizing Opening of PCC Pavements to Traffic”. Texas Department of Transportation Report No. 4188-2, p.29.

GLOSSARY

2-D Tomographic Inversion. Tomographic reconstruction using two dimensional matrix inversion. Each test panel is inverted independently. Therefore, if four tubes are present in a drilled shaft, 6 independent 2-D inversion is performed (4 perimeter plus 2 diagonal).

3-D Display. 2-D or 3-D tomographic inversion results displayed in side-by-side cross-sectional view, or plan view, or by a contoured velocity covering the shaft volume inside the rebar cage.

3-D Tomographic Inversion. Tomographic reconstruction using three dimensional matrix inversion. Data from all test panels are inverted simultaneously (and only once).

Accuracy. Refers to closeness of a measurement to the true value.

Amplitude. The maximum departure of a wave from the average value.

Anomaly. Refers herein to deviation from uniformity in a concrete structure. No determination is yet made regarding its exact size; just identification has been made. An independent verification (using another logging method) is needed to determine if it does not correspond to a false positive.

Artifacts. Artifacts are erroneous values produced by the tomographic matrix inversion due to inadequate scanning of the test volume, inaccuracies in travel time picking, and inversion process that is non-linear and non-unique. These artifacts mostly occur near the image boundaries.

Attenuation, attenuate. A reduction in energy or amplitude caused by the physical characteristics of a transmitting system.

Bulk density. Bulk density is the mass of material per unit volume; in logging, it is the density, in grams per cubic centimeter, of the rock with pore volume filled with fluid.

Bulk modulus. A modulus of elasticity, relating change in volume to the hydrostatic state of stress. It is the reciprocal of compressibility.

Calibration. Determination of the log values that correspond to environmental units, such as porosity or bulk density; calibration usually is carried out in pits or by comparison with laboratory analyses of core.

Coherence. A measure of the similarity of two oscillating functions.

Compressional wave. Compressional (or compression) acoustic waves (P) are propagated in the same direction as particle displacement; they are faster than shear waves.

Compton scattering. The inelastic scattering of gamma photons by orbital electrons; Compton

scattering is related to electron density and is a significant process in gamma-gamma (density) logging.

Crosshole. In this report, refers to concrete logging carried out between access tubes (see also tomography).

Crosshole Sonic Logging (CSL) – A crosshole method used for integrity testing of concrete whereby source and receiver probes in opposite access tubes are pulled simultaneously as to maintain near horizontal ray paths between them (See zero-offset logging).

CSLT. Please see offset tomography.

Curie. The quantity of any radionuclide that produces 3.70 x 1010 disintegrations per second.

Cut-off Velocity. An important velocity value that separates sound concrete velocity distribution from anomalous concrete velocity distribution. The cut-off velocity is used for velocity contouring in volumetric imaging of defects.

Defect. Refers herein to a velocity anomaly in a concrete structure with a velocity lower than a (statistically determined and significant) cut-off velocity. Whether this defect is structurally significant, depends on location, size, and design factors to be determined by the engineer (integrity testing).

Density log. Also called gamma-gamma density log (GDL); gamma photons from a radioactive source in the sonde are backscattered to a detector; the backscattering is related to the bulk density of the material (concrete) around the sonde.

Depth of investigation. See volume of investigation, also called radius of investigation.

Detector. Can be any kind of a sensor used to detect a form of energy, but usually refers to nuclear detectors, such as scintillation crystals.

Dispersion. A property of seismic surface waves in which their velocity (as well as their penetration into the subsurface) is dependent on their frequency.

Dual Testing. Field testing that incorporates both CSL (Sonic) and GDL (Density) logging for assessing the integrity of drilled shaft foundations.

Elastic moduli (elastic constants). Elastic moduli specify the stress- strain properties of isotropic materials in which stress is proportional to strain. They include bulk and shear moduli.

Epithermal neutron. A neutron source emits fast neutrons that are slowed by moderation to an energy level just above thermal equilibrium, where they are available for capture; most modern neutron probes measure epithermal neutrons, because they are less affected by chemical composition than thermal neutrons.

Gamma-Gamma Density Logging (GDL or GGL). Gamma rays from a weak Cesium-137 source are measured at one or several detectors after they migrate through concrete in, and adjacent to, the access tube. Log response primarily results from the electron density of the surrounding medium, which is proportional to the mass per unit volume.

Gamma ray. A photon that has neither mass nor electrical charge that is emitted by the nucleus of an atom; measured in gamma logging and output from a source used in gamma-gamma logging.

Hydration. Hydration is the chemical reaction between cement and water or mineral admixtures and water. When concrete hydrates it dissipates heat; this is called the heat of hydration.

Isotropic. Having a physical property, which does not vary with direction.

The Maturity Method. This method assumes that concrete derives strength from the hydration of cement, the hydration of cement produces heat, and if one can measure the amount of heat generated that the strength of the concrete can be estimated.

Median Velocity. The median velocity value of an individual (one dimensional) log. It is considered to be a better representative of background shaft velocity than mean (average) velocity because it is less affected by the low velocity anomalies that may be present.

Modeling. Computer simulation of data using a presumed model which can then be compared to observations. Agreement between observation from modeling and field conditions does not prove the model represents actual situation due to lack of uniqueness in the geophysical problems.

Neutron Moisture logging (NML). Neutrons from an isotopic source are measured at one or several detectors after they migrate through concrete in, and adjacent to, the access tube. Log response primarily results from hydrogen content as it can be related to moisture content.

Noise. Any unwanted signal; a disturbance that is not part of signal from a specified source.

Nondestructive Testing (NDT). Condition evaluation of a civil structure for integrity assessment or unknown geometry.

Non-unique. In geophysical interpretation and mathematical modeling, a problem for which two or more subsurface models satisfy the data equally well.

Nuclear log. Well logs using nuclear reactions either measuring response to radiation from sources in the probe or measuring natural radioactivity present in the rocks.

Offset. Vertical separation between the source and receiver probes in a Crosshole sonic measurement.

Offset Log. Continuous crosshole sonic log measurement performed with the source or the receiver offset in depth (by some nonzero angle).

Offset Tomography. A scanning method whereby data is collected by running a zero-offset CSL log in combination with several positive offset (receiver is shallower) and negative offset (source is shallower) logs. See CSLT.

Permeability. Permeability is the property of allowing passage of fluid or gases.

Probe. Also called sonde or tool; downhole well-logging instrument package.

Processing. Geophysically, to change data so as to emphasize certain aspects or correct for known influences, thereby facilitating interpretation.

Radius of Investigation. See depth of investigation.

Receiver. The part of an acquisition system that senses the information signal.

Resolution. Refers to the smallest unit of measurement that can be distinguished using a particular instrument or method; based on the ability to separate two measurements which are very close together.

RMS. The root mean square. The square root of the average of the squares of the differences between a series of measurements and their mean value; the standard deviation.

Roughness Model. In a roughness model, the roughness values are calculated by computing changes in velocity from its six neighboring points (or spatial derivative) and it represents the curvature (or roughness) of the velocity field. It identifies regions where a large change in velocity values has taken place.

Standard CSL. Data obtained using (standard practice) CSL method (see also CSL and zero-offset log).

Static Shift. Constant time shift corrections applied to individual offset CSL logs.

Temperature log. A log of the temperature of the fluids in the borehole; a differential temperature log records the rate of change in temperature with depth and is sensitive to very small changes.

Thermal Conductivity. The thermal conductivity is the quantity of heat transmitted within a material if a certain temperature gradient exists.

Thermal neutron. A neutron that is in equilibrium with the surrounding medium such that it will not change energy (average 0.025 eV) until it is captured.

Tomography. A method for determining the distribution of physical properties within the earth by inverting the results of a large number of measurements made in three dimensions (e.g. seismic, radar, resistivity, EM) between different source and receiver locations.

Transducer. Any device that converts an input signal to an output signal of a different form; it can be a transmitter or receiver in a logging probe.

Velocity Equalization. A process performed prior to tomography that equalizes all offset CSL logs to the same median velocity by applying constant static shift to individual logs.

Zero-Offset Log. Crosshole sonic measurement done with no separation between the source and receiver probe (in near horizontal plane). See CSL

APPENDIX A – DUAL CROSSHOLE SONIC LOGGING (CSL) AND GAMMA-GAMMA DENSITY LOGGING (GDL) - CASE HISTORIES

As stated by Jerry DiMaggio (2004), FHWA Principal Geotechnical Engineer, "*unfortunately* (NDT) *tests, due to their qualitative nature, sometimes raise more questions than provide exact answers, and the quality of all testing firms and test results appear to be somewhat variable and inconsistent."*

In this appendix, seven (7) case histories are presented to outline the benefits of **dual** logging for accurate interpretation of anomalies in drilled shafts both inside and outside the rebar cage (including rebar exposure to soil). Dual logging is performed using both crosshole sonic logging (CSL) and gamma-gamma density logging (GDL) methods. Dual logging provides with independent verification of anomalies and provides a better picture for the possible causes for the observed anomalies. It also helps eliminate false positives or false negatives in the data that results in costly construction delays. The seven (7) case histories are all from the Arizona Department of Transportation (ADOT) project sites where dual logging was performed:

Case History 1 (CSL False Negative):

Field Testing: GDL indicates an anomaly with no indication on the CSL record.
Interpretation: Density anomalies were located outside the rebar cage.

Case History 2 (GDL False Negative):

Field Testing: CSL indicates an anomaly in all tubes with no indication on the GDL.
Interpretation: Velocity anomalies were located in the interior portion of the shaft.

Case History 3:

Field Testing: GDL indicates an anomaly with only low amplitudes indicated in CSL.
Interpretation: Density anomalies were located outside the rebar cage and intruding in and just touching the tubes.

Case History 4 (CSL False Positive):

Field Testing: CSL indicates low amplitude anomalies with no anomalies on the GDL.
Interpretation: Tube instillation problem.

Case History 5 (Anomaly Confirmation):

Field Testing: GDL indicates 3 anomaly zones. CSL indicates 1 low amplitude zone and 1 low amplitude/velocity zone.
Interpretation: First anomaly located outside the cage, second anomaly located outside the cage just touching the tube, the third anomaly intrudes inside the cage.

Case History 6 (Anomaly Confirmation):

Field Testing: Three methods: CSL, GDL, and neutron moisture logging (NML) all indicate the same anomaly. CSLT was used to image the defect.
Interpretation: Low velocity/density zone with high moisture that extend inside the cage.

Case History 7 (Anomaly Confirmation):

Field Testing: Both CSL and GDL indicate an anomaly.
Interpretation: Anomaly extends inside the cage. CSLT was used to image the defect in three-dimension for coring confirmation followed by remediation.

Case History 1	Inspection Tubes	Testing Age (Days)		GDL Anomalies	CSL/T Anomalies	
		CSL	GDL		Travel Time	Amplitude
5' Dia. Shaft	4 PVC	17	7	YES	NO	NO

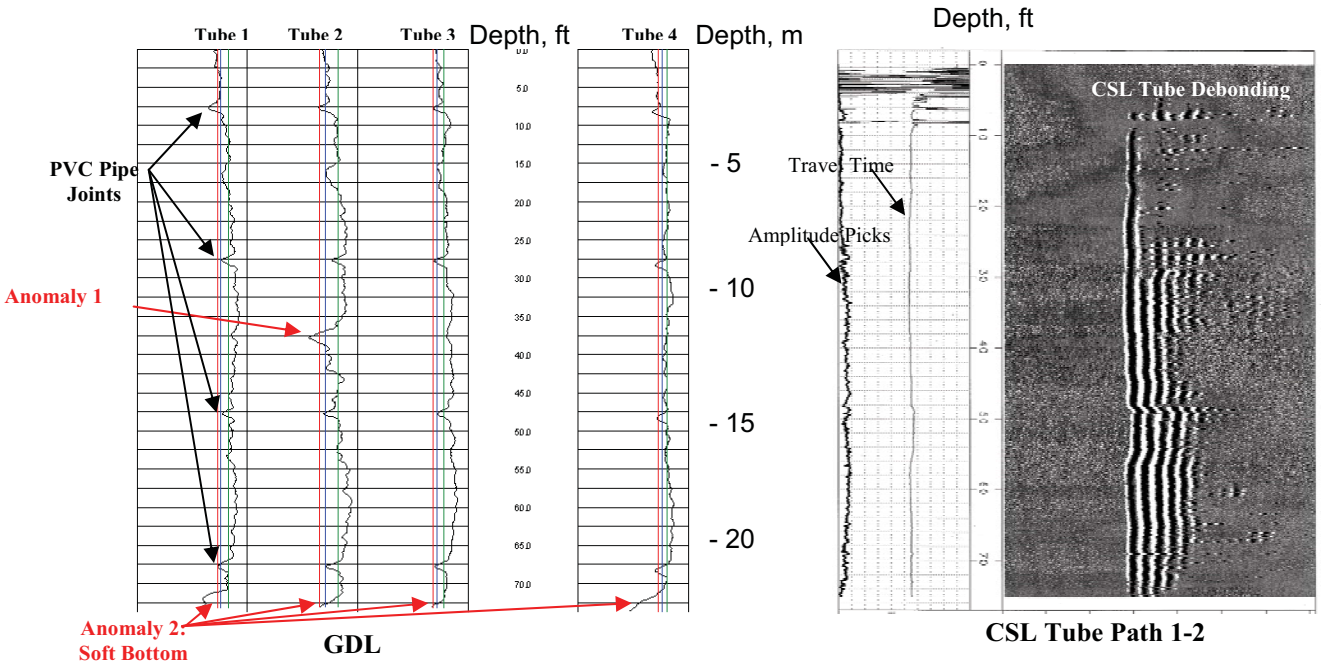

Analysis: GDL test was performed first which indicated a soft bottom condition and a poor quality density zone at Tube 2 between 11.3-11.8 m (37-39 ft). CSL and CSLT did not indicate velocity anomalies (just PVC tube debonding for 17-days old shaft).

Interpretation: Density anomalies were located outside the rebar cage.

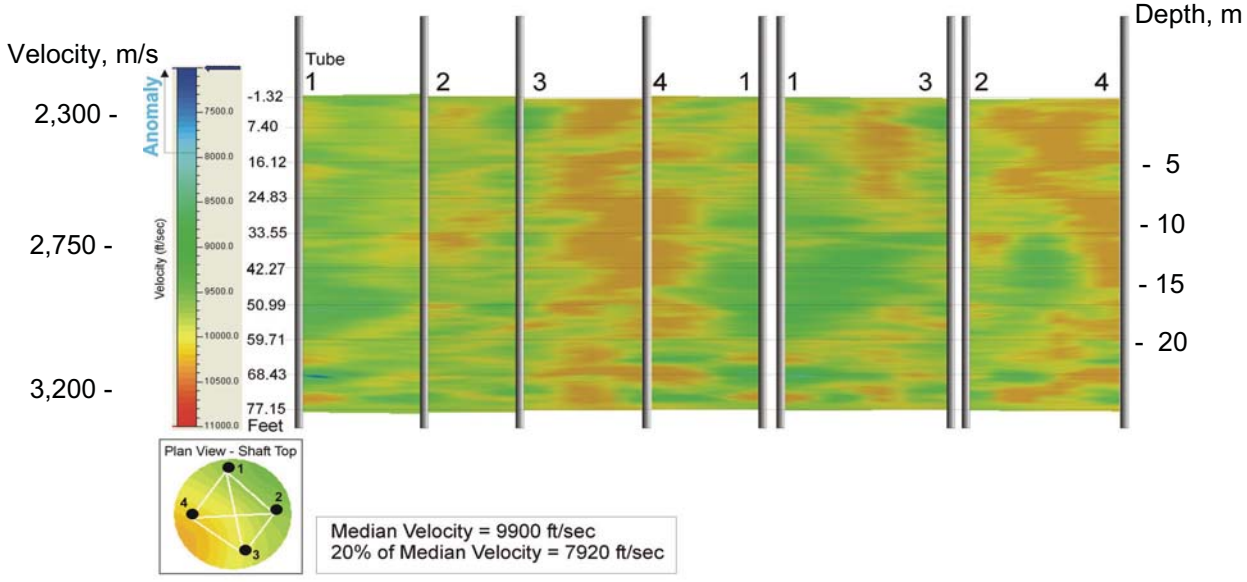

3-D Tomography (CSLT)

Case History 2	Inspection Tubes	Testing Age (Days)		GDL Anomalies	CSL/T Anomalies	
		CSL	GDL		Travel Time	Amplitude
3' Dia. Shaft	3 STEEL	6	18	NO	YES	YES

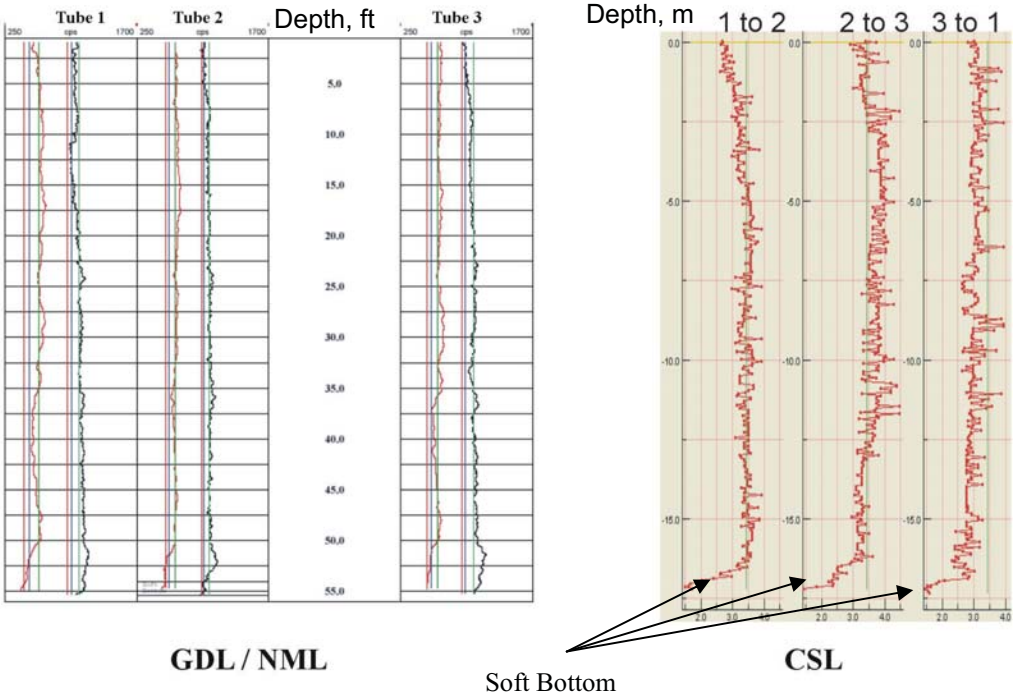

Comprehensive geophysical logging program was performed including: crosshole sonic logging (CSL), 3-D zero-offset tomography (CSLT), gamma-gamma density (GDL), and neutron-moisture logging (NML).

Analysis: ALL three (3) CSL logs indicated a soft bottom. However, GDL, shown in black, indicated no major density anomaly. NML (red), indicated a high moisture zone.

Interpretation: "Soft bottom" condition located in the interior portion of the shaft just missing the tubes.

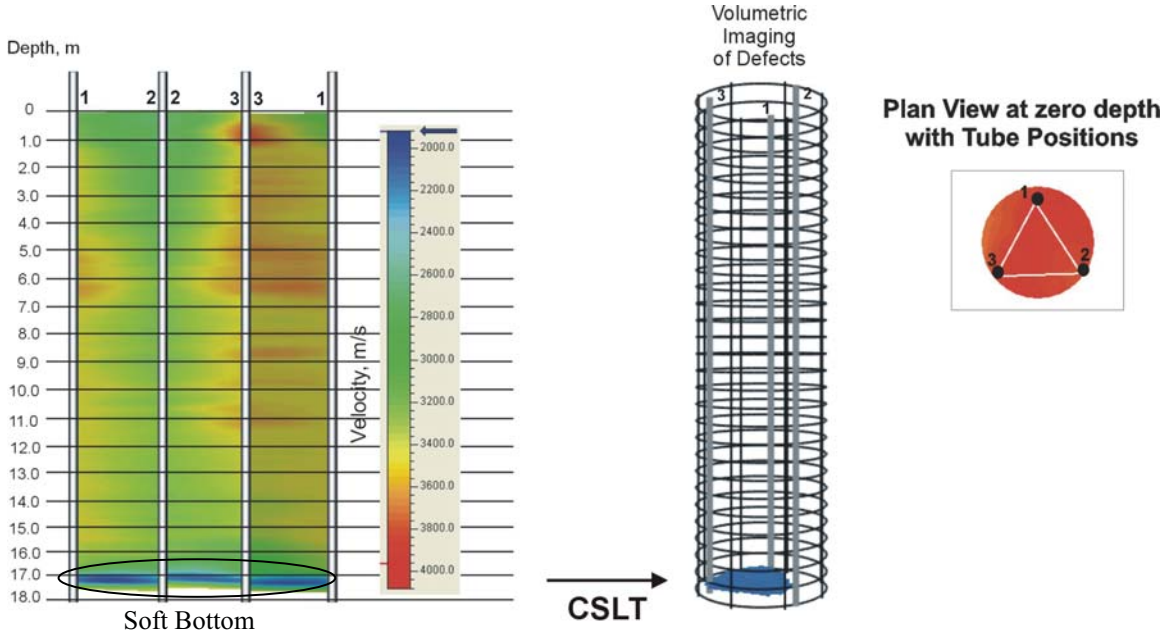

Case History 3	Inspection Tubes	Testing Age (Days)		GDL Anomalies	CSL/T Anomalies	
		CSL	GDL		Travel Time	Amplitude
6' Dia. Shaft	6 PVC	6	6	YES	NO	YES

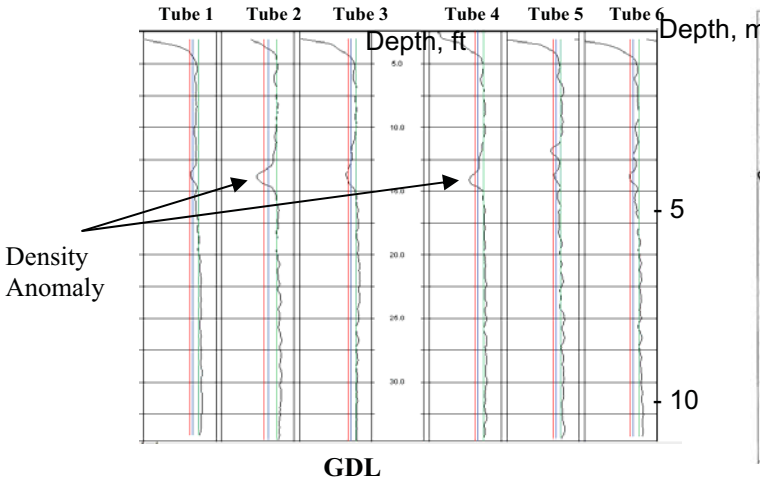

GDL

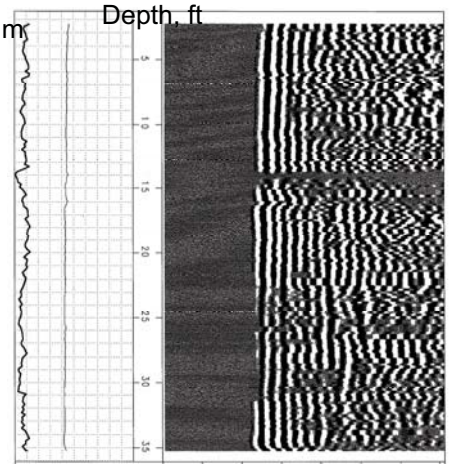

CSL Tube Path 2-3

Analysis: CSL and GDL performed at the same time. GDL indicates a density a 4.1-4.4 m (13.5-14.5 ft). CSL indicates low amplitude (reduced signal energy) at the same depth; but no velocity anomaly.

Interpretation: Density anomalies outside rebar cage and is intruding in just touching the tubes. Therefore, the rebar cage is probably exposed to the density anomaly.

Case History 4	Inspection Tubes	Testing Age (Days)		GDL Anomalies	CSL/T Anomalies	
		CSL	GDL		Travel Time	Amplitude
6' Dia. Shaft	6 PVC	4	22	NO	NO	YES

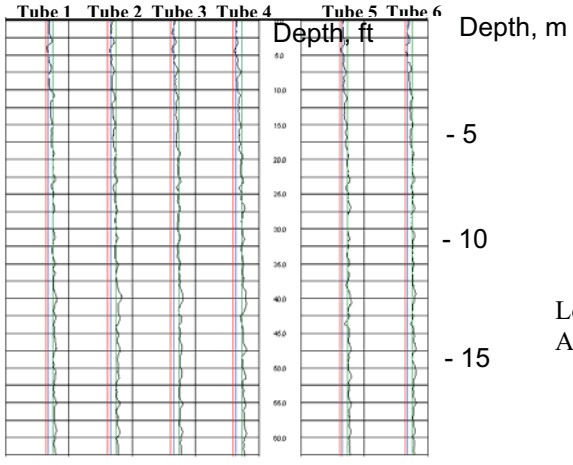

GDL

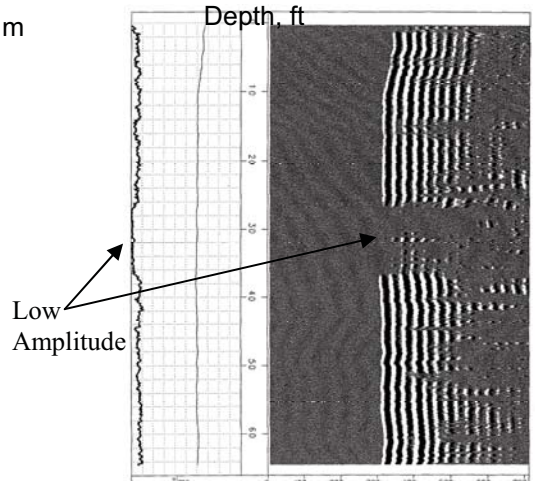

CSL Tube Path 2-5

Analysis: CSL test was performed first which indicated low amplitude (reduced signal energy) near Tubes 2 and 3 between 8.3-11.3 m (27-37 ft); but no velocity anomaly. GDL indicates no density anomalies.

Interpretation: Tube bonding problem, possibly due to excessive vibration during instillation.

Case History 5	Inspection Tubes	Testing Age (Days)		GDL Anomalies	CSL/T Anomalies	
		CSL	GDL		Travel Time	Amplitude
4' Dia. Shaft	4 PVC	43	7	YES	NO/YES	YES

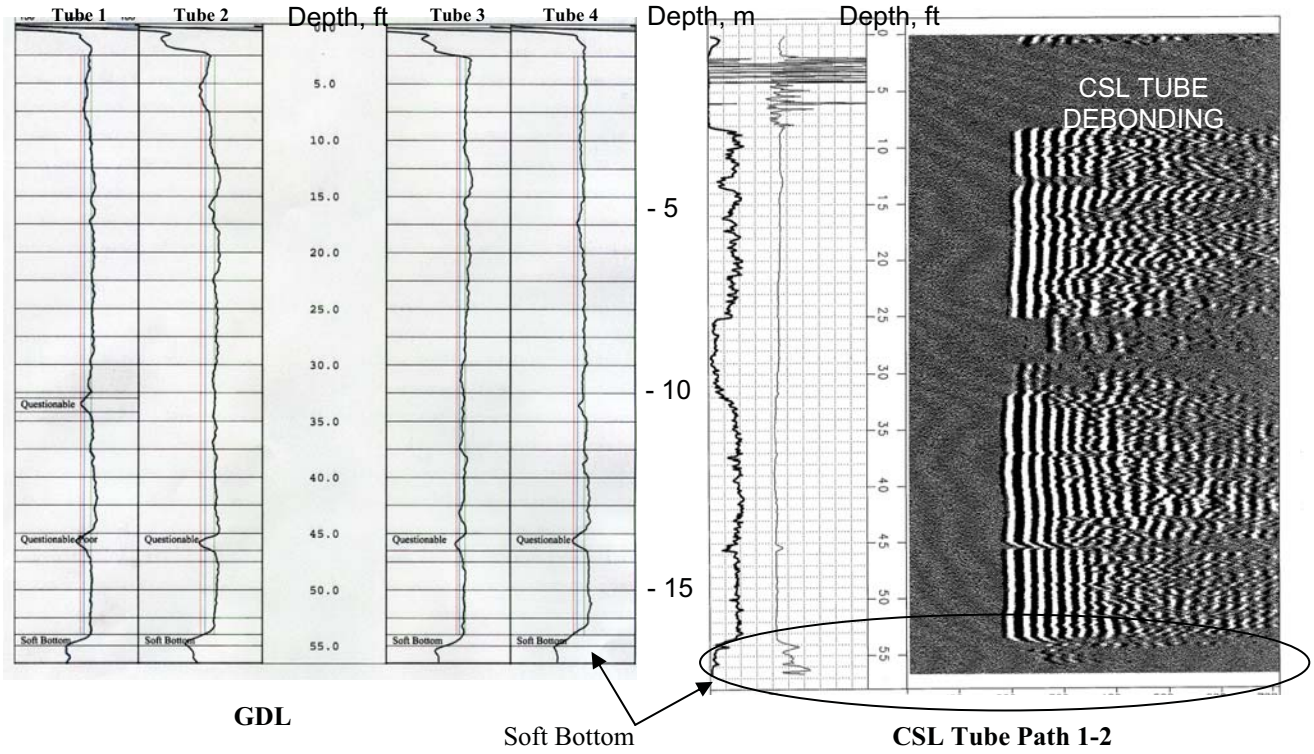

GDL test was performed first which indicated three zones of density anomalies. CSL was performed next with severe PVC tube debonding observed in the 43-days old shaft.

Anomaly 1: GDL indicated a questionable density zones near Tube 1 between 10-10.4 m (33-34.2 ft). CSL testing does not indicate a significant velocity anomaly.

Interpretation: Density anomaly is located outside the rebar cage.

Anomaly 2: GDL indicated a questionable-poor density anomaly in all four tubes between 13.7-14.2 m (45-46.5 ft). CSL data indicate only a drop in signal amplitudes in all four tubes without a significant reduction in velocity (<10%).

Interpretation: Density anomalies outside rebar cage and is intruding in just touching the tubes. Therefore, the rebar cage is probably exposed to the density anomaly.

Anomaly 3: GDL indicated a soft bottom condition in all tubes at the bottom 0.76 m (2.5 ft). CSL testing also confirms the soft bottom condition (>20% drop in velocity).

Interpretation: The soft bottom condition is located both inside and outside the rebar cage.

Case History 6	Inspection Tubes	Testing Age (Days)		GDL Anomalies	CSL/T Anomalies	
		CSL	GDL		Travel Time	Amplitude
3' Dia. Shaft	3 STEEL	6	18	YES	YES	YES

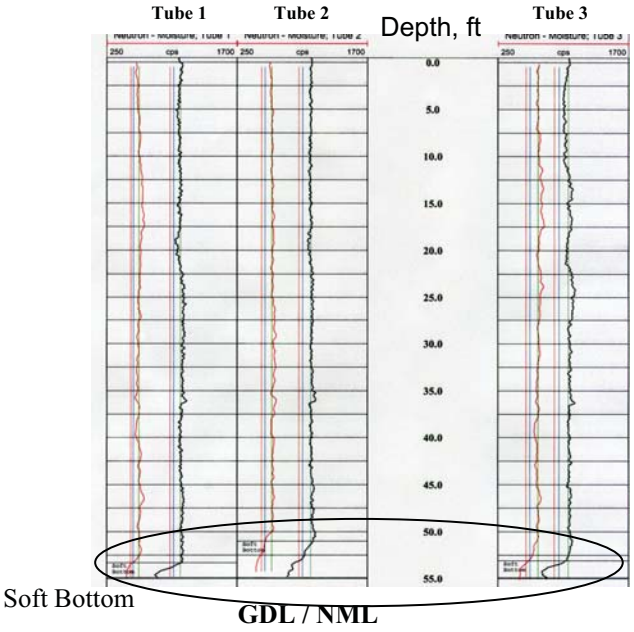

GDL / NML

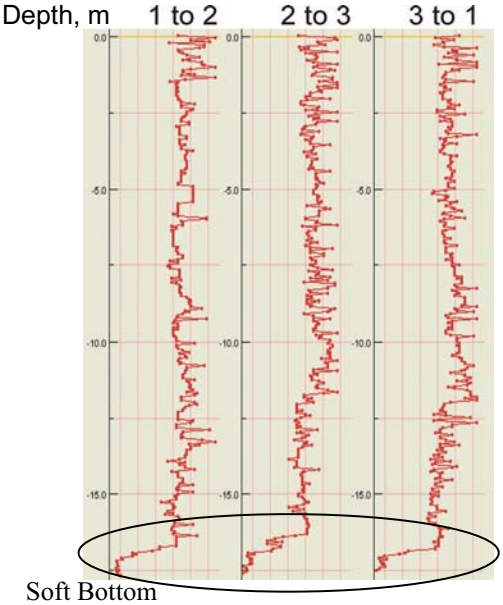

CSL

Comprehensive geophysical logging program was performed including: crosshole sonic logging (CSL), 3-D zero-offset tomography (CSLT), gamma-gamma density (GDL), and neutron-moisture logging (NML).

Analysis: ALL three (3) CSL, GDL, and NML logs indicated a soft bottom condition. Therefore, complementary results were indicated; however, note for Tube 3, neutron-moisture (NML) indicates higher extent of high-moisture anomaly.

Interpretation: "Soft bottom" condition which extends to the interior of the shaft.

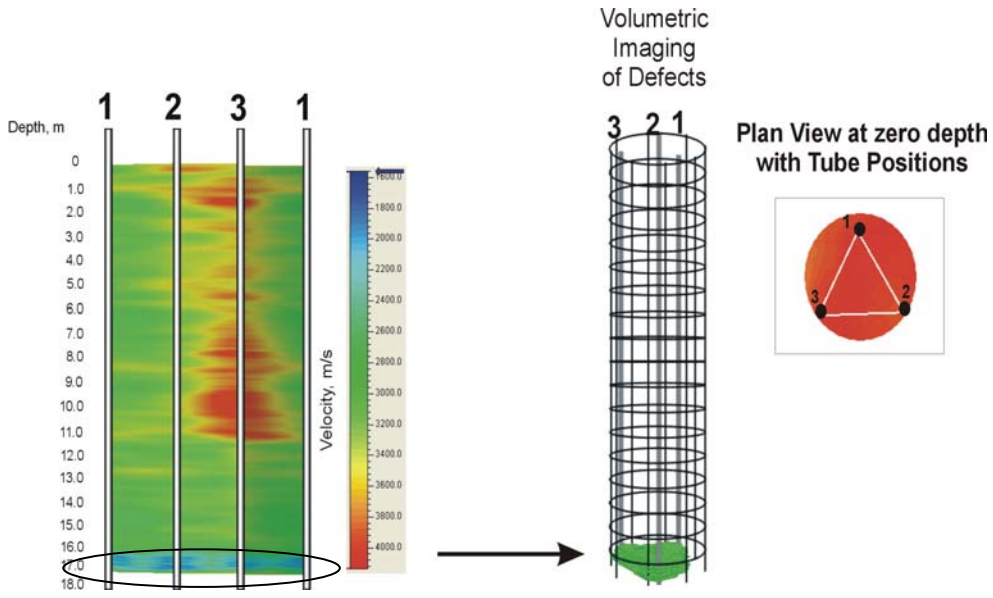

CSLT

Case History 7	Inspection Tubes	Testing Age (Days)		GDL Anomalies	CSL/T Anomalies	
		CSL	GDL		Travel Time	Amplitude
6' Dia. Shaft	6 STEEL	5	5	YES	YES	YES

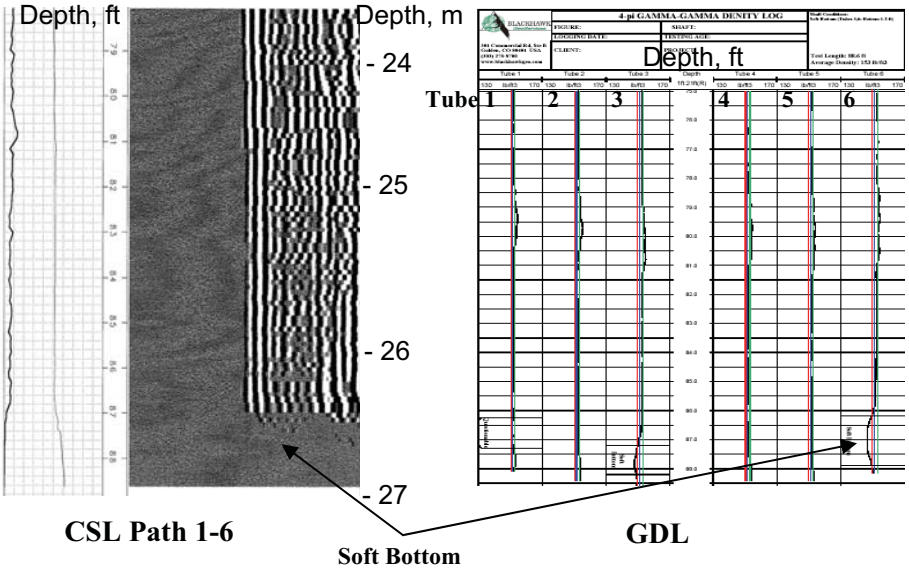

Comprehensive Geophysical logging including: crosshole sonic logging (CSL), 3-D multi-offset tomography (CSLT), and gamma-gamma density logging (GDL) was performed from **steel** pipes.

Analysis: CSL and GDL data indicated 0.3-0.6 m (1-2 ft) "soft bottom" condition. Three-dimensional tomographic imaging (CSLT) was performed for coring followed by remediation.

Interpretation: Soft bottom condition which extends to the interior of the shaft. 3-D images defined poor quality concrete zones shown in green, blue, and purple colors. Good quality concrete is shown in red. The defect zones are shown at the bottom of the shaft primarily around Tubes 6, 5, and 3.

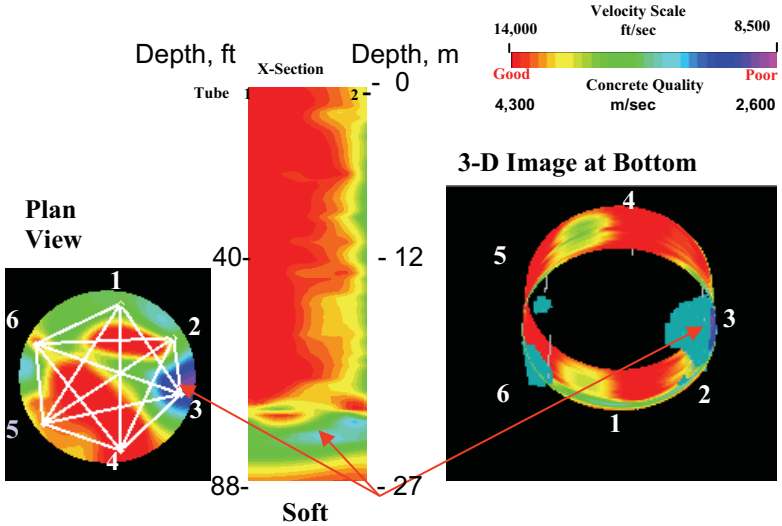

CSLT